Czech Technical University in Prague

Faculty of Electrical Engineering

Doctoral Thesis

June, 2020 *Michal Ulvr*

Czech Technical University in Prague
Faculty of Electrical Engineering
Department of Measurement

AC MAGNETIC FLUX DENSITY STANDARDS AND THEIR USE IN METROLOGY

Doctoral Thesis

Michal Ulvr

Prague, June 2020

Ph.D. Programme: P2612 - Electrical Engineering and Information Technology
Branch of study: 2601V006 - Measurement and Instrumentation

Supervisor: ***Doc. Ing. Petr Kaňpar, CSc.***

Declaration

I declare, that this doctoral thesis is based at all my own work and I have cited all sources I have used in the bibliography.

In Prague, June 22nd, 2020

Prohlášení

Prohlašuji, že jsem předloženou disertační práci vypracoval samostatně a že jsem uvedl veškerou použitou literaturu.

V Praze, 22. 6. 2020

é é é é .....é é é é é é é ..
Michal Ulvr

Acknowledgements

I would like to express my gratitude to my supervisor, associate professor Petr Kaġpar, and to my colleague, Dr. Josef Kupec, for their scientific and university guidance, invaluable comments and patience with my studies.
Also I would like to thank my family for their support and patience throughout the study period.

Abstract:

This dissertation describes the development of AC magnetic flux density standards and their use in metrology. The dissertation focuses mainly on the design and realization of new standards, which will extend the existing ways of calibrating AC magnetometers in the primary laboratory of the Department of Electromagnetic Quantities of the Czech Metrology Institute.

Various coil systems and various types of solenoids are commonly used for calibrating magnetometers (teslameters with a Hall probe, or 3-axis coil probe analyzers) up to several mT. The maximum value of the AC magnetic flux density generated in the center of the standard, and its homogeneity, depend on the dimensions and the type of the coil standard and the winding parameters. The induction and parasitic capacity of the winding affects the value of the resonance frequency and thus the frequency range in which the standard can be used. An electromagnet has to be used when a higher magnetic flux density value needs to be generated for calibration up to hundreds of mT. Here, some standard sensor (Hall probe, search coil) with traceable calibration should be used for precise measurements of the AC magnetic flux density generated in the center of the air gap.

In the first part of the dissertation, various types of coil standards (Helmholtz, Maxwell, Garrett, Barker, Braunbek, etc.) and available AC electromagnets are described and are compared in terms of their parameters and their uses in AC applications. The standards for AC calibrations available in the primary laboratory of the Department of Electromagnetic Quantities of the Czech Metrology Institute before starting this dissertation work are also presented here.

The second part of the dissertation describes the design and realization of the Helmholtz-type single-layer coil standard for calibrating magnetometers in the frequency range up to 100 kHz. The standard was designed primarily for calibrating magnetic field analyzers with a 3-axis coil probe (EFA 300, ELT 400). An AC magnetic flux density value of 105 εT up to 40 kHz and an AC magnetic flux density value of 40 εT at a frequency of 100 kHz can be generated by means of the coil standard that is developed. The serial resonance effect was used in order to generate a magnetic flux density of 105 εT up to 100 kHz. For this purpose, a capacitive programmable array was designed and realized. This array is connected in series with the winding of the coil standard. To ensure the metrological traceability of the generated AC magnetic flux density, a calibration method was developed involving special search coils and an AC current shunt with calibrated AC/DC differences, by which the coil standards can be calibrated up to 100 kHz with expanded uncertainty of (0.12 to 0.25)%. This section of the dissertation also describes the possibilities of using coil standards in metrology.

The last part of the dissertation is devoted to the design and realization of the system with an AC electromagnet, which can be used for calibrating teslameters with a Hall probe up to 1 T at low frequencies (mainly at a frequency of 50/60 Hz). An AC electromagnet with a UNICORE core has been developed from oriented electrotechnical steel with a cross-section of 36 cm^2 and with a length of the air gap of 10 mm. A single-layer, a double-layer and a 10-layer special PCB search coil were designed and fabricated for precise measurements/adjustments of the AC magnetic flux density generated in the center of the air gap, ensuring the metrological traceability of the teslameter calibration using the system with an AC electromagnet. The serial resonance effect was used when powering the electromagnet. It was possible to use a conventional amplifier for power supply thanks to the HV capacitors connected in series with the electromagnet winding. A feedback was also implemented to improve the stability of the AC magnetic flux density generated inside the air gap. The value of the generated AC magnetic flux density can be measured/adjusted in the center of the air gap with expanded uncertainty of 0.2%. To extend the frequency range of the calibrations, an AC electromagnet made from amorphous MetGlass 2605HB1 material was also realized, enabling it to generate magnetic flux density of about 100 mT up to a frequency of 1 kHz.

Keywords: AC magnetic flux density, calibration, coil standard, electromagnet, metrology.

Abstrakt:

Tato disertační práce se zabývá etalony střídavé magnetické indukce a jejich využitím v metrologii. Práce je zaměřena především na návrh a realizaci nových etalonů, které by rozšířily stávající možnosti kalibrací střídavých rozsahů magnetometrů v primární laboratoři oddělení elektromagnetických veličin Českého metrologického institutu.

Pro kalibrace magnetometrů (teslametrů s Hallovou sondou nebo analyzátorů elektromagnetického pole s 3-osou cívkovou sondou) do několika mT se běžně využívají různé cívkové systémy nebo různé typy solenoidů. Maximální hodnota generované střídavé magnetické indukce ve středu etalonu a její homogenita závisí na rozměrech a typu etalonu a na parametrech vinutí. Z parametrů vinutí etalonu je nejdůležitější indukčnost a parazitní kapacita, která ovlivňuje velikost rezonanční frekvence a tím i frekvenční rozsah, ve kterém lze etalon používat. Pro kalibrace do vyšších hodnot střídavé magnetické indukce (stovky mT) je nutné použít silnější zdroj pro generování magnetické indukce (střídavý elektromagnet) ve spojení s etalonem (etalonový senzor), kterým se nastavená hodnota magnetické indukce ve vzduchové mezeře elektromagnetu přesněji změří.

V první části disertační práce jsou popsány a srovnány různé typy cívkových etalonů (Helmholtz, Maxwell, Garrett, Barker, Braunbek atd.) a dostupných střídavých elektromagnetů z hlediska jejich parametrů a využití ve střídavých aplikacích. Také jsou zde popsány etalony pro střídavé kalibrace dostupné před zahájením řešení této disertační práce v primární laboratoři oddělení elektromagnetických veličin Českého metrologického institutu.

Druhá část práce je věnována návrhu a realizaci jednovrstvého cívkového etalonu Helmholtzova typu pro kalibrace magnetometrů v rozsahu do 100 kHz. Tento etalon byl navržen primárně pro kalibrace analyzátorů magnetického pole s 3-osou cívkovou sondou (EFA 300, ELT 400). Tímto etalonem bylo možné generovat střídavou magnetickou indukci 105 μT do 40 kHz a 40 μT na frekvenci 100 kHz. Aby bylo možné generovat hodnoty magnetické indukce 105 μT až do 100 kHz, byla využita sériové rezonance. Pro tento účel byla navržena a realizována programovatelná kapacitní dekáda, která byla připojena do série s vinutím etalonu. Aby byla zajištěna metrologická návaznost generované střídavé magnetické indukce, byla vyvinuta kalibrační metoda zahrnující speciální měřicí cívky a AC/DC boční k s kalibrovanou AC/DC diferencí, kterou je možné kalibrovat cívkové etalony do 100 kHz s rozšířenou nejistotou 0,12 % až 0,25 %. V této části práce jsou popsány možnosti využití cívkových etalonů v metrologii.

Poslední část práce je věnována návrhu a realizaci systému se střídavým elektromagnetem, kterým je možné kalibrovat teslametry s Hallovou sondou do 1 T na nízkých frekvencích (především na frekvenci 50/60 Hz). Byl vyvinut střídavý elektromagnet s UNICORE jádrem z orientované elektrotechnické oceli o průřezu 36 cm^2 a s délkou vzduchové mezery 10 mm. Pro přesné měření/nastavení generované střídavé magnetické indukce ve vzduchové mezeře byla navržena a realizována jednovrstvá, dvouvrstvá a 10-vrstvá speciální PCB měřicí cívka, která zajišťuje metrologickou návaznost kalibrace teslametrů při použití systému se střídavým elektromagnetem. Při napájení elektromagnetu byla opět využita sériová rezonance. Díky vn kapacitorům zapojeným do série s vinutím elektromagnetu je možné použít pro napájení běžný zesilovač. Pro zlepšení stability generované střídavé magnetické indukce byla také použita zpětná vazba. Tímto systémem je možné měřit/nastavit hodnotu magnetické indukce ve vzduchové mezeře s rozšířenou nejistotou 0,2 %. Pro rozšíření frekvenčního rozsahu kalibrací byl také realizován střídavý elektromagnet z amorfního materiálu MetGlass 2605HB1, díky kterému je možné generovat magnetickou indukci kolem 100 mT do frekvence 1 kHz.

Klíčová slova: cívkový etalon, elektromagnet, kalibrace, metrologie, střídavá magnetická indukce.

Table of Contents

Abbreviations

A/D	analog-to-digital
AC	alternating current
CMI	Czech Metrology Institute
DC	direct current
EMC	electromagnetic compatibility
FEM	finite element method
FF	fringing factor
FIT	finite integration technique
LF	low frequency
MFD	magnetic flux density
NMR	nuclear magnetic resonance
PCA	programmable capacitor array
PCB	printed circuit board
ppm	parts per million
PTB	Physikalisch-Technische Bundesanstalt
PTFE	polytetrafluorethylene
RMS	root mean square
RF	radio frequency
VMI	variable mutual inductance
VNIIM	D. I. Mendeleyev Institute for Metrology
ZDM	zero differential method

1 Introduction and motivation

AC magnetic flux density standards are very important in metrology of magnetic quantities for calibrations of the AC teslameter (with Hall probes) and for calibrating AC magnetic field analyzers (magnetometers) with a 3-axis coil probe. Others fields in which these standards are used are electromagnetic compatibility (EMC) testing and biomedical applications. In recent years, there have been increasing numbers of inquiries about calibrating Hall probes up to 1 T at 50 Hz and for calibrating magnetometers up to 100 kHz. To fulfill these demands from industry, it was necessary to design and realize new standards at the Department of Electromagnetic Quantities of the Czech Metrology Institute (CMI). The standards can be split up into two groups.

The first group is coil standards. The structure of DC and AC magnetic flux density (MFD) standards does not differ greatly. Solenoids of the same types are used. In general, the coil standards can be compared according to the homogeneity in the inner space of the coil standard, according to the access into the inner space of the coil and according to the relative difficulty of exact realization (e.g. a cylindrical frame with circular turns is easier to realize than frame a with square/rectangular turns). The magnetic flux density value B (T) inside the coil standard is given by the coil constant K_B (T/A) or K_H (Am^{-1}/A), and by the current value I (A) through the coil standard as

$$B = K_B I = \mu_0 \mu_r K_H I \,, \tag{1}$$

where ε_0 is a constant of magnetic vacuum permeability (1.25663706212(19)×10^{-6} H/m [1]) and ε_r is the relative permeability of air. The coil standards of B are also the coil standards of the magnetic field strength H with the uncertainty given by the difference between ε_r and 1. This difference is negligible. The efficiency of the coil standards can also be compared using the Fabry factor G, which is dependent only on the coil shape. The magnetic flux density in the center of the coil standard can be expressed as [2]

$$B = \mu_0 G \sqrt{\frac{P_i \lambda_0}{R_i \rho_i}} \,, \tag{2}$$

where G is the Fabry factor, P_i is the loss power of the winding, ϑ_0 is the filling factor, R_i is the inner radius of the winding, and ρ_i is the resistivity of the conductor. However, there are some limitations in the use of coil standards in AC applications. The coil standard should have no metal parts except the winding. In AC applications, an imaginary part of the coil impedance (its inductance L) is important. The value of L is related to the power supply possibility, and thus to the maximal value of generated B. The frequency range of coil standards is given by the winding impedance and the parasitic capacity of the winding, which determine the resonance frequency value and thus the usable frequency range.

The second group consists of AC electromagnets, which can generate a B value of at least several tens of mT. The value of the generated B is measured either by a teslameter with a Hall probe or by a special search coil. These special electromagnets must be produced from suitable material with regard to its parameters and its use. The material of the yoke should have high permeability, low losses and high saturation.

1.1 Coil systems

Coil systems for generating a DC magnetic field are described in this section. These coil systems can also be used for generating an AC magnetic field, with some limitations.

1.1.1 Helmholtz coils

Helmholtz coils are the most widely-used type of coil standard. Helmholtz coils consist of two parallel, circular, identical loops of thin wire that are placed symmetrically along a common axis [3]. The distance l between the loops is equal to the radius R of the loop (Fig. 1a). The magnetic field value on the axis of the Helmholtz coils can be calculated as [4]

$$B = \mu_0 \frac{NIR^2}{2} \left\{ \left[R^2 + \left(\frac{l}{2} + z \right)^2 \right]^{-3/2} + \left[R^2 + \left(\frac{l}{2} - z \right)^2 \right]^{-3/2} \right\}, \tag{3}$$

where z is the distance from the center of the coils on the axis of the coils. Equation (3) can be re-written for z=0 and l=R as

$$B = \mu_0 \frac{NI}{R} 0.7155 . \tag{4}$$

Generally, homogeneity of the generated magnetic field of about the 4th order can be

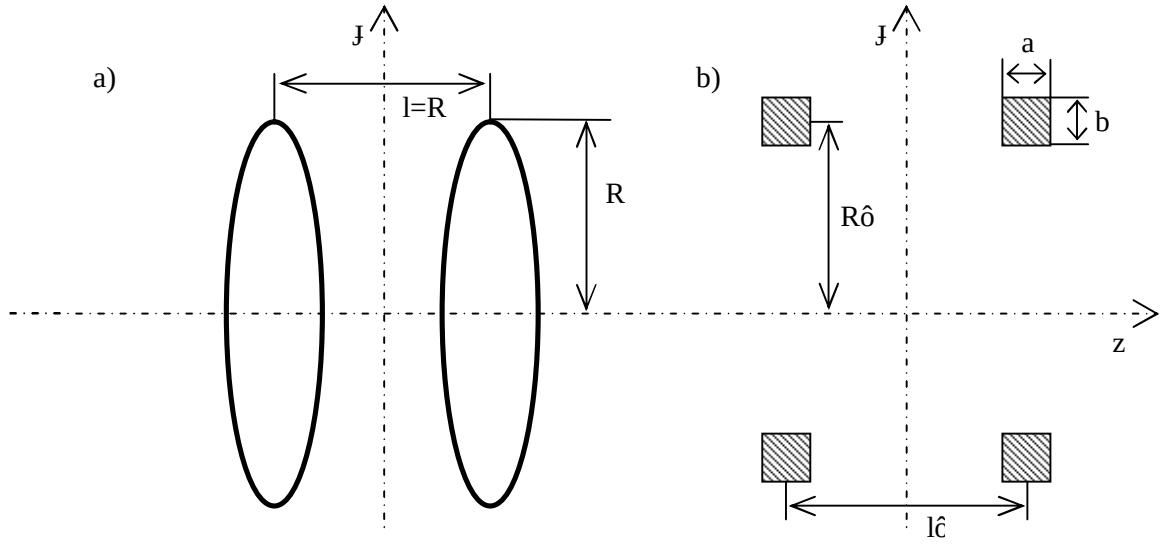

Fig. 1 a) Helmholtz coils, b) multi-layer Helmholtz coils.

achieved using Helmholtz coils. Helmholtz coils can be modified in their winding shape or in their dimensions to improve the homogeneity in the desired volume inside the coils. Optimization of the coils spacing of circular Helmholtz coils is presented in [5]. An analysis of the magnetic field homogeneity between circular and square Helmholtz coils has also been published [6], [7]. An example of simulation results for the improved homogenity of Helmholtz coils when a third coil of the same diamater is added between the coils can be found in [8]. A comparison of the magnetic field homogeneity of circular, square and triangular Helmholtz coils is presented in [9]. Multi-layer Helmholtz coils can be used for generating higher magnetic flux density values. Here, the width a and height b of the winding must be taken into account and the mean radius Rô and mean distance lô should still fulfill the condition ló=Rô (Fig. 1b). The recommended value of the height to width ratio is b/a=1.078 [4].

1.1.2 Maxwell coils

A Maxwell coil setup consists of three coils oriented on the surface of a virtual sphere [10]. Both outer coils should have a radius of $\sqrt{4/7}R$, and should have a distance of $\sqrt{3/7}R$ from the central coil with radius R (Fig. 2a). Each of the outer coils should have number of turns exactly in the ratio of 49/64 of the central coil. Maxwell coils are very often used for

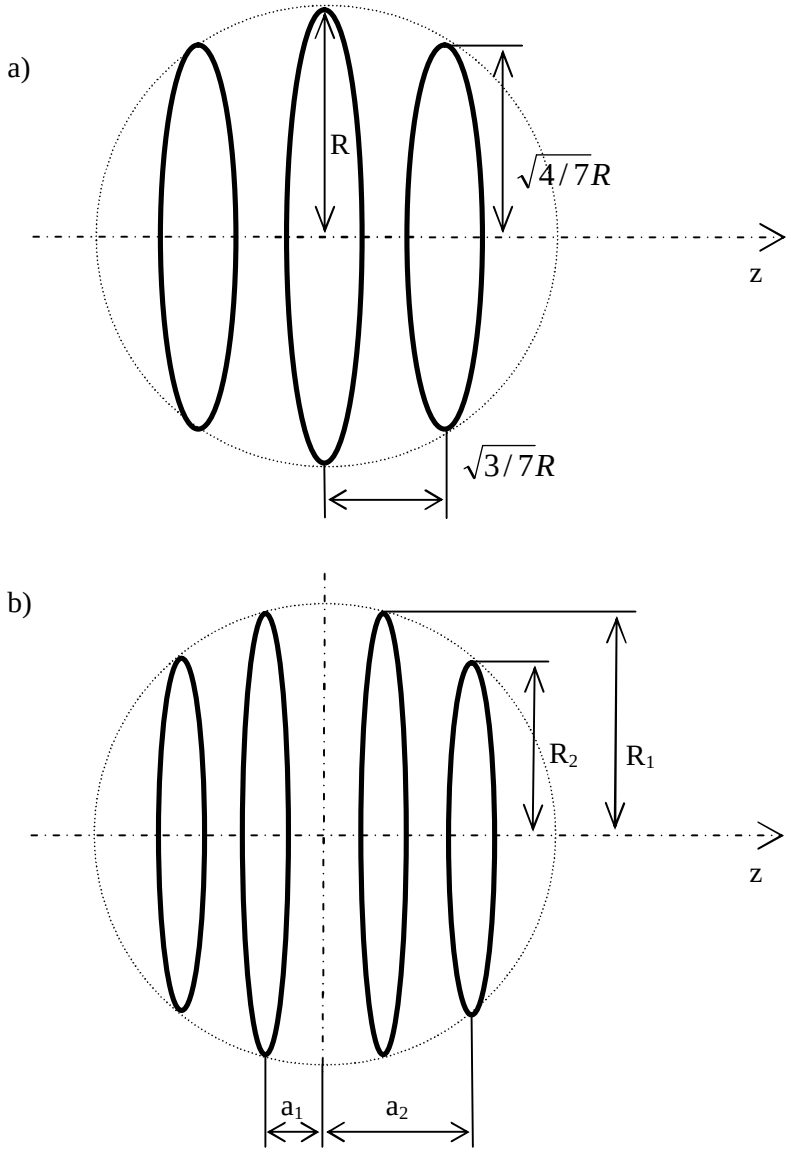

Fig. 2 a) Maxwell 3-coil configuration, b) Maxwell 4-coil configuration.

generating a magnetic field gradient [11], for example in the 4-coil configuration (Fig. 2b). The 4-coil configuration should have following ratios [24]:

$$\frac{R_2}{R_1} = 0.6719, \quad \frac{a_1}{R_1} = 0.2976, \quad \frac{a_2}{R_2} = 1.1880, \quad \frac{N_2}{N_1} = 0.6821.$$

A comparison of the homogeneity between Helmholtz coils and Maxwell coils can be found in [12].

1.1.3 Barker coils

Another coil system is called Barker coils, which are 3, 4 or 6 symmetrically arranged coils of the same radius. The advantage of Barker coils is that they are simpler to realize (than Helmholtz or Maxwell coils), and all coils are on one and the same frame. Barker coils (for the 4-coil arrangment) should have following ratios [24]:

$$\frac{a_1}{R} = 0.2432, \quad \frac{a_2}{R} = 0.9407, \quad \frac{N_2}{N_1} = 2.2606 .$$

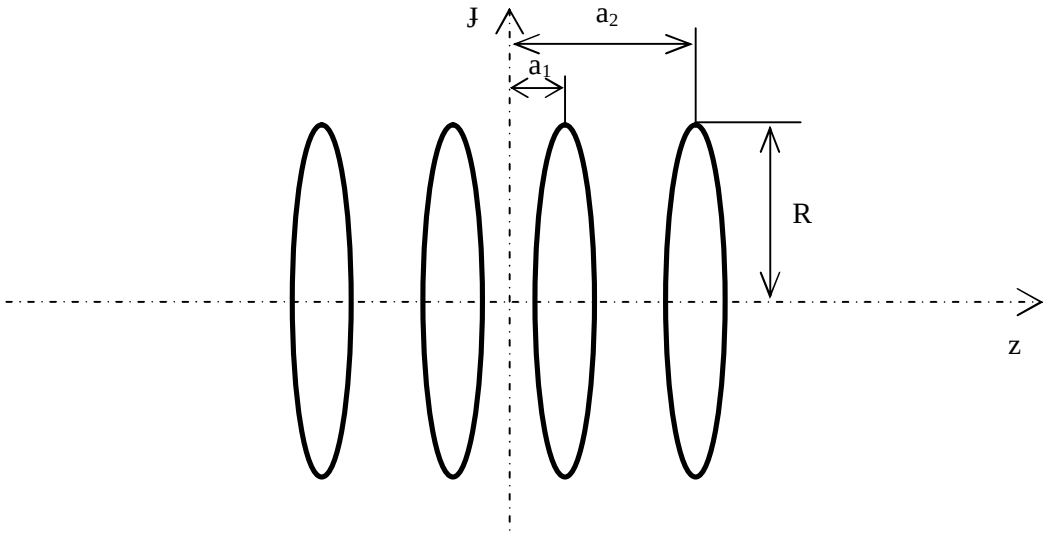

Fig. 3 Barker coils (4-coil arrangment).

1.1.4 Braunbek coils

A multi-coil system (3 or more coils) is used when a larger area of homogeneous magnetic field is needed. Braunbek coils consist of four coils (two pairs of coils) [13] with dimensions according Fig. 4. Each coil has the same number of turns. The ratios between the distance of the inner coil pair from the center d_2, the distance of the outer coil pair from the center d_1, the radius of the inner coil pair R_2 and the radius of the outer coil pair R_1 are [14]:

$$\frac{d_1}{R_1} = 1.107, \quad \frac{R_2}{R_1} = 1.309, \quad \frac{d_2}{R_1} = 0.364, \quad \frac{d_2}{R_2} = 0.278.$$

A comparison of the homogeneity between Braunbek coils and Helmholtz coils can be found in [15].

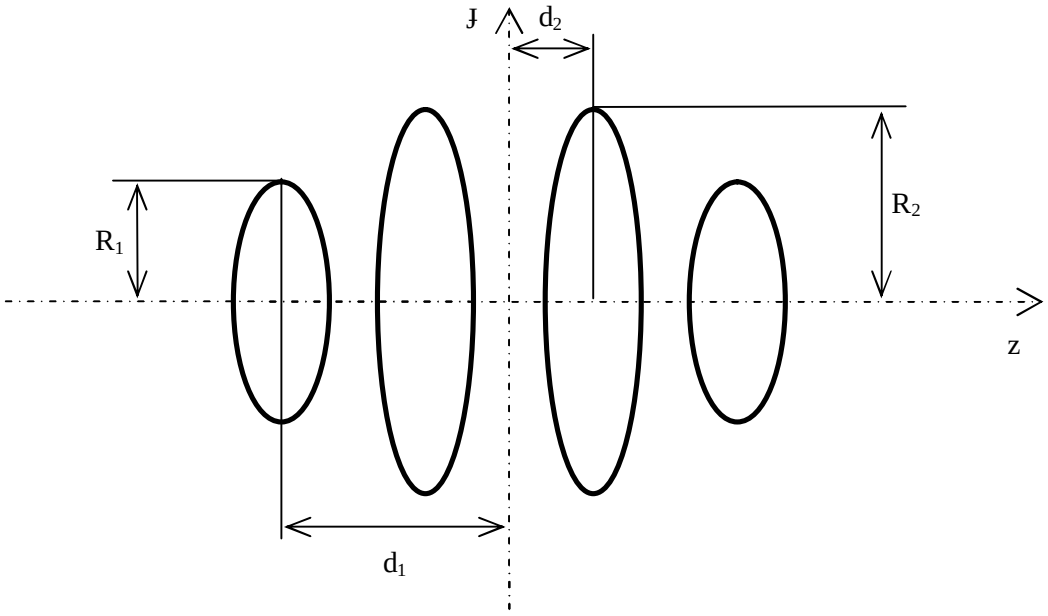

Fig. 4 Braunbek coil system.

1.1.5 Merritt coils

A system of three (Fig. 5) or four (Fig. 6) square coils with given dimensions is referred to as Merritt coils. For a three-coil system, the ratio of the length of the coil side l and the width of the coil system w is $w/l = 0.821116$, and the ratio of the current in the middle coil I_1 to the current of the outer coils I_2 is $I_1/I_2 = 0.512797$. For a four-coil system, the ratio between the side length of the coil l and the distance of the inner coil pair from the center of the system x is $x/l = 0.128106$. The ratio between coil side length l and the distance of the outer coil pair

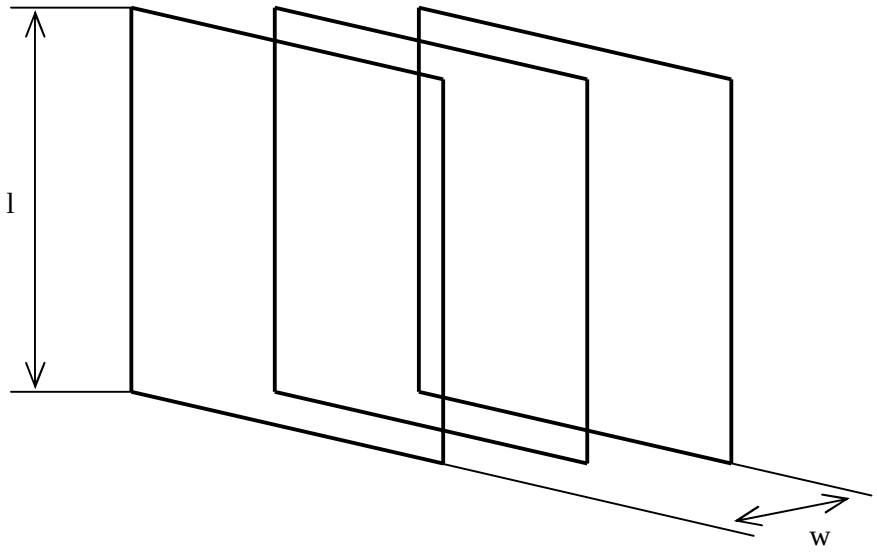

Fig. 5 Merritt 3-coil system.

from the center of the system y is $y/l = 0.505492$. The ratio of the current in the inner coil pair I_1 to the current in the outer coil pair I_2 is $I_1/I_2 = 0.423514$ [16].

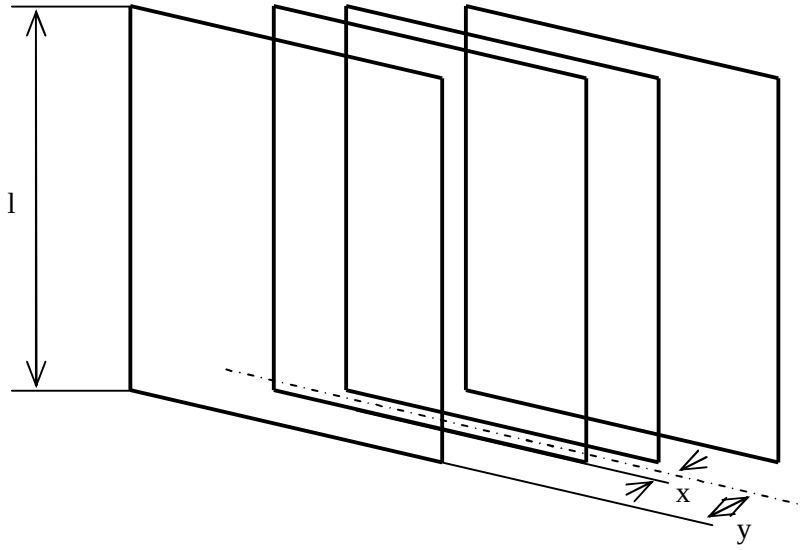

Fig. 6 Merritt 4-coil system.

1.1.6 Other coil systems

The Braunbek and Merritt coil systems are the most widely used multi-coil systems. However, they are not the only systems. There are some other multi-coil systems that can be used when a larger area of homogeneity is needed. For example, there is the Rubens coil system of 5 square coils [17], the Lee-Withing system of 4 circular coils [18] and the Alldred-Scollar system of 4 square coils [19]. A comparison between these multi-coil systems and Helmholtz coils can be found in [20]. A decription of a new axial system of 8 circular coils for calibrating sensors for measuring weak magnetic fields is described in [21]. The most widely-used coil systems are circular or square in shape, while a hexagonal coil system is discussed in [22]. This type of coil system gives more than 99% uniformity over half of the space occupied by the coil system.

1.2 Solenoid-type systems

1.2.1 Solenoid

A solenoid is a long, thin single-layer conductor that is homogeneously wound as a cylindrical helix on a non-magnetic frame. A solenoid can be characterized by the number of turns N of the conductor and the length of the solenoid l. The magnetic field inside an ideal solenoid (of infinite length) can be expressed as

$$B = \frac{\mu_0 IN}{l}, \tag{5}$$

where I is the current through the solenoid and $\boldsymbol{\varepsilon}_0$ is the permeability of the vacuum. An equation can be obtained for determining the magnetic field value of a long thin solenoid (of

finite length) in the longitudinal z-axis of the solenoid (Fig. 7), applying the Biot-Savart law [23]

$$B_z = \mu_0 \frac{NI}{2l}\left[\frac{0.5l+z}{\sqrt{R^2+(0.5l+z)^2}}+\frac{0.5l-z}{\sqrt{R^2+(0.5l-z)^2}}\right], \tag{6}$$

where N is the count of the winding turns, I is the current through the solenoid (A), R is the radius of the winding (m), l is the total winding length (m), and z is the distance from the center of the solenoid on the axis of the solenoid (m). This equation is valid if the solenoid winding is wound homogeneously along the whole length and is not interrupted. An axial magnetic field can be generated by the solenoid.

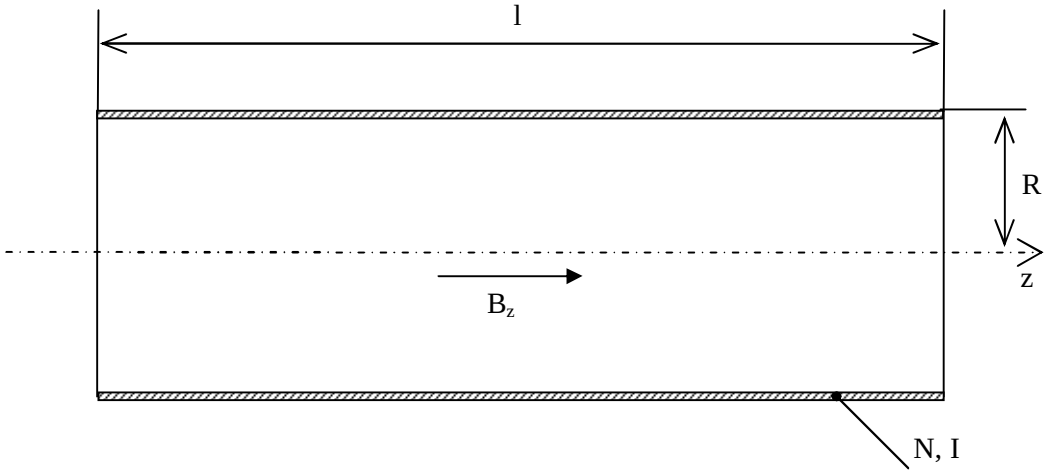

Fig. 7 Cross-sectional view of the solenoid.

1.2.2 Helmholtz-type solenoid

Two approaches can be used in the analytical design of a Helmholtz-type solenoid. The first approach is based on the Biot-Savart law, from which equation (6) can be obtained for determining the MFD of a long thin solenoid in the longitunidal z axis of the solenoid. It is necessary to subtract one solenoid from another in order to calculate the MFD - the internal solenoid with number of turns N_2 and length l_2, which represents the empty turns, has to be subtracted from the external solenoid with number of turns N_1 and length l_1 of the winding, including the empty turns between the two Helmholtz-type solenoid windings (Fig. 8). The equation for MFD inside the Helmholtz-type solenoid is then

$$B_z = B_{z1} - B_{z2} \tag{7}$$

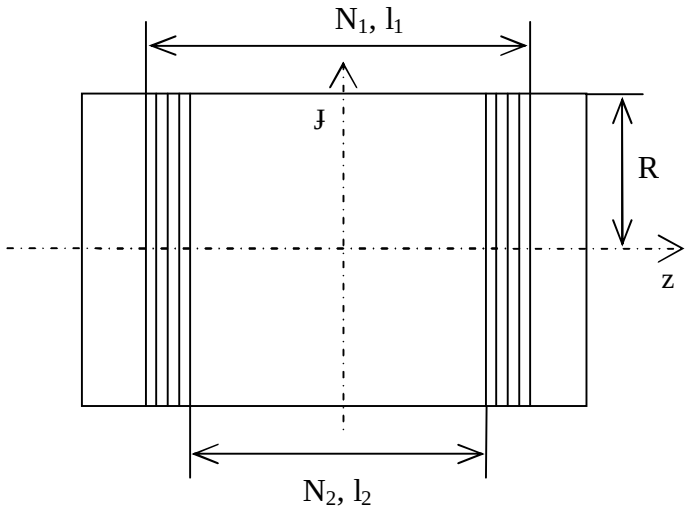

Fig. 8 Helmholtz-type solenoid

After substituting into (7), we obtain the equation for calculating the MFD inside the Helmholtz-type solenoid as

$$B_z = \mu_0 \frac{N_1 I}{2l_1}\left[\frac{0.5l_1 + z}{\sqrt{R^2 + (0.5l_1 + z)^2}} + \frac{0.5l_1 - z}{\sqrt{R^2 + (0.5l_1 - z)^2}}\right] - \\ - \mu_0 \frac{N_2 I}{2l_2}\left[\frac{0.5l_2 + z}{\sqrt{R^2 + (0.5l_2 + z)^2}} + \frac{0.5l_2 - z}{\sqrt{R^2 + (0.5l_2 - z)^2}}\right] \quad (8)$$

Equation (8) will be simplified for calculating the MFD in the center of the solenoid (z =0) as

$$B_z = \mu_0 \frac{(N_1 - N_2)I}{l_1 - l_2}\left[\frac{0.5l_1\sqrt{R^2 + (0.5l_2)^2} - 0.5l_2\sqrt{R^2 + (0.5l_1)^2}}{\sqrt{\left(R^2 + (0.5l_1)^2\right)\left(R^2 + (0.5l_2)^2\right)}}\right]. \quad (9)$$

A second option is the calculation published, for example, in [24], which also offers the possibility of calculating the MFD in the ***J*** axis perpendicular to the z axis of the solenoid. The vector of magnetic field ***B*** inside the single-layer solenoid can be described by the equations

$$B_z = \mu_0 I \alpha k_{\text{û}}\left(1 + k_2\frac{u_2}{R^2} + k_4\frac{u_4}{R^4} + k_6\frac{u_6}{R^6} + k_8\frac{u_8}{R^8} + \ldots\right), \quad (10)$$

$$B_\rho = \mu_0 I \alpha k_{\text{û}}\left(-k_2\frac{v_2}{R^2} - k_4\frac{v_4}{R^4} - \ldots\right), \quad (11)$$

where I (A) is the current through the solenoid, Ŭis the number of turns to one meter, R (mm) is the radius of the winding, $k_{\text{û}}$, k_2, k_4 and k_6 are values dependent on the geometry of the solenoid (some of them, and a recurrent formula for calculating others, can be found in [24]), and u_2, u_4, v_2 and v_4 are functions of the coordinates derived from the Legendre polynomials. In addition, all odd constants k_1, k_3,é are equal to zero due to symmetry. Generally, after substituting for u_2, u_4, u_6, v_2, v_4 into equations (10) and (11), we obtain

$$B_z = \mu_0 I \alpha k_\sigma \left(\begin{array}{l} 1 + k_2 \dfrac{2z^2 - \rho^2}{2R^2} + k_4 \dfrac{8z^4 - 24z^2\rho^2 + 3x\rho^4}{8R^4} + \\ + k_6 \dfrac{16z^6 - 120z^4\rho^2 + 90z^2\rho^4 - 5\rho^6}{16R^6} + \\ + k_8 \dfrac{28z^8 - 1792z^6\rho^2 + 3360z^4\rho^4 - 970z^2\rho^6 + 35\rho^8}{128R^8} + \ldots \end{array} \right), \quad (12)$$

$$B_\rho = \mu_0 I \alpha k_{\check{u}} \left[- k_2 \frac{z\rho}{R^2} - k_4 \frac{z\rho\left(4z^2 - 3\rho^2\right)}{2R^4} - \ldots \right], \quad (13)$$

where z (mm) and ρ (mm) are cylindrical coordinates with their origin in the center of the solenoid, and z is the coordinate in the direction of the longitudinal axis of the solenoid. Values k_2, k_4, k_6 from (12) and (13) can be calculated and, by solving the non-linear equations, dimensions can be found such that the solenoid can be designed with $k_2 = 0$ (a solenoid with homogeneity of the 4th order ï a Helmholtz-type solenoid). Alternatively, a solution can be found where $k_2 = k_4 = 0$ (a Garrett solenoid) or $k_2 = k_4 = k_6 = 0$ (a Barker solenoid).

1.2.3 Garrett solenoid

A modification of the solenoid described in 1.2.1 is the Garrett solenoid [25] (Fig. 9). This type of single-layer solenoid has better homogeneity than the more common Helmholtz solenoid. This solenoid has 3 sections of windings of the same diameter connected in series: the middle section with length 2l with current density $\check{U}$ and side sections with length l_k-l with a current density per length unit $\check{U}_k > \check{U}$. Different current densities can be achived by different pitch values of the winding. However, this is not easy to realize in practice. Different current densities can also be realized by having additional sections of turns placed on the two ends of

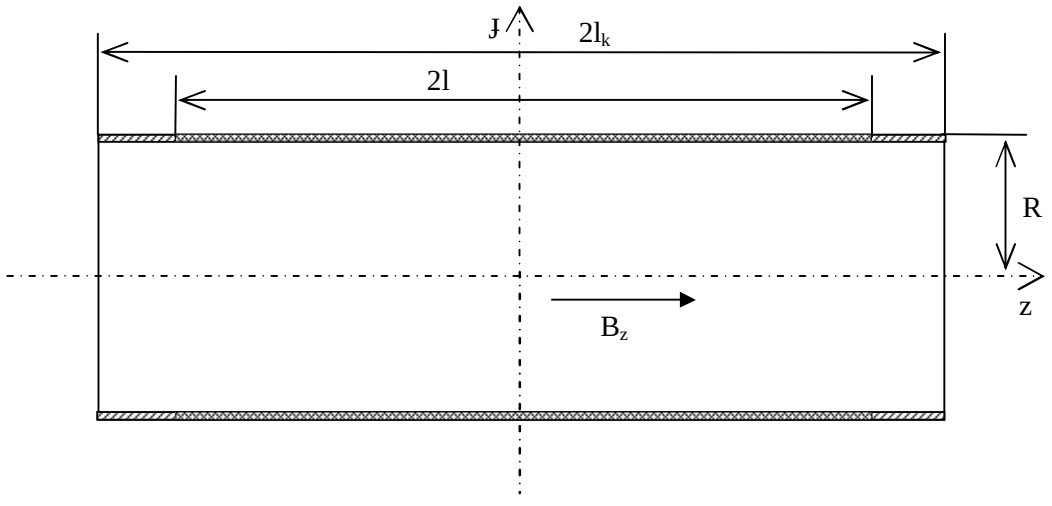

Fig. 9 Cross-sectional view of the Garrett solenoid.

the solenoid. For a certain ratio of $\check{U}_k/\check{U}$ it is possible to find l/R and l_k/R values such a Garrett solenoid can be realized with homogenity of the 6th order. Tabulated values for different ratios can be found in [26].

1.2.4 Barker solenoid

The Barker solenoid consists of 4 symmetrically arranged sections of the same radius (Fig. 10). The internal sections are l_2-l_1 in length, and the external sections are l_4-l_3 in length. The gap in the middle of the solenoid is $2l_1$ in length. The gap between the external and internal sections is l_3-l_2 in length [27]. For a certain ratio of l_1/R, it is possible find l_2/R, l_3/R and l_4/R values such that a Barker solenoid can be realized with homogeneity of the 8th order.

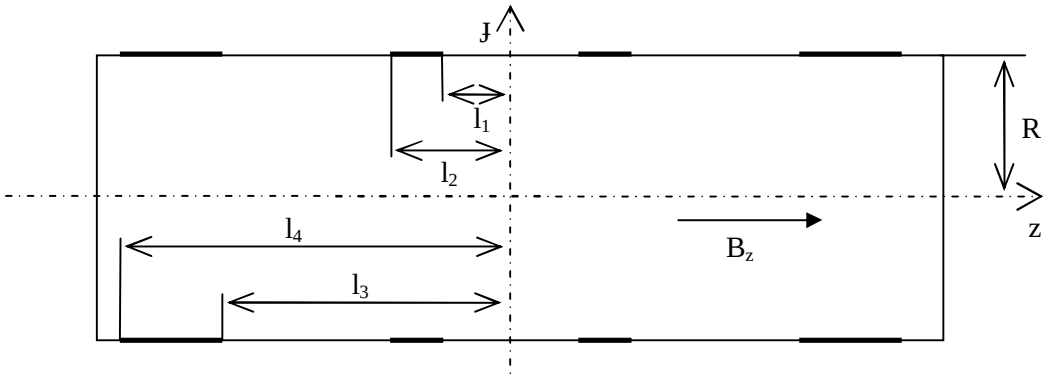

Fig. 10 Barker solenoid.

The difficulty lies in finding ratios of l_1/R, l_2/R, l_3/R and l_4/R that will suit the integer number of turns of individual sections of the winding. The current value and the pitch value of the winding are the same in all sections of the Barker solenoid. A comparison of the homogeneity between Helmholtz coils and the Barker solenoid is presented in [28]. Values for some of the different section ratios can be found in [24].

1.2.5 Massive solenoids

The vector of magnetic field ***B*** inside a multi-layer solenoid can be described by components B_z and $B_ϳ$ as

$$B_z = \mu_0 \lambda \frac{I}{S_d} R_{in} k_j \left(1 + k_2 \frac{u_2}{R_{in}^2} + k_4 \frac{u_4}{R_{in}^4} + \ldots \right), \tag{14}$$

$$B_ϳ = \mu_0 \lambda \frac{I}{S_d} R_{in} k_j \left(-k_2 \frac{v_2}{R_{in}^2} - k_4 \frac{v_4}{R_{in}^4} - \ldots \right), \tag{15}$$

where ε_0 (H/m) is a constant of magnetic vacuum permeability, I (A) is the current through the solenoid, S_d (mm^2) is the cross section of the wire that is used, ∂ is the filling factor, R_{in} (mm) is the inner radius of the winding, k_j, k_2 and k_4 are values dependent on the geometry of the solenoid (some of them can be found in [24]), and u_2, u_4, v_2 and v_4 are functions of coordinates derived from the Legendre polynomials. All odd constants k_1, k_3, é are equal to zero as a result of symmetry. After editing and substituting for u_2, u_4, v_2, v_4 into equations (14) and (15), we get

$$B_z = \mu_0 \lambda \frac{I}{S_d} R_{in} k_j \left(1 + k_2 \frac{2z^2 - \rho^2}{2R_{in}^2} + k_4 \frac{8z^4 - 24z^2\rho^2 + 3\rho^4}{8R_{in}^4} + \ldots \right), \tag{16}$$

$$B_{\jmath} = \mu_0 \lambda \frac{I}{S_d} R_{in} k_{\jmath} \left[-k_2 \frac{z\rho}{R_{in}^2} - k_4 \frac{z\rho\left(4z^2 - 3\rho^2\right)}{2R_{in}^4} - \ldots \right], \tag{17}$$

where z (mm) and $\jmath$ (mm) are cylindrical coordinates with their origin in the center of the solenoid and z is the coordinate in the direction of the longitudinal axis of the solenoid. We can approximately determine the magnetic flux density value and the homogeneity inside the solenoid by substituting for coordinates z and $\jmath$ into (16) and (17). The solenoid can be

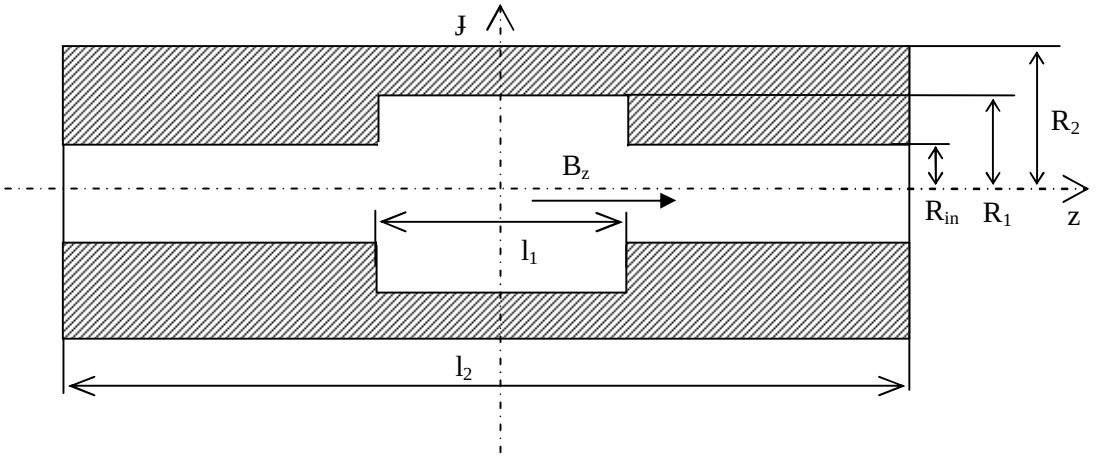

Fig. 11 Cross-sectional view of the Montgomery solenoid.

designed, for example, with $k_2 = 0$ (a Helmholtz-type massive solenoid), for better homogeneity.

A Montgomery solenoid is one of the massive (multi-layer) solenoid types. It can be used for generating a higher value of the magnetic flux density (up to 100 mT) in the center of the solenoid. The magnetic flux density can be calculated using the superposition of two concentric massive coils (the smaller coil with inner radius R_{in}, outer radius R_1 and length l_1; the larger coil with inner radius R_{in}, outer radius R_2 and length l_2) with rectangular cross-sections with identical current densities in the winding, but with opposite directions of the currents, while the winding of the smaller coil is contained in the space of the larger coil [29]. This solenoid can be designed with $k_2 = k_4 = 0$ for better homogeneity.

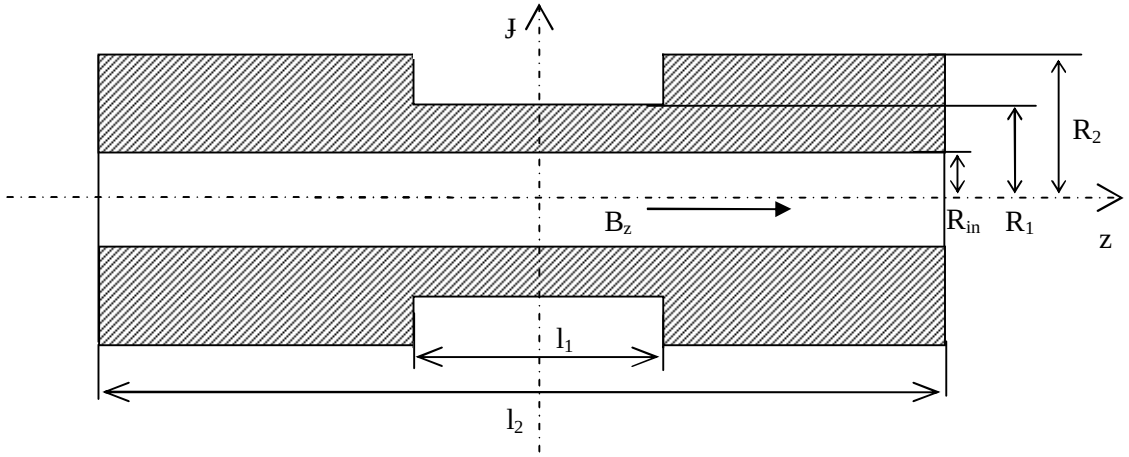

Fig. 12 Cross-sectional view of the Girard-Sauzade solenoid.

In the realization of this type of massive coil, the shape of the frame is omitted by the winding in the space of the smaller coil, symmetrically in the middle of the length at the inner edge of the winding area. The remaining space, according to the shape of the frame, is homogeneously filled with the winding (Fig. 11). Tabulated values for different ratios can be found in [30] or [24]. Another type of massive solenoid is the Girard-Sauzade solenoid [31]. This type of massive solenoid can also be calculated using the superposition of two concentric massive coils, like the Montgomery solenoid ï the smaller coil with inner radius R_1, outer radius R_2 and length l_1; the larger coil with inner radius R_{in}, outer radius R_2 and length l_2 (Fig. 12). This solenoid can be also designed with $k_2 = k_4 = 0$ for better homogeneity. Tabulated values can be found in [31], [24].

These massive solenoids are very useful for generating homogeneous, high DC magnetic flux density. However, they are generally not suitable for generating AC magnetic flux density, due to the high impedance value.

1.3 Sources of high magnetic fields

A magnetic flux density value B in the range of εT up to several tens of mT can be generated by the coil standards described in Chapters 1.1 and 1.2. An electromagnet had to be used when a higher magnetic flux density value needed to be generated. The typical C-shape of the electromagnet yoke is presented in Fig. 13. The homogeneity of the magnetic flux density B inside the air gap depends especially on the parallelism of the pole caps, on the shape of the yoke, and on the homogeneity of the yoke material that is used. The maximum AC-generated B value depends especially on the material of the yoke (on its total losses and on its maximal saturation value) on the length of the air gap, on the impedance of the winding, and on the power source that is used. The design of the AC electromagnet is described in Chapter 5.

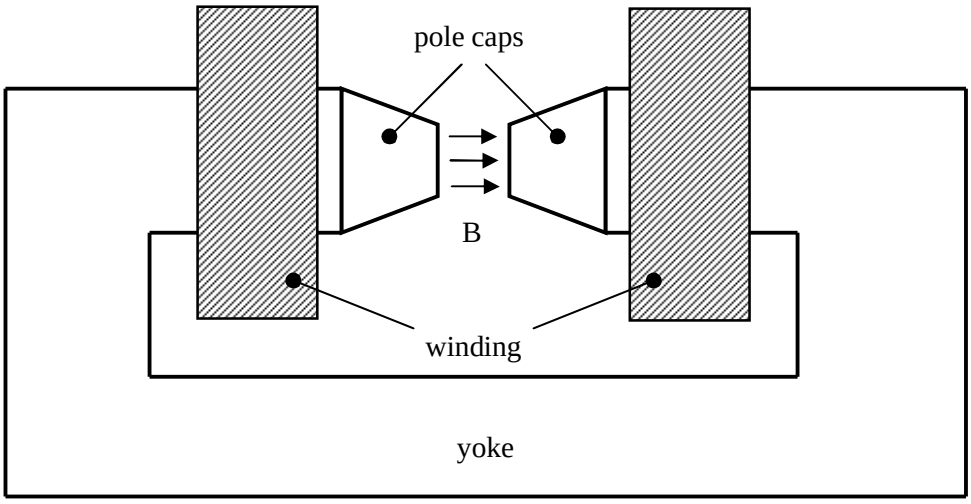

Fig. 13 A C-shaped electromagnet.

Other ways to generate a high *B* value (from a few T up to several tens of T) can be with the use of a Bitter electromagnet (also referred to as a Bitter solenoid or as a resistive electromagnet) or with the use of a superconducting solenoid. A Bitter solenoid is constructed of circular metal plates made from conducting material (Bitter plates) with insulator plates in between stacked in a helical configuration. The Bitter solenoid requires a high drive current value (several tens of kA). This current flowing through the plates generates enormous mechanical pressure produced by the Lorentz force, and dissipates large quantities of heat (Fig. 14). The solenoid is cooled by water circulating through the holes in the plates [32], [33]. A Bitter electromagnet can generate an axial magnetic field. However, if the plane of each turn of the conducting coil is rotated with respect to the central axis, a transverse magnetic field can be generated [34]. It can be tricky to use a Bitter electromagnet in an AC application, due to the eddy currents generated by the AC current passing through the metal plates.

A superconducting solenoid is wound by a superconducting wire (e.g. niobium-titanium). The winding of a superconducting solenoid must be cooled down to cryogenic temperatures during operation. The winding has no electrical resistance in its superconducting state, and can therefore conduct much higher currents than an ordinary wire. A superconducting solenoid can generate higher magnetic fields than a non-superconducting electromagnet. A disadvantage of commercial superconducting solenoids (5 T and more) is the high inductance value (several H), which means a very high impedance value for AC applications. Superconducting solenoids can be made as a room-temperature (cryogen-free) bore solenoid system with radial or axial access, or with multi-axis access (see Fig. 15).

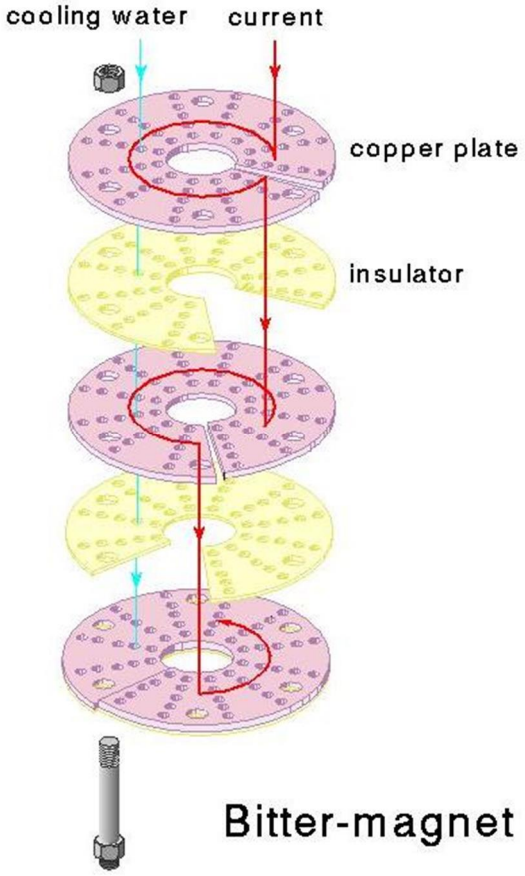

Fig. 14 Schematic principle of the Bitter electromagnet [from the website of The High Field Magnet Laboratory (HFML) of Radboud University, Netherlands].

Fig. 15 Standard split pair magnets provide both axial and transverse field access [from the website of Cryomagnetics, Inc., USA].

2 State of the Art

2.1 AC coil standards

Generating a stable, homogeneous reference AC magnetic field is important not only for traceable calibrations of AC magnetic field analyzers with a 3-axis coil probe (e.g., EFA 300, C.A. 42), but also for many types of biomedical applications, and for EMC testing.

Solenoids are widely used for generating the AC magnetic field in biomedical experiments. Some studies have described the use of a single-layer solenoid (water cooled) for magnetic hyperthermia applications at a frequency of 300 kHz with variable magnetic flux density up to 11 mT [35], in the frequency range from 10 kHz up to 1 MHz with magnetic field amplitudes up to 5 mT [36], or at a frequency of 500 kHz with a peak magnetic field value of 11 mT [37]. A water-cooled double solenoid exposure system for in-vitro studies is presented in [38]. A magnetic flux density of about 125 mT (peak-to-peak) at a frequency of 150 kHz can be generated for biomedical applications. A solenoid for exposure of radish seeds with a magnetic field of 6 mT at 50 Hz can be found in [39]. A description of a different type of solenoid for AC magnetic flux density generation ï a multi-layered laminated eddy-current type of solenoid ï can be found in [40]. The laminated plate coil type and the whirled coil type are presented. The laminated plate coil type is suitable for use in low voltage and a high current. The whirled coil type is suitable for use in high voltage and with a small current. Both types can be used in the frequency range up to several kHz.

Helmholtz coils, as a magnetic flux density standard in various sizes and designs, are widely used in sensor calibration for generating a reference AC magnetic field in a wide frequency range ï up to 25 εT at 100 kHz [41], up to 0.1 mT at 120 kHz [42], or up to 0.4 εT at 200 kHz [43] - or for a single frequency value ï up to 0.4 mT at 60 Hz [44], up to 9 εT at 50/60 Hz [45], up to 200 εT at 60 Hz [46]. The design of the MFD standard should meet the requirements for the amplitude value and the frequency range of the generated magnetic field for occupational and general public exposure levels [47], and also for homogeneity in the volume of the probe size [48]. Helmholtz coils can also be used in biomedical research [49]-[54] and in EMC testing [55]-[56]. Square Helmholtz coils with a side length of 1 m, with the constant about 1.1 εT/A, with a zig zag winding structure and with a usable frequency range up to 50 kHz are discussed in [57].

Multi-coil systems are used when a larger area of homogeneous magnetic field is needed for a research application. Examples of the use of Merritt coils in biomedical applications can be found for generating a magnetic flux density of about 80 εT [58] or 10 mT [59] at 50 Hz, for generating 3.4 mT [60] or 0.2 mT [61] at 20 kHz, or for generating 2 mT at 60 Hz [62]. Rubens coils for generating magnetic flux density up to 1.7 mT up to 60 Hz [63] and the Braunbek coil system for generating pulsed magnetic flux density of 4 εT at 5 Hz [64] have also been presented.

2.1.1 Multi-layer AC coil standards at CMI

Two massive multi-layer Helmholtz solenoids with a textit frame, for sensor calibrations, are used at CMI in the low frequency range. A cross-sectional view is presented in Fig. 16. The parameters and the dimensions of these two coil standards are listed in Table 1. The design of these coil standards was calculated according formulas (16) and (17). Both coil standards were wound with enameled copper wire 2 mm in diameter. The value of the coil standards constant was determined by the nuclear magnetic resonance (NMR) method with flowing water as (8.1424 ± 0.0033) mT/A (No. 051) and (1.94428 ± 0.00097) mT/A

(No. 052). Coil standard No. 51 was fabricated for Hall probe calibration at a frequency of 50 Hz. A B_{RMS} value of 20 mT at 50 Hz can be generated by means of coil standard No. 051. A resistance value of 2.8 q , an inductance value of 93 mH and a resonance frequency value of 52 kHz was determined. Coil standard No. 052 was manufactured for calibrating magnetic field analyzers with a 3-axis coil probe (e.g. EFA 300, ELT 400). This solenoid can generate a maximum magnetic flux density value of 7 mT at 50 Hz for a relatively short period of time (about 2 minutes), and can be used up to 2-3 kHz. A resistance value of 2.6 q , an inductance value of 69 mH and a resonance frequency value of 28 kHz was also determined. The homogeneity values were measured experimentally using special search coil EP 601 with a suppressed octupole (see Chapter 2.1.3), and the results for the theoretical and measured homogeneity values are presented in Fig. 18 and Fig. 19. The search coil was moved from the center on the *z* and *J* axis, and the true homogeneity value was calculated from the change in the measured output voltage.

Table 1. Dimensions and parameters of coil standard No. 051 and No. 052.

Coil standard	**D_i (mm)**	**D_e (mm)**	**L (mm)**	**M (mm)**	**number of turns in 1 layer**	**number of layers**	**nominal DC constant value (mT/A)**
No. 051	76	184.8	50.1	18	25	27	8.2
No. 052	238	286	53.4	82.8	26	12	1.9

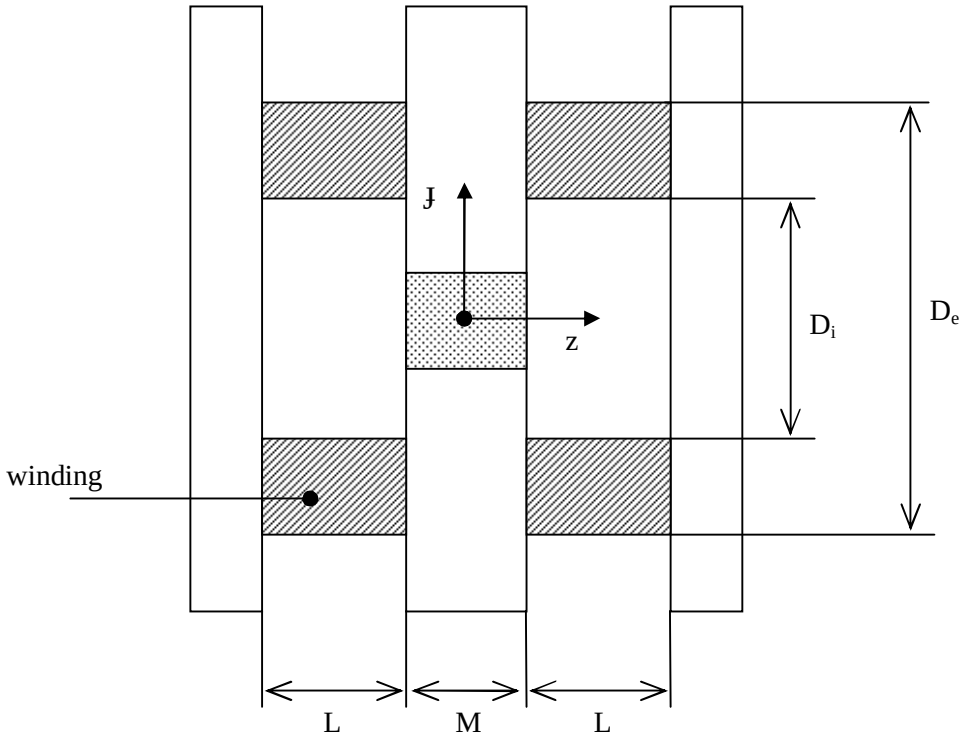

Fig. 16 Cross-sectional view of the massive Helmholtz-type solenoid.

Fig. 17 Helmholtz-type solenoid standard No. 051.

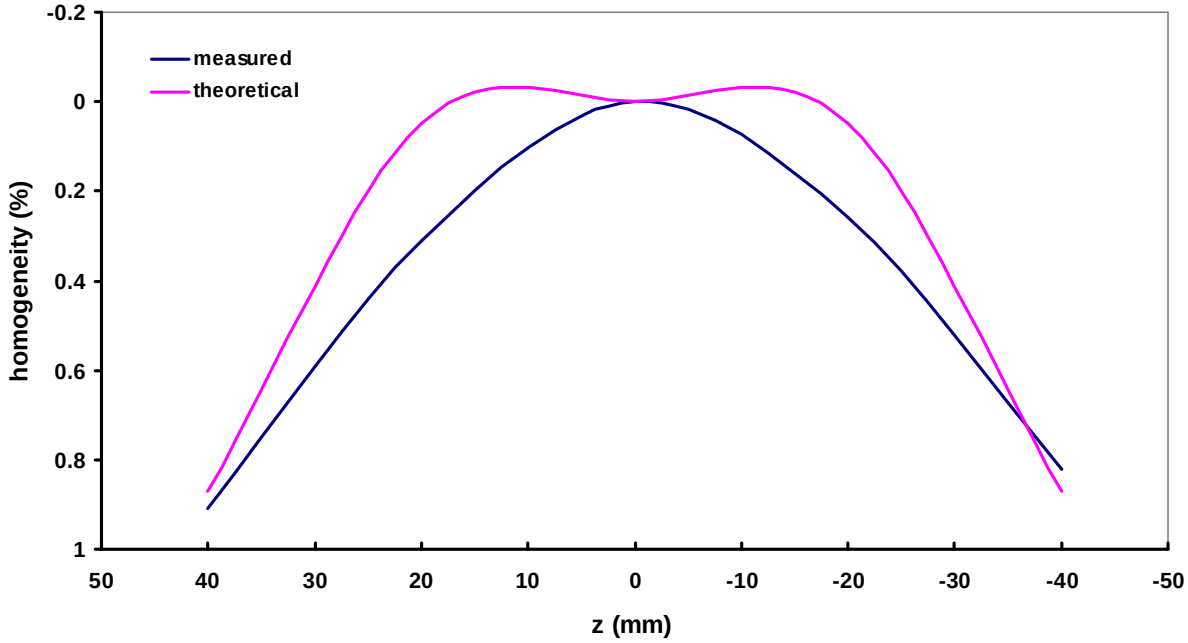

Fig. 18 Theoretical and measured values of the homogeneity of solenoid No. 052 on the *z*-axis.

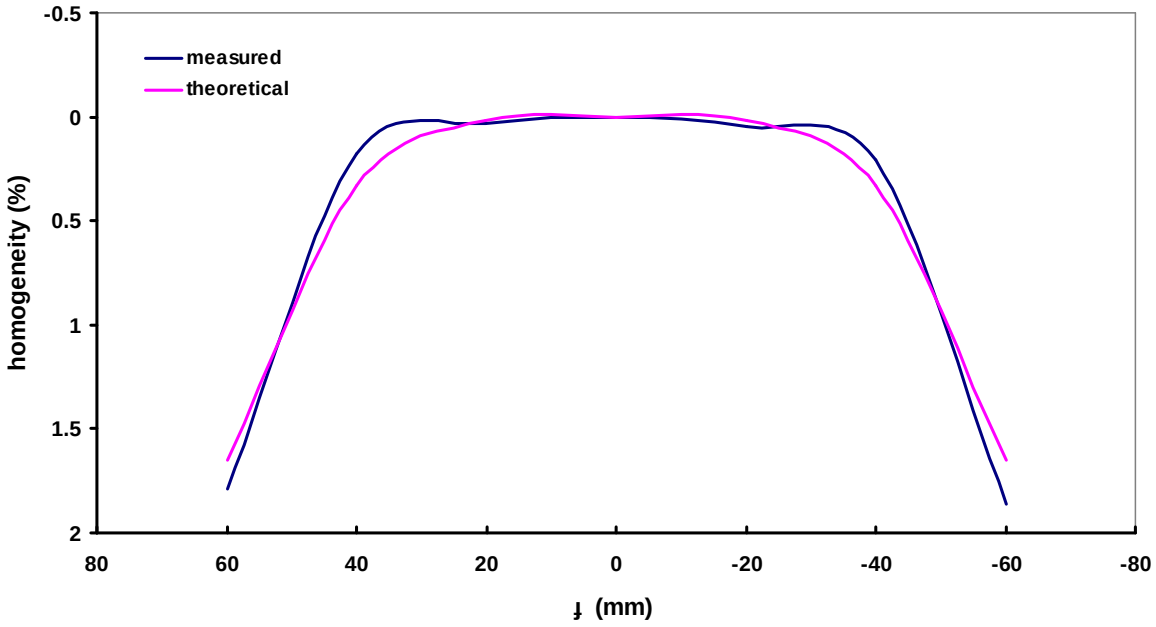

Fig. 19 Theoretical and measured values of the homogeneity of solenoid No. 052 on the z-axis.

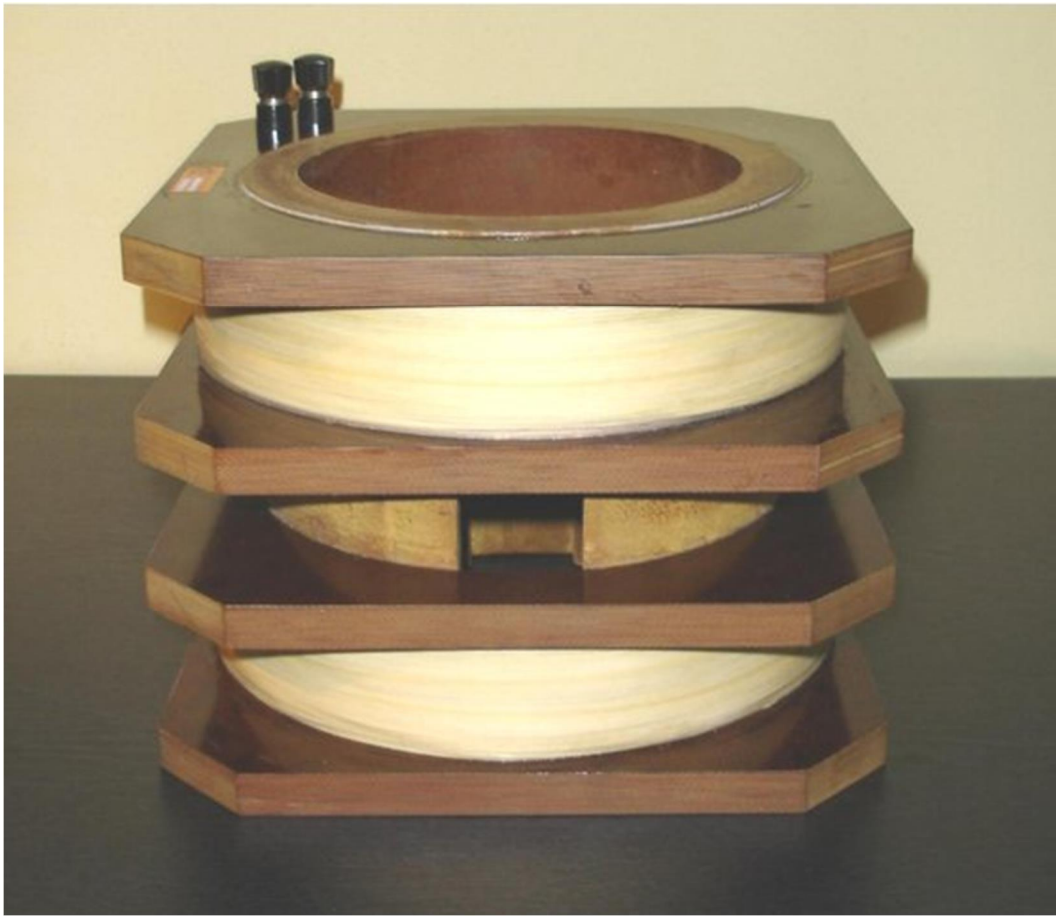

Fig. 20 Helmholtz-type solenoid standard No. 052.

2.1.2 Thin AC solenoid standards at CMI

Two thin solenoid standards are used at CMI: a Garrett solenoid with a textite frame and with a constant with a nominal value of 0.46 mT/A (Fig. 21), and a Barker solenoid with 4 sections of winding on a quartz frame (Fig. 22), with a nominal value of 0.6 mT/A. The value of DC constant of the coil standards was determined by the NMR method with flowing water as (0.4627 ± 0.0033) mT/A (No. 8003) and (0.64428 ± 0.00097) mT/A (No. 8701). Garrett solenoid No. 8003 was wound with enameled copper wire 2.8 mm in diameter. This solenoid has an inner diameter of 190 mm, length of 440 mm, resonance frequency 84.5 kHz, and it can be used for B_{RMS} generation up to 4 kHz. Two identical Barker solenoids were realized, and one of them is a part of the national standard for DC magnetic flux density [65]. The Barker solenoid with inner diameter of 162 mm, length of 228 mm and resonance frequency of 280 kHz can be used for B_{RMS} generation up to 20 kHz. It was wound with pure copper wire 0.8 mm in diameter. The homogeneity of the two solenoids is presented in Fig. 23 and Fig. 24.

Fig. 21 Garrett solenoid standard No. 8003.

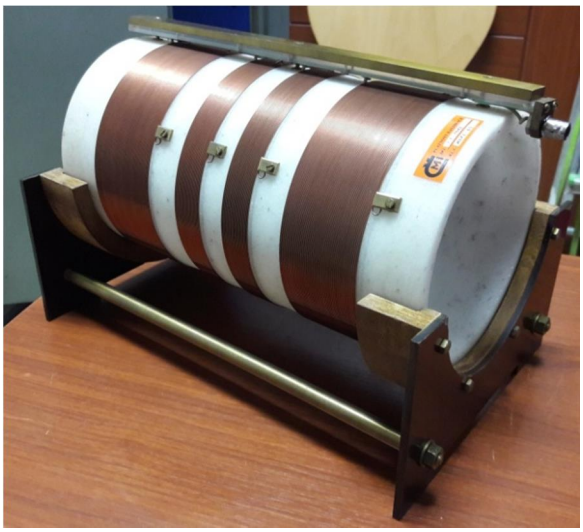

Fig. 22 Barker solenoid standard No. 8701.

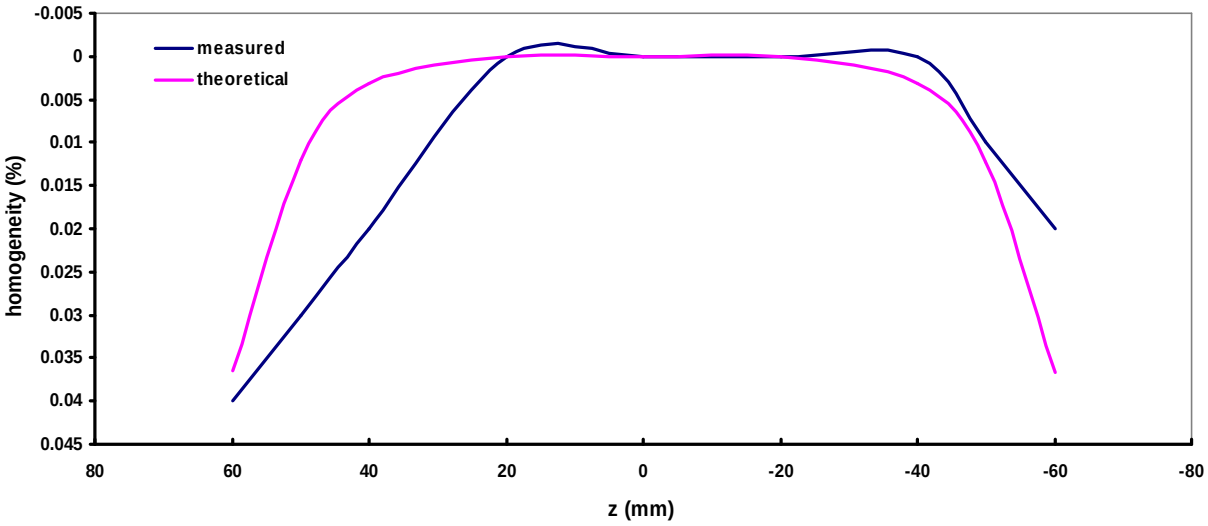

Fig. 23 Theoretical and measured values of the homogeneity of Garrett solenoid No. 8003 on the *z*-axis.

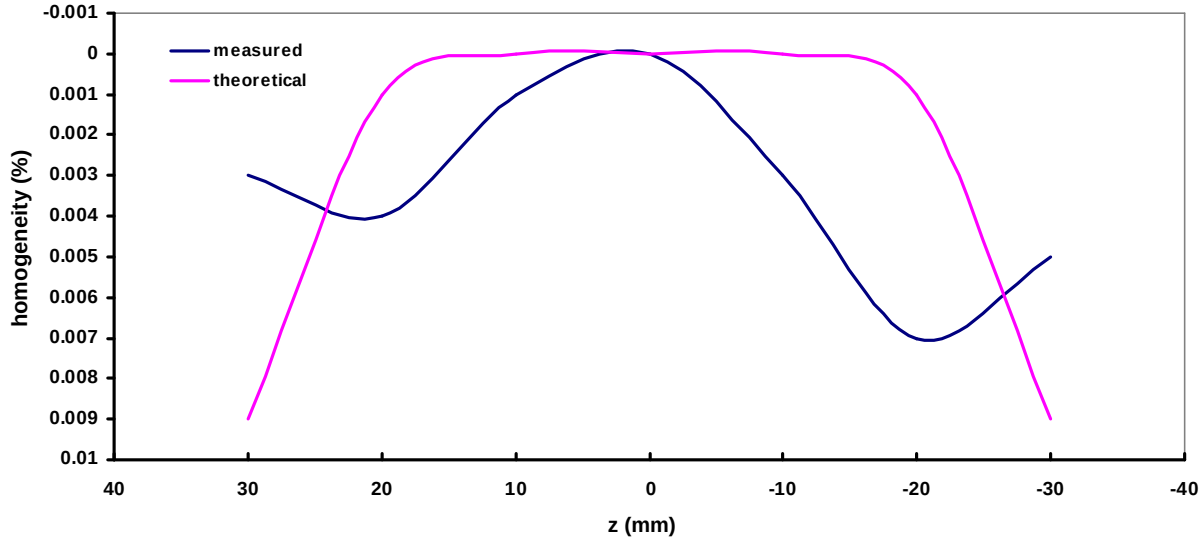

Fig. 24 Theoretical and measured values of the homogeneity of Barker solenoid No. 8701 on the *z*-axis.

The differences between the theoretical homogeneity and the measured homogeneity of the Garrett solenoid were probably caused by small differences in the winding of the turns. The differences between the theoretical homogeneity and the measured homogeneity of the Barker solenoid was caused by an adjustment to the winding ï one turn from each side was removed.

2.1.3 Search coils at CMI

Search coils are commonly used to make precise measurements of the AC or pulsed magnetic flux density. Search coils can also be used in calibrating the AC constant of coil standards. The theoretical background of the search coil design can be found in [24], [66]. If the search coil has only a dipole character (other multipoles are perfectly suppressed), the search coil measures the magnetic field at the center point. The system of axially symmetric

conductive loops with area turns *NA* passed by current *I* can be described by the magnetic moment $\boldsymbol{m} = I \cdot NA$, which is a vector quantity describing the magnetic dipole of the search coil. In the real case of a system of loops, an accurate description is a series of multipoles with multipole constants p_0, p_1, p_2, p_3,..., p_n. A multipole with constant p_0 equals zero, because of the absence of a magnetic monopole. A multipole with constant p_1 is an elementary magnetic dipole; p_1 is the area turns for a coil. A multipole with constant p_2 is a quadrupole that equals zero, and all even multipole constants are equal to zero, due to the symmetry of the system. The third multipole, with a constant of p_3, is an octupole, etc. The influence of the higher multipoles (their participation in the magnetic field generated by the coil) declines with distance. The influence can be significant in real distances (e.g. a 5 - 10 multiple of the dimensions of the coil). For this reason, we attempt to suppress the higher multipoles, especially p_3, when designing the search coil. The search coils used in the calibration method described above are designed as symmetrical cylindrical windings ï the constants of the even multipoles are zero. For a single-layer search coil, the constant of an octupole is zero, when we choose the ratio of the length of the coil to the diameter $\sqrt{3}/2$. This ratio can also be used for the multi-layer search coil, but the thickness of the windings must also be taken into account. Several different search coils types (single-layer and multi-layer) with a cylindrical frame and a suppressed octupole were fabricated at CMI (Fig. 25). Their parameters can be found in Table 2.

Fig. 25 Special search coils (from left): EP 02/95, K_{II}, EP 01/00 and EP 601.

Table 2. Dimensions and some of the parameters of the special search coils used at CMI.

Search coil	**Frame material**	**Coil inner diameter (mm)**	**Coil outer diameter (mm)**	**Coil length (mm)**	**Winding thickness (mm)**	**DC constant (m^2)**	**Usable frequency range (kHz)**
EP 02/95	PTFE	50	74	52.4	6	5.2325	0.050
K_{II}	textit	18	46	40	7	1.3312	up to 3
EP 01/00	PTFE	39.8	41	80	0.6	0.045394	2 - 100
EP 601	PTFE	16	24	18	2	0.14752	up to 1 kHz

2.2 AC electromagnets

There was no AC electromagnet for use in Hall probe calibration at CMI before the work presented in this dissertation began. There are commercial AC electromagnets with a C-frame configuration, produced by GMW company, that generate an AC MFD amplitude of up to 1 T at very low frequencies (below 10 Hz) through a 32 mm air gap with a square pole face of (32x32) mm [67], or that generate an amplitude of 70 mT up to 10 kHz through a 35 mm air gap with a pole face diameter of 46 mm [68]. The GMW 5403 electromagnet has been applied up to 4 mT for frequencies up to 50 Hz [69]. A small toroidal electromagnet with a ferrite core and with an air gap of 7.5 mm for generating amplitude up to 25 mT within a few minutes for frequencies of about several hundreds of kHz is described in [70], (Fig. 26a). This type of electromagnet can be used in biomedical applications. A different type of electromagnet is presented in [71]. Here, two pairs of coils 11 cm in length are wound on iron bars with enameled copper wire 0.41 mm in diameter. Amplitude up to 150 mT at 60 Hz can be generated between the iron bars by means of this electromagnet.

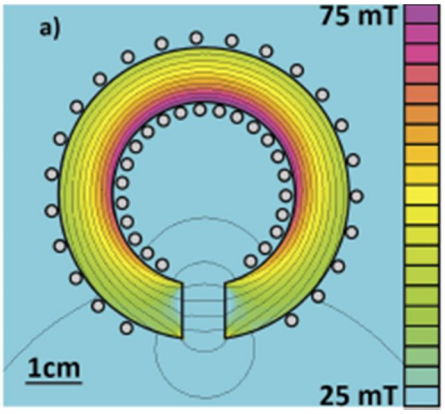

a)


b)

Fig. 26 a) an FE model of a gapped toroidal electromagnet with a ferrite core [70], and b) nested Helmholtz coils formed by Bitter disks (b) [72].

A very interesting AC application of a Bitter coil can be found in [72]. This paper describes the nested 2D Helmholtz coils design formed by Bitter disks (Fig. 26b). A strong rotating magnetic field up to 200 mT at frequencies of several kHz can be generated by means of this system without a need for cooling. The Bitter coil can also be used for generating a pulse magnetic field of about 1.5 T [73].

Superconducting electromagnets can be used for generating an AC magnetic field, but only at very low frequencies ï e.g. a magnetic field value of (0.14 to 1.73) T can be generated at a frequency of 0.05 Hz [74]. The development of a 2.5 T/100 kVA AC superconducting magnet is presented in [75]. It has an inner bore diameter of 30 mm and is 60 mm in length. The winding has 1050 turns in 14 layers, the inductance is 26 mH, and the coil constant is 16.6 mT/A. This magnet was wound by NbTi multifilamentary wires with artificial pins, and could generate a peak value of 2.5 T at 60 Hz with a current value of 140 A.

3 Thesis objectives

The main goal of this dissertation was to develop the new standards of AC magnetic flux density to be used for expanding the calibration possibilities of Hall probes up to 1 T in the low frequency range (up to 100 Hz) and the calibration possibilities of magnetometers up to 100 μT in the frequency range up to 100 kHz. These standards should have tracability to the national magnetic flux density standard, which is kept at the Department of Electromagnetic Quantities of CMI.

To achieve this main goal, it was necessary to:

- Design and realize a single-layer coil standard for generating AC magnetic flux density up to 100 kHz.
- Develop a setup with the single-layer coil standard for generating AC magnetic flux density up to 100 μT in the frequency range up to 100 kHz.
- Develop a method for calibrating the coil standard up to 100 kHz.
- Design and realize the AC electromagnet for generating the AC magnetic flux density up to 1 T in the low frequency range.
- Design and realize the special search coil for precise measurements of the AC magnetic flux density inside the air gap of the AC electromagnet.

In addition, there is a discussion about the use of AC magnetic flux density standards in metrology. An AC electromagnet made from amorphous material for expanding the frequency range of the AC magnetic flux density up to 1 kHz is also presented.

4 Setup for generating an AC magnetic flux density value up to 100 kHz

4.1 Single-layer Helmholtz-type solenoid

A single-layer Helmholtz-type solenoid was designed for generating an MFD value up to 100 kHz. The solenoid was designed analytically using formulas described in 1.2.2, and also by the FEM method, using FLUX 3D software, which is described in [J1]. A single-layer Helmholtz-type solenoid No. 1201 was produced (Fig. 27). The frame with an inner diameter of 285 mm was made from glass epoxy, with a refined groove and with a turn pitch of 1.8 mm. The turn pitch was chosen large enough to reduce the influence of the parasitic capacitance of the winding. The winding was wound with enameled copper wire 0.75 mm in diameter. The winding is terminated by the BNC connector. The solenoid was calibrated by direct comparison with the national MFD standard. The original calibrated solenoid DC constant of 0.105497 mT/A was determined with expanded uncertainty of 0.05% for k = 2. As stated in Table 3, the relative difference $\check{u}_{ORG}$ (the difference between the theoretical value in the center of the solenoid and the original calibrated value Calibration ORG) is in the range from 0.21% to 0.36%, depending on the method that is used. After several months, it was found that the coil winding had been wound with insufficient tension. It was therefore re-wound. A new calibration was made after this, and the relative difference $\check{u}_{AFT}$ (the difference between the theoretical value in the center of the solenoid and the new calibrated value Calibration AFT) is in the range from 0.04% to 0.19%. A real winding DC resistance value of 2.51 Ω and an inductance value of 600 εH was measured by the digital multimeter and by the LCR meter. The full, detailed characterization of the solenoid is presented in [J1].

Table 3 A comparison of the theoretical DC values of the magnetic flux density in the center of the solenoid with the calibrated original value (Calibration ORG) and the new calibrated value (Calibration AFT) after rewinding the winding.

	Calc. (9)	**Calc. (12)**	**FLUX 3D**	**Calibration ORG**	**Calibration AFT**
B (mT/A)	0.105724	0.105882	0.105808	0.105498	0.105683
$\check{u}_{ORG}$ (%)	0.21	0.36	0.30	0	-
$\check{u}_{AFT}$ (%)	0.04	0.19	0.12	-	0

The real homogeneity values were measured using special search coil No. EP 601 with a suppressed octupole at a frequency of 50 Hz. The results for the theoretical values calculated from (8), (12), (13) and by FEM (Fig. 28), and the measured homogeneity values, are presented in Fig. 29 and in Fig. 30, at a distance of ±40 mm. The search coil was moved from the center on the *z* and *y* axes, and the true homogeneity value was calculated from the change in the measured output voltage. The theoretical homogeneity values calculated from (8) and (12) were the same.

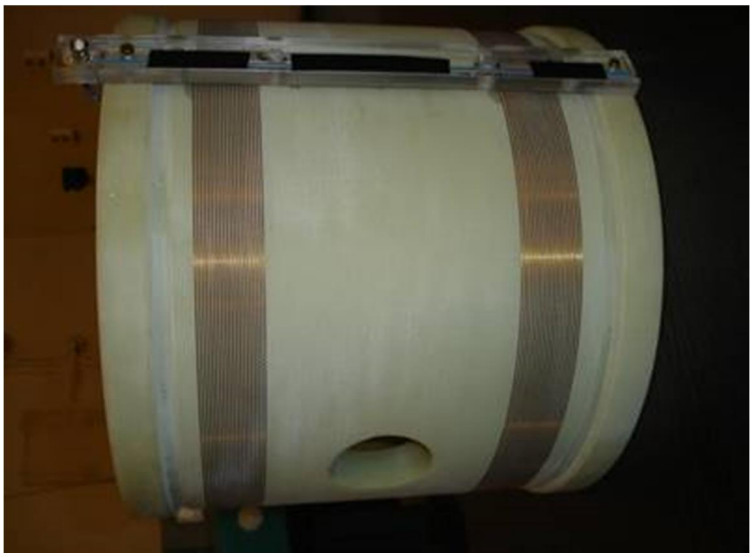

Fig. 27 Single-layer Helmholtz-type solenoid No. 1201.

a)

b)

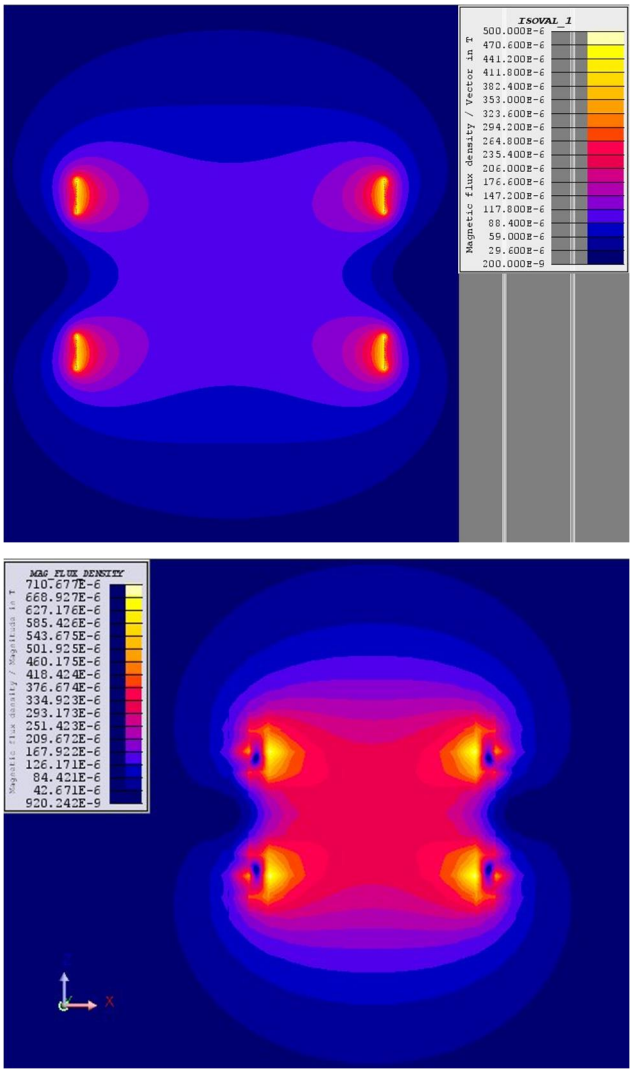

Fig. 28 MFD distribution in a solenoid model ï a) DC analysis, b) AC analysis ï 500 Hz.

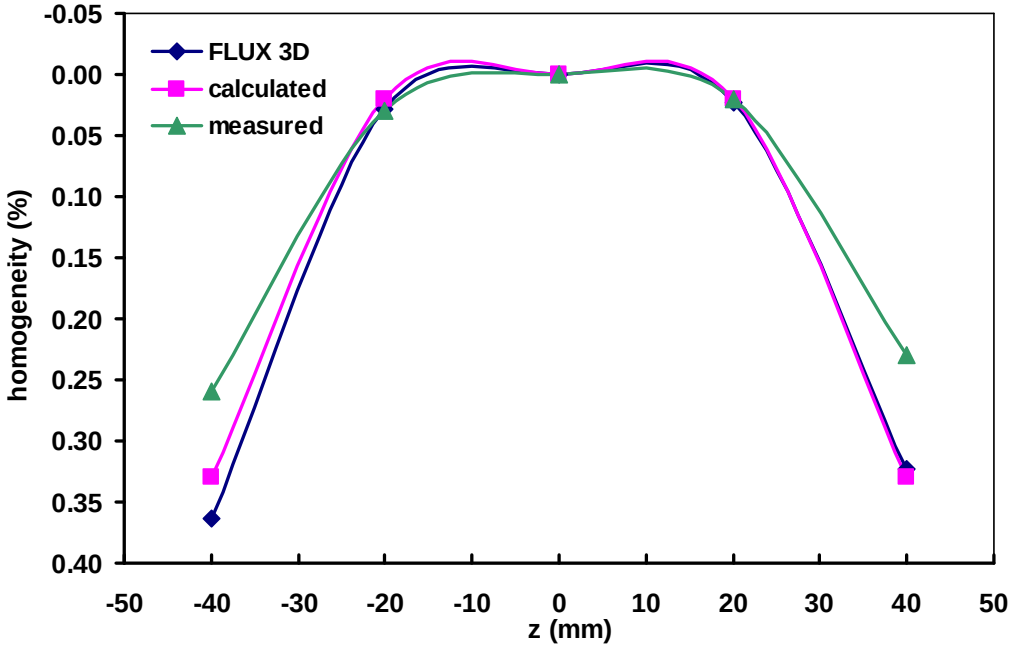

Fig. 29 Homogeneity inside the solenoid on the z-axis.

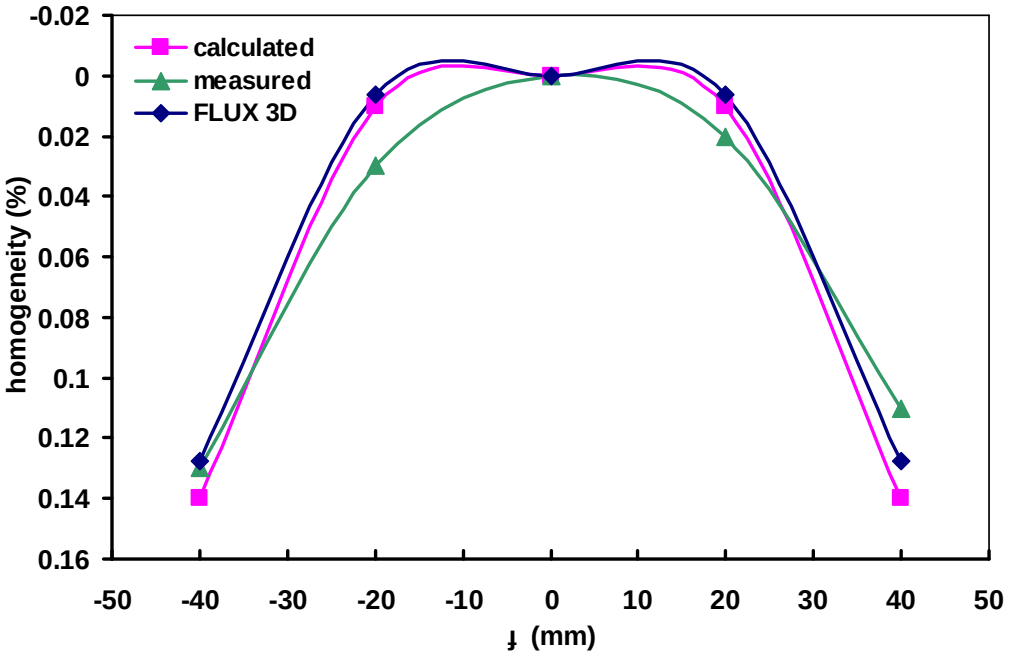

Fig. 30 Homogeneity inside the solenoid on the y-axis.

There are some methods that can be used to enable the frequency dependence of the MFD generated by the solenoid to be determined. This dependency is usually quadratic, and can be determined approximately from [76]

$$K_{\mathrm{bAC}} = K_{\mathrm{bDC}}\left(1+\frac{f^2}{f_r^2}\right), \tag{18}$$

where K_{bDC} is the solenoid constant with a DC current value of 1 A (mT), f is the frequency of the generated AC MFD (Hz), and f_r is the resonance frequency value (Hz). The change of K_{bAC} from K_{bDC} is 1% for $f/f_r = 0.1$, and 4% for $f/f_r = 0.2$. Formula (18) is then valid in its approach for small changes of K_{bAC} from K_{bDC}. A resonance frequency value of 535 kHz was measured using a digital oscilloscope. Alternatively, the frequency dependence of K_{bAC} can be measured directly by a special search coil with calibrated area turns. This method was also used for precise adjustment of AC MFD in the solenoid. The special search coil design was described in 2.1.3. The measurement method is described in detail in [66]. A special multi-layer search coil No. K_{II} with calibrated constant K_S = (1.3312 ± 0.0011) m^2 was used for measuring the adjustable magnetic field value inside a solenoid in the frequency range up to 3 kHz. A single-layer search coil No. EP 01/00 with calibrated constant K_S = (0.045394 ± 0.000036) m^2 was used for measuring the magnetic field value inside the solenoid in the frequency range from 3 kHz up to 100 kHz.

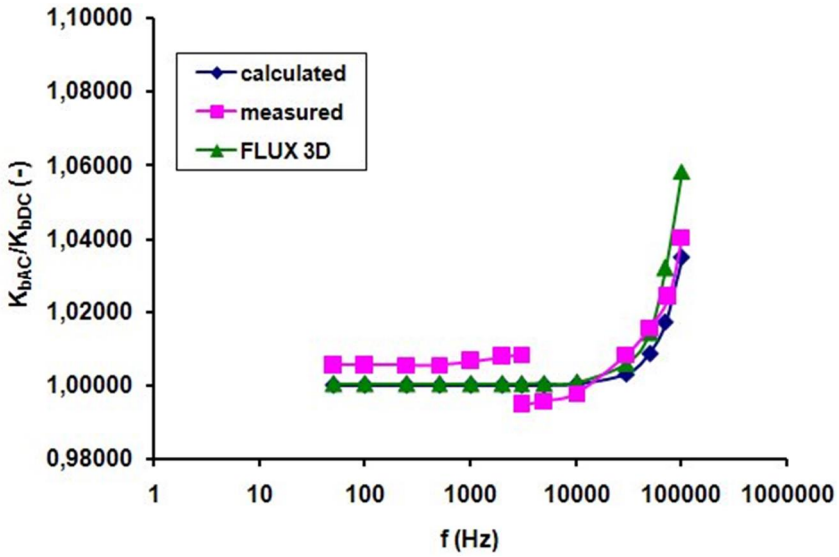

Fig. 31 Frequency dependence of the solenoid constant.

For a sinusoidal waveform, the adjusted amplitude value of MFD B_{m} (or effective MFD value B_{RMS}) inside the solenoid is then calculated from

$$B_{\mathrm{RMS}} = \frac{U_{\mathrm{RMS}}}{2\pi K_{\mathrm{S}} f} \tag{19}$$

$$B_{\mathrm{m}} = \frac{U_{\mathrm{AVG}}}{4K_{\mathrm{S}} f}, \tag{20}$$

where U_{RMS} is the RMS value of the output voltage of the search coil, which we measured using an Agilent 3458A digital multimeter, U_{AVG} is the arithmetic mean value of the output voltage of the search coil, which we measured using a Keithley 2001 digital multimeter, K_{S} is the value of the constant of the search coil, and f is the frequency, which we measured with an HP 53131A digital counter. The frequency dependence of the solenoid constant calculated from (18), calculated by FEM in FLUX 3D and measured by special search coils is shown in Fig. 31. The relative difference of the calculated values from the measured values is less than

0.6% in the frequency range up to 500 Hz, and is in the range from 0.25% up to 0.7% in the frequency range from 3 kHz up to 100 kHz. Only the constant value at 100 kHz calculated by FEM has a relative difference of about 2% from the measured value. The AC MFD amplitude value up to 140 εT up to 40 kHz and 40 εT at 100 kHz inside the solenoid can be measured/set in the frequency range of (3 to 100) kHz, using a power amplifier only.

4.2 Generating an AC magnetic flux density value up to 100 εT

Because the impedance of the solenoid described above is directly proportional to the frequency (e.g. 386 q at 100 kHz), an increasingly higher voltage is needed for higher frequencies. A straightforward solution is to use a high-voltage high-frequency amplifier [38]. However, these devices are not only expensive but also inefficient, because the energy stored in the magnetic field has to be dissipated in each cycle. A serial resonance effect can be exploited to minimize the required voltage range of the amplifier [77]. An 11-bit programmable capacitor array (PCA) was designed, which was then connected in series with the solenoid to create an LC tank circuit (Fig. 32). This enabled an AC amplitude MFD value of 150 μT to be created even at 150 kHz. A detailed description of PCA design can be found in [J2]. Because the output voltage of the EP 01/00 single-layer search coil is very small at lower frequencies ï due to the small area turns value ï tests were performed to extend the frequency range of multi-layer search coil K_{II}. For this purpose, a transimpedance amplifier (a current-to-voltage convertor) was constructed that enabled to measure the current from the search coil. The transimpedance amplifier had an input impedance of 0.11 Ω, which was low enough not to influence the measurement. Shorting the output of the coil reduces the effect of its parasitic capacitance and greatly expands the upper range of usable frequencies. At angular frequencies much larger than the ratio of coil series resistance to coil inductance, the output voltage is independent of frequency [78].

Fig. 32 Programmable capacitor array PC1101.

The measured/set value of B_m is then calculated from (21),

$$B_m = \frac{U_{SC} L_s}{R_Z K_S}, \tag{21}$$

where U_{SC} is the output RMS voltage of the transimpedance amplifier, L_S is the search coil inductance value, R_Z is the value of the transimpedance gain, and K_S is the value of the constant of the search coil. The design and the parameters of the transimpedance amplifier are described in [J2]. Using the transimpedance amplifier, the resonance frequency of the multi-layer search coil was measured, and was found to be 405 kHz. The equivalent parasitic capacitance value was then reduced to about 6 pF. This increase should allow the multi-layer search coil to be easily used up to 40 kHz. However, a search coil with a transimpedance amplifier has also a low corner frequency, below which the frequency reponse is not flat.

Generating an AC amplitude MFD value of 150 εT (or generating an AC RMS MFD value of 100 εT) was tested using the PCA and a multi-layer search coil with a transimpedance amplifier (see Fig. 33). Measurements were carried out with a sinusoidal waveform up to 150 kHz and for a current value of 1 A and 1.5 A through the solenoid (Fig. 34, 35). The uncertainty evaluation is described in [J2]. The AC amplitude MFD value inside the solenoid can be measured/set up to 150 εT up to 140 kHz or 230 εT up to 120 kHz with expanded uncertainty of (0.2 to 1.0)% for k = 2 for frequencies up to 150 kHz (Table 4).

Table 4 Relative expanded uncertainty (k = 2) of the AC amplitude MFD value measured/set in the center of the solenoid using formula (20).

Frequency (kHz)	**0.1**	**3**	**10**	**50**	**100**	**150**
Uncertainty (%)	0.2	0.2	0.25	0.3	0.6	1.0

Table 5 Relative expanded uncertainty (k = 2) of the AC RMS MFD value measured/set in the center of the solenoid using formula (19).

Frequency (kHz)	**0.1**	**3**	**10**	**50**	**100**	**150**
Uncertainty (%)	0.2	0.2	0.2	0.25	0.3	0.6

An AC amplitude MFD value of 110 εT can be generated at a frequency of 150 kHz for a short period of time. The AC RMS MFD value can be measured/set with expanded uncertainty of (0.2 to 0.6)% for k = 2 (Table 5). The differences of the measured values using the EP 01/00 single-layer search coil in comparison with multi-layer search coil K_{II} were smaller than 0.25% in the frequency range from 1 kHz to 3 kHz. Search coil K_{II} can be used with the transimpedance amplifier from 2 kHz (the search coil low corner frequency is 1.2 kHz) up to 30 kHz (the differences the from measurements with the EP 01/00 search coil are lesss than 0.28%), with expanded uncertainty of 0.4% for k = 2.

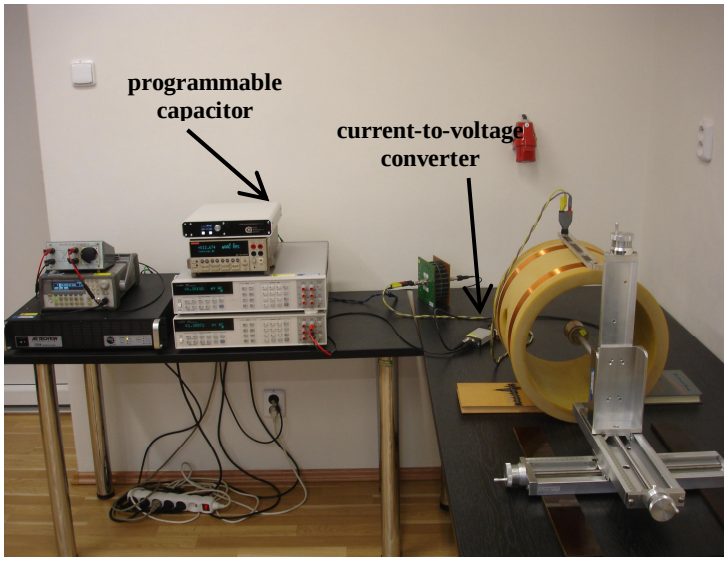

Fig. 33 The setup for AC amplitude MFD measurement.

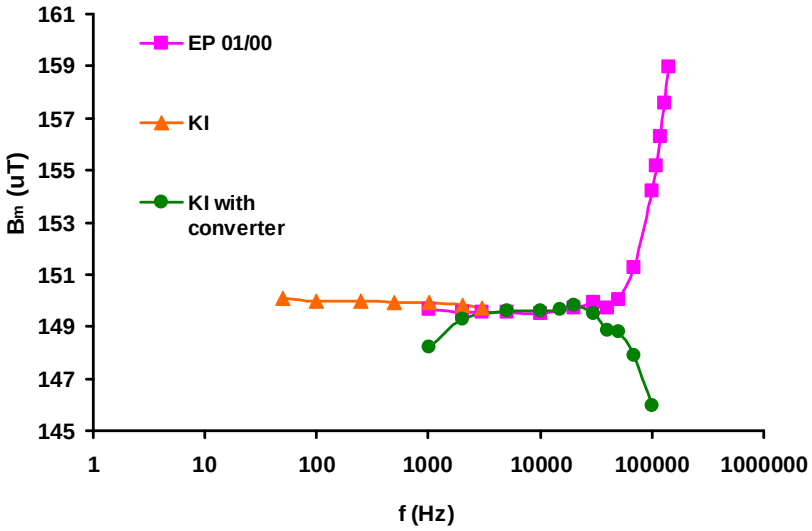

Fig. 34 Measured AC amplitude MFD value for a current value of 1 A.

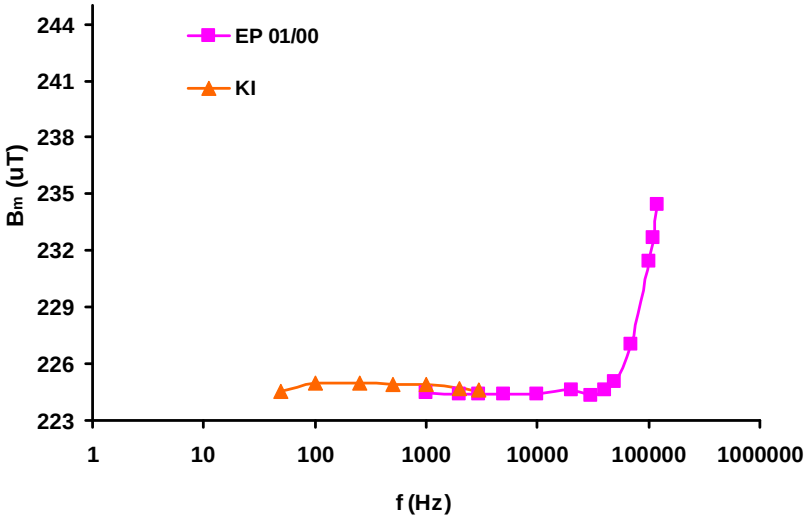

Fig. 35 Measured AC amplitude MFD value for a current value of 1.5 A.

4.3 Methods for AC calibration of a single-layer Helmholtz-type solenoid

AC calibration of the coil standard involves determining the frequency dependence of the coil standard constant. This is needed in order to generate the AC magnetic flux density precisely. Methods that were applied involve using a search coil in quite different ways. In [79], a method is presented where the induced voltage from the search coil and the voltage drop on the AC resistor, which correspond to the current through the coil standard, are measured by the same digital voltmeter. A combination of these two voltage values measured at the same frequency gives the mutual inductance between the search coil and the magnetic field as a function of the frequency. This can be applied, provided that the value of the AC resistor does not change within the given frequency range. The expanded uncertainty (k = 2) is 0.2% in the range up to 30 kHz. The main part of the system described in [80] is a low-frequency magnetic field converter. The main application of the converter is in precise conversion of the measured AC magnetic flux density to AC voltage [81]. This means that the converter with an AC voltmeter can produce precise measurements of the AC magnetic flux density. The converter output voltage and the voltage of a standard resistor (by which the current through the coil standard is measured) is then compared by the voltage comparator. The expanded uncertainty (k = 2) is less than 0.2% in the range of 1 Hz to 20 kHz.

The frequency range is mostly limited by the frequency dependence of the constant of the search coil, and also by the AC resistor that is used. This paper will present an analysis of methods that can be used for calibrating the coil standard up to 100 kHz. In addition, the frequency dependence of the search coils will be calibrated and verified in special Helmholtz coils.

4.3.1 Description of methods

A method using two search coils with nominally the same values (Method 1)

Fig. 36 presents a method using two search coils, S_1 and S_2, with nominally the same values. One search coil is placed in calibrated coil standard *X*, and the other one is placed in coil standard *E*; the frequency dependence of constant K_E is well known. The two coil standards are positioned three meters apart, and they are connected in series, so that they carry the same current during the measurements. RMS voltages U_1 and U_2, which are induced in the two search coils S_1 and S_2 with constant K_{S1} and K_{S2}, are measured by means of a 3458A digital multimeter. The current *I* through the two coil standards is measured as the voltage drop U_R on the AC current shunt *R*, using a 3458A digital multimeter. Current *I* is measured for information only. Assuming a sinusoidal waveform, the constant of the calibrated coil standard is calculated from the equation

$$K_X = \frac{U_2 K_{S1} K_E}{U_1 K_{S2}}. \tag{22}$$

This procedure can also be repeated after transposing the search coils. The coil factors of the search coils can be eliminated from the results, when the geometric mean value (23) is used (K_{x1} is the value calculated from (22) before transposing the search coils, and K_{x2} is the calculated value after transposing the search coils).

$$\overline{K}_X = \sqrt{K_{X1} K_{X2}} \tag{23}$$

The unchanged type B uncertainty of the voltmeters can be eliminated in a similar manner by transposing the voltmeters. These transpositions may be advantageous, but the measurements are lengthened and they are complicated. This method also needs a lot of space for

implementation.

In a modified method, the voltages induced in the two search coils are compared by means of inductive voltage dividers and a selective nanovoltmeter, and this procedure is repeated after transposing the search coils to eliminate their coil factors from the result. This method was used successfully up to 20 kHz during the CCEM.M.-K1 international key comparison [82]. However, this modification cannot be used for higher frequencies, due to the high error and the instability of the inductive dividers.

A method using a precise AC current shunt (Method 2)

The method presented in Fig. 37 involves measuring the RMS voltage U_X induced in search coil S with constant K_S placed inside calibrated coil standard X, and measuring the current I through the coil standard as the RMS voltage drop U_R across the AC current shunt R. A precise AC current shunt with a known AC-DC difference and a search coil with the flat frequency characteristic within a given frequency range is needed. Assuming a sinusoidal waveform, the constant of the calibrated coil standard is calculated from the equation

$$K_X = \frac{U_X R}{4\sqrt{2} U_R K_S f}. \tag{24}$$

The influence of the parasitic capacitance of the connecting cable is negligible. A method using a precise AC current shunt is much simpler, and a lower uncertainty value can be achieved than by the method using two search coils with nominally the same values. This method can also be used for search coil calibration when a coil standard with flat frequency dependence of the constant within a given frequency range is used.

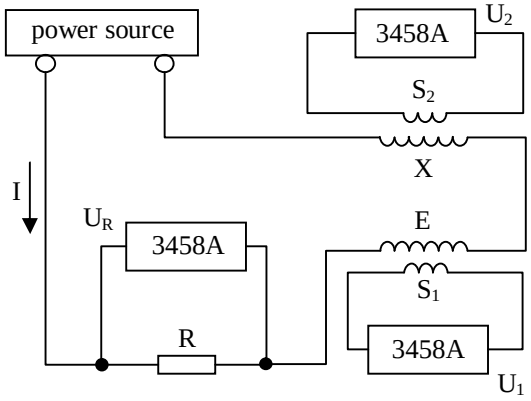

Fig. 36 Schematic diagram of the method using two search coils

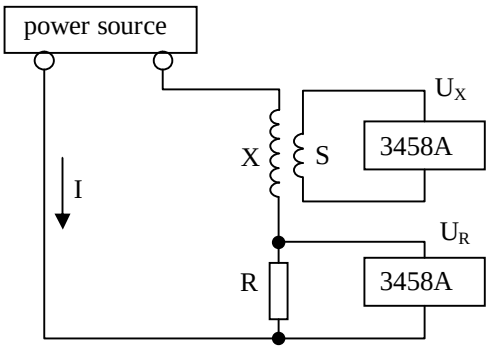

Fig. 37 Schematic diagram of the method using a precise AC current shunt.

Approximate formula (Method 3)

Another option is to use an approximate formula (18) that was described above.

4.3.2 Search coils

Two special search coils with cylindrical frames and suppressed octupoles were used for calibrating the frequency dependence of the coil standard constant (Chapter 2.1.3). A single-

layer printed-circuit-board (PCB) search coil 0.5 mm in thickness, 30 cm in length and with dimensions of (10x10) mm was used for experimental measurements in the frequency range of 50 kHz up 150 kHz (Fig. 38). It was possible to extend the usable frequency range of coil standard calibration above 100 kHz, which was stated in [C2]. The design can be found in Chapter 5.2 and in [J3]. The parameters of the search coils can be found in Table 6. When a search coil is used far below its resonance frequency, it can be considered that the search coil is frequency-independent in the described frequency range. Multi-layer search coil K_{II} can be used up to 3 kHz. However, a change in its constant can be observed at a frequency of 3 kHz. A transimpedance amplifier was therefore implemented to extend the usable frequency range of this search coil. The frequency dependence of search coil K_{II} with the transimpedance amplifier was measured with expanded uncertainty of 0.1%. Search coil K_{II} can be used with the transimpedance amplifier from 2 kHz (the search coil corner frequency is 1.2 kHz) up to 30 kHz [J2].

Due to its resonance frequency, the EP 01/00 single-layer search coil can be used up to 100 kHz, and the single-layer PCB SC1L_30 search coil can be used up to 150 kHz, without changing its constant. However, this needs to be verified by simulation and by measurement, and to be compared with the calculated frequency dependence, according to (18). First, a simulation by the finite integration technique (FIT) was performed using the CST Studio environment. A low-frequency domain solver, full wave analysis and a tetrahedral mesh were used for the simulations of the EP 01/00 search coil. Simulations of the PCB search coil have been published in [J3].

Table 6 Parameters of the search coils.

Parameter	**K_{II}**	**EP 01/00**	**SC1L_30**
Frame material	cotton-phenolic laminate (Textit)	PTFE	FR4
Calibrated DC constant (m^2)	(1.3312 ± 0.0011)	(0.045394 ± 0.000036)	(0.000860 ± 0.000001)
Resistance (Ω)	24.5	0.5	4
Inductance	26.3 mH	38.1 µH	2.9 µH
Resonance frequency (MHz)	0.0496	3.2	6.23
Parasitic capacitance (pF)	392	63	227
Useful frequency range (kHz)	< 3	2-100	50-150

The area turns value K_S of the simulated EP01/00 search coil was calculated from the induced voltage U_{RMS} on a resistor of 10 Mq when the peak magnetic field strength value H = 10 kA/m (B_{RMS} = 8.888 mT) was applied perpendicular to the search coil, according the formula

$$K_S = \frac{U_{RMS}}{2\pi B_{RMS} f}. \tag{25}$$

A 10 Mq resistor represents the input resistance of a common digital multimeter. However, a

serious error in the area turns calculations was observed during the simulations in the CST Studio when the 10Mq resistor was exposed to the applied magnetic field strength. The shielding of the resistor was therefore needed. A shileding was therefore designed for the resistor (Fig. 39, Fig. 40 and Fig. 41), with the following parameters: conductivity of 5.10^8 S/m, relative permeability of 50000, and a hollow cylindrical shape.

Special Helmholtz coils 25 cm in diameter and with 2x4 turns of shielded coaxial cable wound on a wooden frame were used for calibrating and verifying the frequency dependence of the search coil constant up to 150 kHz. The resistance value of the Helmholtz coils is 0.59 q , the inductance value is 50.6 εH and the constant is (14.581 ± 0.029) εT/A. The measured resonance frequency of the Helmholtz coils was 2.6 MHz (shielding not grounded).

The method using the precise AC current shunt described above was used for measurements of the search coil constant frequency dependence. The search coil wires for connecting with the multimeter should be made from a shielded cable, and should have a coaxial choke to reduce the common voltage. The shielding of the Helmholtz coils has to be connected to the ground to eliminate parasitic capacitance between the search coil and the Helmholtz coils, and to reduce the capacitance of the Helmholtz coils. Fig. 42 and Fig. 43 present the measured, calculated and simulated frequency dependence of the EP01/00 and SC1L_30 search coils. The differences between the measured and simulated results are less than 0.11% for EP01/00 in the frequency range up to 100 kHz, and less than 0.06% for SC1L_30 in the frequency range up to 150 kHz. The differences between the measured and calculated results are less than 0.15% for EP01/00 in the frequency range up to 100 kHz and less than 0.05% for SC1L_30 in the frequency range up to 150 kHz. When the shielding is not connected to the ground, a serious error in the induced voltage can been observed, especially at frequencies above 50 kHz (Fig. 42), caused by the parasitic capacitance mentioned above. This effect can be described by the frequency coefficient of the mutual inductance between the connected search coil and the Hemholtz coils, using a simplified approach calculated as [83]

$$M = M_0 \left\{ 1 + \varpi^2 \left[\begin{array}{l} C_1 L_1 + C_2 L_2 - \\ C_M \dfrac{\left(L_1 - M_0\right)\left(L_2 - M_0\right)}{M_0} \end{array} \right] \right\}, \tag{26}$$

where C_1, L_1 are the capacitance and the inductance of the Helmholtz coils, C_2, L_2 are the capacitance and the inductance of the search coil, C_M is the parasitic capacitance between the Helmholtz coils and the search coil, and the mutual inductance M_0 is calculated as

$$M_0 = k\sqrt{L_1 L_2}\,, \tag{27}$$

where k is a coupling factor. The value of k can be calculated from formula (27), when the value of M_0 is measured, or it can be calculated as follows

$$k = \frac{U_2}{U_1}\sqrt{\frac{L_1}{L_2}}\,, \tag{28}$$

where U_1 is the RMS voltage across inductance L_1, and U_2 is the induced RMS voltage at L_2. The value of k = 0.0145 is valid when M_0 is measured, and k = 0.0147 is valid when the value is calculated according to (28). The value of C_M = 8.7 pF was measured using an LCR bridge. The calculated dependence of mutual inductance M for search coil EP01/00 is presented in Fig. 44. The change in the mutual inductance at 100 kHz is 0.1% when the shielding is grounded (assuming a value of C_M = 0 and a value of C_1 that is reduced by one order magnitude), and 1.3% when the shielding is not grounded. The corresponding measured change of the EP01/00 constant at 100 kHz is 0.25% (shielding grounded) and 0.84% (shielding not grounded). These results confirm the correctness of the setup for search coil calibration and verification.

Fig. 38 The SC1L_30 single-layer PCB search coil.

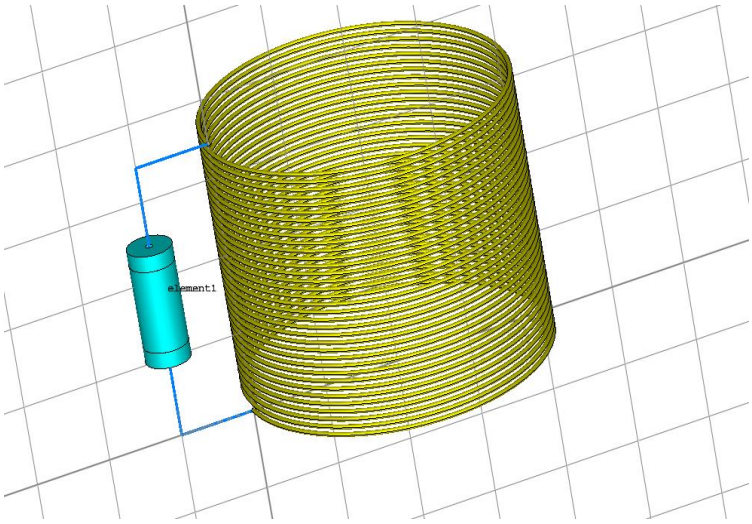

Fig. 39 A model of the EP 01/00 search coil in the CST Studio.

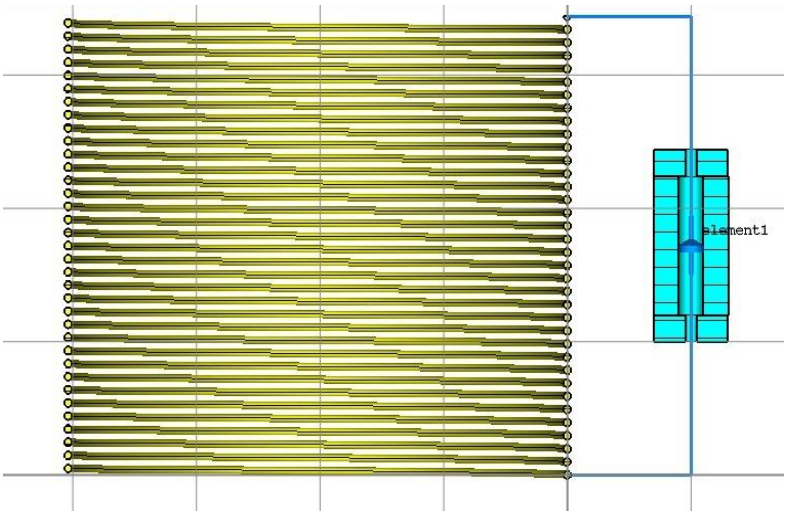

Fig. 40 Resistor shielding design: cross-section view.

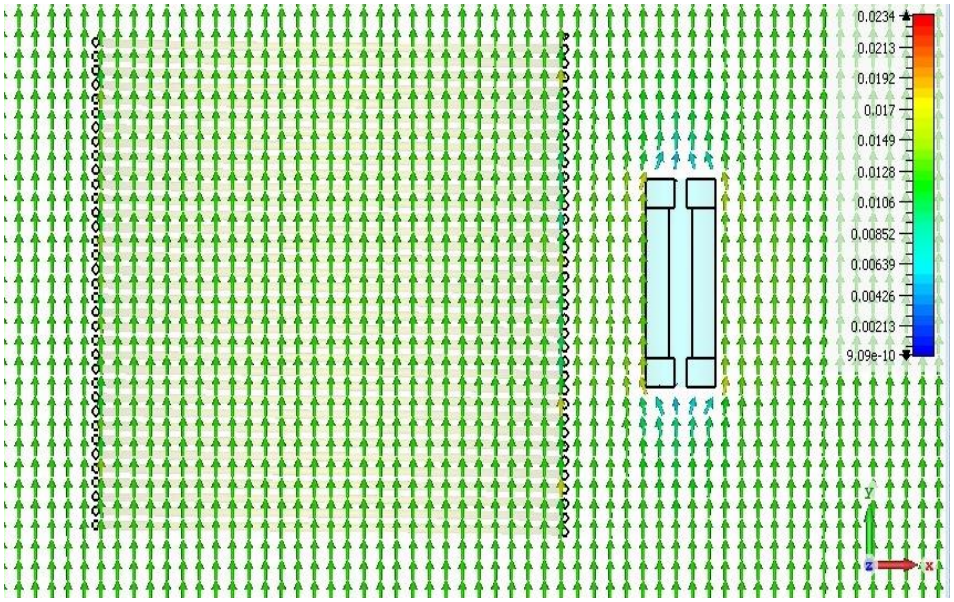

Fig. 41 Resistor shielding design: the effect of shielding during the simulations when H_{peak} = 10 kA/m was applied.

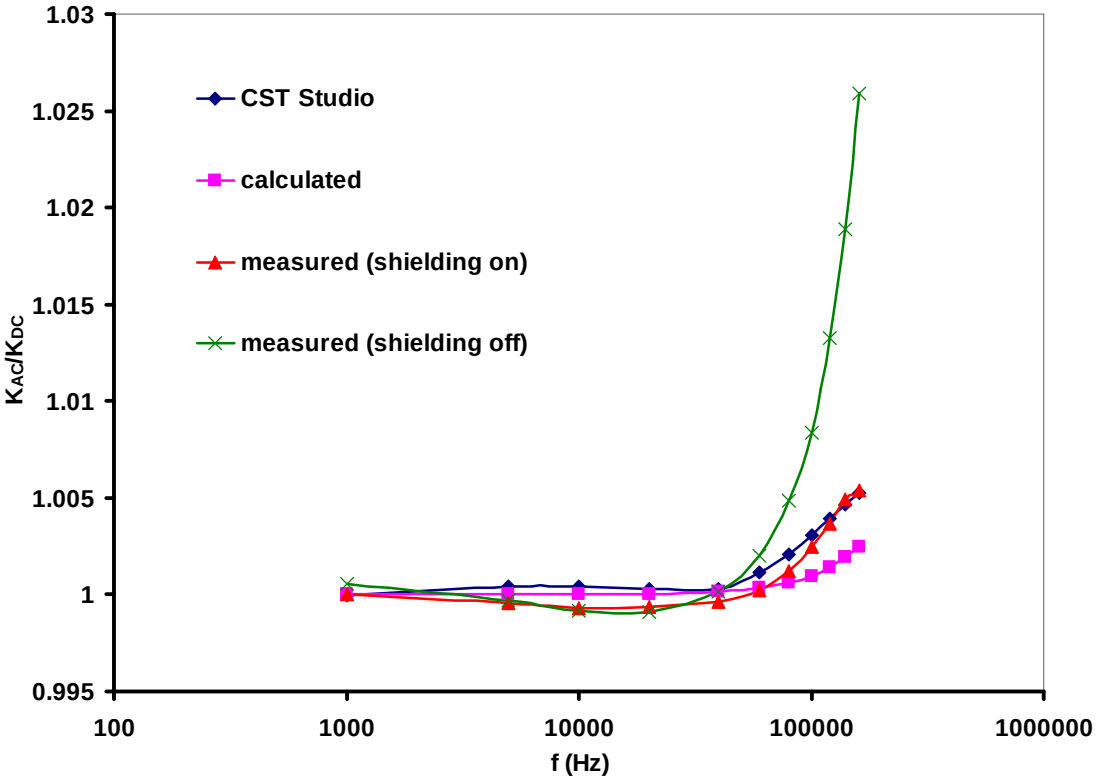

Fig. 42 Calculated, simulated and measured frequency dependence of the EP01/00 search coil.

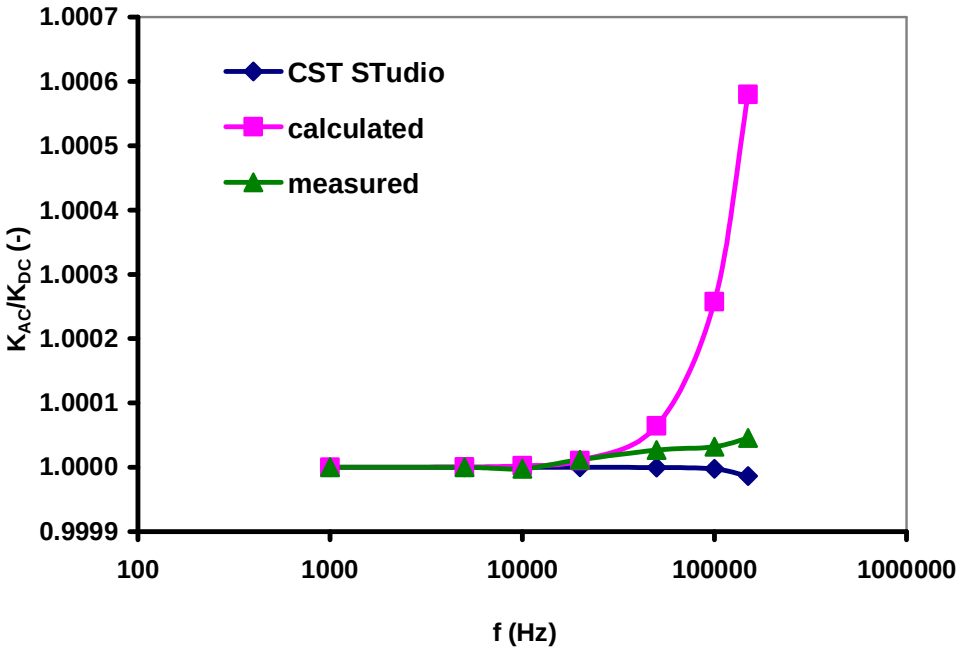

Fig. 43 Calculated, simulated and measured frequency dependence of the SC1L_30 search coil.

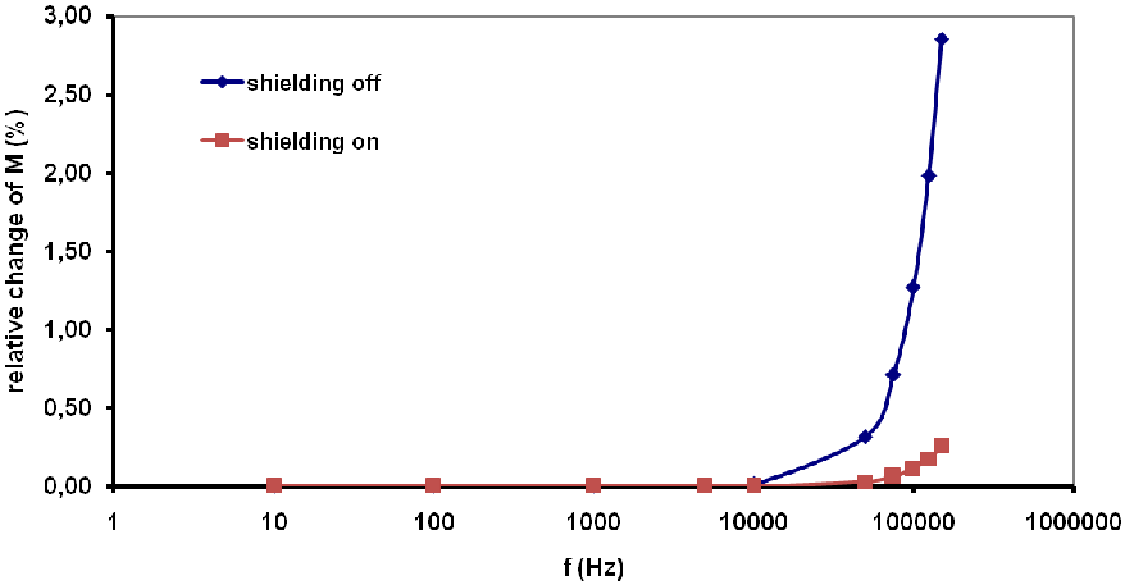

Fig. 44 Relative change in the calculated dependence of mutual inductance *M* for the EP01/00 search coil.

4.3.3 Uncertainty analysis

Two AC coil standard calibration methods and one approximate formula for calculating the frequency dependence of the coil standard have been described above.

The type A uncertainty (repeatibility) of these methods depends mainly on the stability of the power source that is used, and on the repeatability of the multimeters. The stability of the

power source is better than 0.02%, and the repeatability of the multimeters (3458A) is better than 0.002%. The repeatibility value is better than 0.02%. The input quantities of the type B uncertainty sources are assumed to be uncorrelated.

Uncertainty of method 1

The type B relative uncertainty of the method using two search coils with nominally the same values, where the constant of the calibrated coil standard is calculated according to (22), can be determined as

$$u_{\mathrm{Bs}} = \sqrt{u_{\mathrm{KE}}^2 + u_{\mathrm{SC1}}^2 + u_{\mathrm{SC2}}^2 + u_{\mathrm{U1}}^2 + u_{\mathrm{U2}}^2 + u_{\mathrm{d}}^2 + u_{\mathrm{h1}}^2 + u_{\mathrm{h2}}^2} \tag{29}$$

where u_{KE} is the relative standard uncertainty of the calibration of the coil standard constant at a given frequency value, u_{SC1} and u_{SC2} are the uncertainties of the search coil constants, u_{U1} and u_{U2} are the uncertainties of the search coil output voltage measurement, u_{d} is the uncertainty of the difference of the directional dependence measurements of the search coils, and u_{h1} and u_{h2} is the uncertainty of the influence of homogeneity inside the coil standard in the volume of the search coils. The uncertainty of the search coil constants determined by calibration with variable mutual inductance was 0.04%. The uncertainty value of u_{KE} can lie in the order of tenths of one percent. The uncertainty of u_{U1} and u_{U2} depends on the digital voltmeters that are used for the voltage value measurements. The value can lie in the order of thousandths to tenths of one percent. The value of u_{d} can lie in the order of hundredths to tenths of one percent, and the value of u_{h1}, u_{h2} can lie in the order of hundredths to tenths of one percent [J2].

Uncertainty of method 2

The type B relative uncertainty of the method with a precise AC current shunt, where the constant of the calibrated coil standard is calculated according (24), can be calculated as

$$u_{\mathrm{Bcs}} = \sqrt{u_{\mathrm{f}}^2 + u_{\mathrm{SC}}^2 + u_{\mathrm{UX}}^2 + u_{\mathrm{UR}}^2 + u_{\mathrm{R}}^2 + u_{\mathrm{d}}^2 + u_{\mathrm{h}}^2}\,, \tag{30}$$

where u_{f} is the relative standard uncertainty of the frequency, u_{UX} is the uncertainty of the search coil output voltage measurement, u_{UR} is the uncertainty of the voltage measured across the precise AC current shunt, u_{R} is the standard uncertainty of the precise AC current shunt value, u_{SC} is the uncertainty of the search coil constant, u_{d} is the uncertainty of the directional dependence measurement of the search coil, and u_{h} is the uncertainty of the influence of homogeneity inside the coil standard in the volume of the search coil. The maximum uncertainty value of the frequency measurement usually varies within tens of ppm. It can therefore be neglected, because the other uncertainties are typically higher. The value of u_{R} lies in the order of tens of ppm. The value of u_{UX} and u_{UR} can lie in the order of thousandths to tenths of one percent.

The type B relative uncertainty of the method with a precise AC current shunt used for search coil calibration is similar to (30), except that the relative standard uncertainty of u_{SC} is replaced by the relative standard uncertainty of u_{KE}, with the same meaning as previously.

Uncertainty of method 3

The type B absolute uncertainty of the results calculated from (18) can be determined as

$$u_{\mathrm{Baf}} = \sqrt{\left[\left(1+\frac{f^2}{f_\mathrm{r}^2}\right)u_{\mathrm{KDC}}\right]^2 + \left(-\frac{2K_{\mathrm{DC}}f^2}{f_\mathrm{r}^3}u_{\mathrm{fr}}\right)^2} \tag{31}$$

where u_{KDC} is the uncertainty of the DC coil constant, and u_{fr} is the uncertainty of the resonance frequency determination. The value of u_{KDC} depends on the method used for the DC coil calibration - at the CMI, we use a direct comparison with the national coil standard, or the NMR method with flowing water (nutation method). This means that the value of u_{KDC} can lie in the order of hundredths of one percent. The resonance frequency value of the coil standard can be determined by an LCR meter or by a method where the frequency value of the current through the coil standard is changing, and the maximum value of the voltage on the coil winding is measured by a digital oscilloscope. The value of u_{fr} can lie in the order of hundredths of one percent. However, the uncertainty value u_{Baf} is disputable, because it is an approximate formula.

4.3.4 Experimental results

A single-layer Helmholtz-type solenoid, the design of which was described in Chapter 4.1, was calibrated by methods 1 and 2. The current value through the solenoid winding was about 1 A for both methods. This means that the magnetic flux density inside the solenoid was about 105 εT. Two 3458A digital multimeters with an external trigger for measuring the voltages at the same time were used for the voltage U_R and U_X measurements. The multimeters were switched after the first measurement to eliminate multimeter reading errors. The measured frequency dependence was also compared with the frequency dependence simulated in FLUX 3D, and with the calculated frequency dependence (method 3), according to formula (18). A precise cage-type AC current shunt [84] with an AC-DC difference of (82 ± 60) ppm at 200 kHz was used. An early change in the K_II search coil constant can be seen in the range of 2-3 kHz (Fig. 45). However, the differences between the EP 02/00 results and the calculated and simulated frequency dependence in the range of 3-20 kHz were larger than expected. Differences of about 0.5% were probably caused by interferences, and by the lower sensitivity of EP 02/00 in this frequency range. Search coil K_II with an I/U converter was therefore used in the range of 2-20 kHz. The I/U converter increased the frequency range of the K_II coil up to 30 kHz. The disadvantages of the EP 02/00 coil were thus eliminated in this range (see the results in Fig. 46). The relative difference between the measured values and the calculated values is up to 0.25% in the frequency range up to 50 kHz; up to 1.2% in the frequency range of 50-70 kHz; and up to 3.2% in the frequency range of 70-100 kHz. It is evident that formula (18) can be used only up to 50 kHz in this case. The relative difference between the measured values and the simulated values is up to 0.15% in the frequency range up to 20 kHz; up to 0.35% in the frequency range of 20-50 kHz; and up to 0.5% in the frequency range from 50 kHz up to 100 kHz. The SC1L_30 search coil has been used experimentally for coil standard calibration in the range of 50 kHz up to 150 kHz. However, the absolute difference was less than 2% in the range of 50 kHz up to 100 kHz and less than 7% at 150 kHz, in comparison with the values measured by EP01/00. These big differences in the values were probably caused by ineffective reduction of the common voltage by the choke that was used. This needs to be further investigated, and improvements need to be made, for example by using a nanocrystalline material for the choke instead of a high-frequency ferrite core. Expanded uncertainty (k = 2) from 0.2% to 0.35% up to 100 kHz (Table 7) can be achieved by method 1 (using two search coils with nominally the same values). Expanded uncertainty (k = 2) from 0.12% to 0.25% up to 100 kHz (Table 8) can be achieved by method 2 (using a precise AC current shunt). However, when search coil K_II with the I/U converter is

used, the expanded uncertainty value is 0.25% in the range of 2-20 kHz, due to the measurement uncertainty of the self-inductance of the K_{II} search coil.

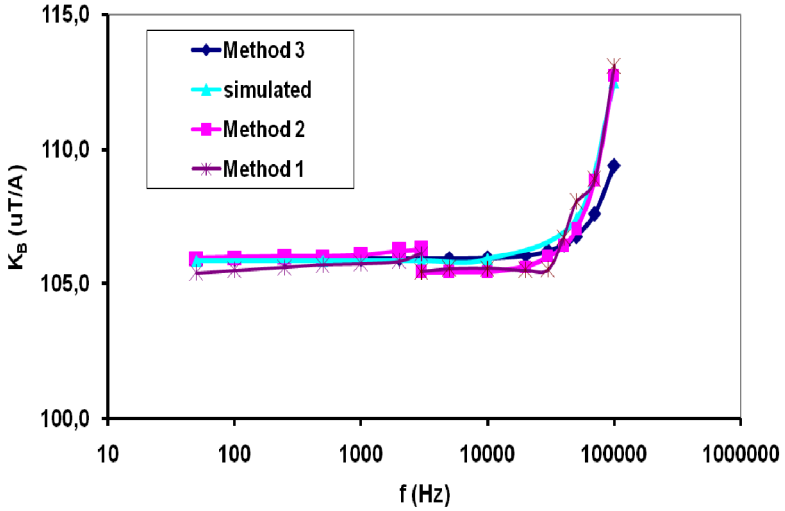

Fig. 45 Frequency dependence of the coil standard constant. The K_{II} and EP01/00 search coils were used for the measurements.

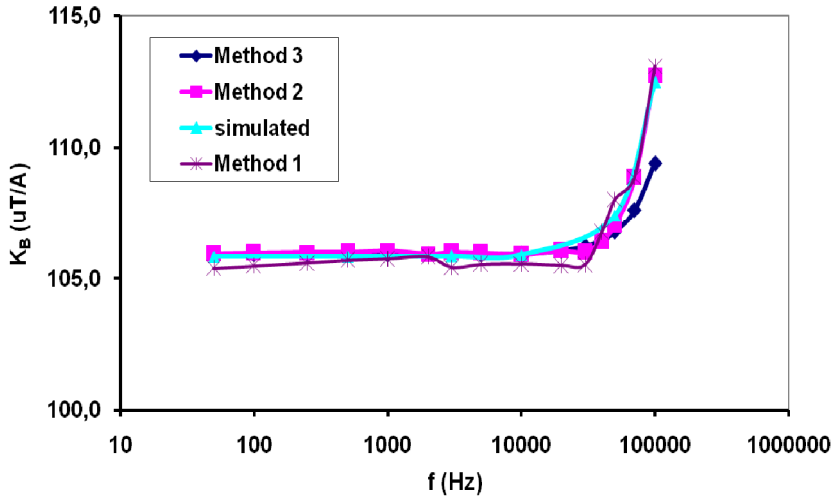

Fig. 46 Frequency dependence of the coil standard constant. The K_{II} and EP01/00 search coils and the K_{II} search coil with an I/U converter were used for the measurements.

Table 7 The relative expanded uncertainty (k = 2) of coil standard calibration using method 1.

Frequency (kHz)	**0.05**	**10**	**30**	**50**	**100**	**150**
Uncertainty (%)	0.20	0.20	0.20	0.25	0.35	0.80

Table 8 The relative expanded uncertainty (k = 2) of coil standard calibration using method 2.

Frequency (kHz)	**0.05**	**10**	**30**	**50**	**100**	**150**
Uncertainty (%)	0.12	0.12	0.12	0.2	0.25	0.55

4.4 The use of coil standards in metrology

4.4.1 Calibration of AC magnetic field meters

The primary use of AC magnetic flux density coil standards is for calibrating AC magnetic field meters. Calibrating the AC ranges of teslameters with a Hall probe involves inserting the probe of the instrument into the coil standard, and then comparing the magnetic flux density value measured by the instrumentôs probe with the magnetic flux density value generated by the coil standard, which is powered by an AC current [65]. The adjusted magnetic flux density value is then calculated from the current value and from the coil standard constant determined e.g. by the NMR method. However, the frequency dependence of the coil standard constant (determined by one of the methods described in chapter 3) and its resonance frequency is needed in order to make a correct calculation of the adjusted value.

AC magnetic field analysers with a 3-axis coil probe (e.g. ELT 400, EFA 300, C.A. 42), which work on the principle of integrating voltage measurements, are widely used by health and safety professionals, in service industries, and in manufacturing (Fig. 47). The calibration of these instruments is therefore important. For these calibrations, we use a method with a special search coil, which has already been mentioned above and is described in detail below.

Fig. 47 A magnetic field analyser with an ELT 400 3-axis coil probe (left) and C.A. 42 (right). Pictures taken from the Narda Safety Test Solutions (ELT 400) website and from Chauvin Arnaux website (C.A. 42).

The calibration method consists in comparing the measured values using a calibrated instrument with values measured by a special search coil. The special search coil is designed to achieve a good approximation of the magnetic dipole. Fig. 48 presents a schematic diagram of instrument calibration. First, the search coil is placed in the center of a coil standard and the output voltage of the search coil is measured by a digital multimeter. The coil standard is powered from a generator and an amplifier, and the current I through the coil standard is measured, using an Agilent 3458A digital multimeter, as the voltage drop U_N on the standard resistor R_N. Current I is measured for information only. The adjusted magnetic flux density value inside the coil standard is then calculated from (19) or from (20). Then the probe of the calibrating instrument is placed in the center of the coil standard, and the measured value is

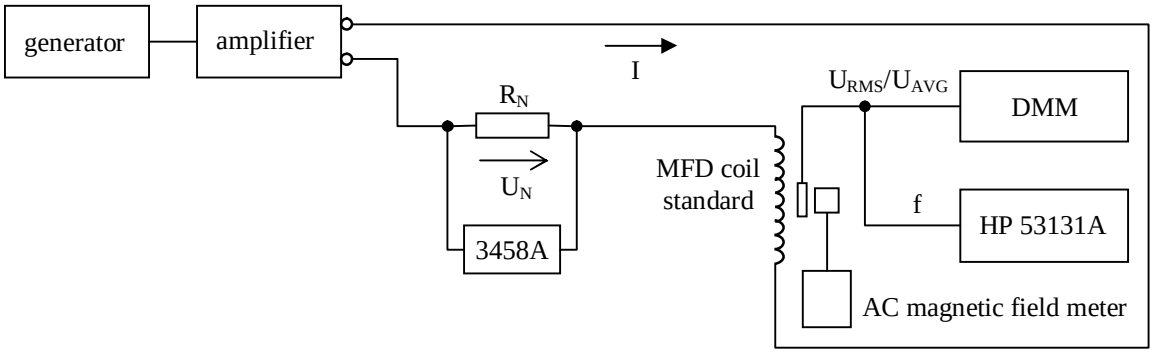

Fig. 48 A schematic diagram of AC magnetic field meter calibration by making comparisons with the search coil.

recorded. The magnetic flux density sine wave also needs to be checked. The advantages of this method are that the adjusted value inside the coil standard is precisely measured, it is not dependent on the parameters of the coil standard, and only constant K_S and the resonance frequency of the search coils need to be known. Only the influence of the magnetic field homogeneity inside the solenoid needs to be taken into account. Examples of the results of EFA 300 calibration are presented in Table 9 and Table 10.

Table 9 An example of EFA 300 calibration on all three axes separately

Frequency (Hz)	**Set value of B_{RMS} in the CMI coil standard (mT)**	**Measured value of B_{RMS} by EFA 300 in direction (mT)**		
		X	**Y**	**Z**
50	**0.200**	0.198	0.197	0.199
	0.400	0.398	0.397	0.397
	0.600	0.594	0.595	0.597
	0.800	0.790	0.794	0.794
	1.000	0.987	0.990	0.992
	3.000	2.962	2.968	2.990
	6.000	5.944	5.960	5.951

Table 10 An example of EFA 300 calibration on the Z-axis (the axis of the coil standard)

Frequency (kHz)	**Set value of B_{RMS} in the CMI coil standard (ε T)**	**Measured value of B_{RMS} by EFA 300 on the Z-axis (ε T)**
1	**50.00**	50.10
	100.0	100.54
	200.0	201.38
	250.0	251.41
	300.0	301.38

Frequency (kHz)	Set value of B_{RMS} in the CMI coil standard (εT)	Measured value of B_{RMS} by EFA 300 on the Z-axis (εT)
5	**25.00**	25.07
	50.00	50.06
	100.0	99.89
	200.0	200.33
	250.0	251.10
	300.0	301.25
10	**25.00**	25.21
	50.00	50.28
	100.0	100.88
	200.0	202.10
	250.0	252.54
	300.0	302.51
30	**20.00**	21.91
	40.00	43.85
	60.00	65.75
	80.00	87.56
	100.0	109.09
	120.0	130.92

4.4.2 Calibration of search coils

Search coils are widely used for measuring AC magnetic fields, and in special cases for measuring DC magnetic fields with a webermeter, and for comparing magnetic flux density standards and magnetic flux standards. Multi-layer and single-layer search coils were used for characterizing the solenoid in Chapter 2.1.1 and 2.1.2, and search coils are also used for AC coil standard calibration (Chapter 2.1.3). Search coil calibration is therefore important, and the use of a coil standard for magnetic flux density is crucial in search coil calibration.

Generally, there are several AC calibration methods for search coils. The first two methods are based on compensating the magnetic flux from a search coil placed in a known reference magnetic field (magnetic flux density coil standard) by variable mutual inductance (VMI) or by the zero differential method (ZDM), where the magnetic flux standard with a calibrated value is used [24], [85]. The frequency range is limited by the magnetic flux standard, or especially by the variable mutual inductance that is used. At CMI, we have a Tinsley type 4229B variable mutual inductance and a special coil with double winding (mutual inductance) with a nominal value of 10 and 100 mWb/A as a magnetic flux standard. We need to know the frequency dependence of the variable mutual inductance and the magnetic flux standard. The frequency dependence was measured by comparison with a Sullivan universal inductance bridge (type A.C.1100) from 40 Hz up to 10 kHz. The measured frequency dependence results are shown in Fig. 49 and Fig. 50. It is obvious that variable mutual inductance and the magnetic flux standard with a nominal value of 10 mWb/A can be used up to 1 kHz. If a magnetic flux standard with a nominal value of 100 mWb/A is needed, the system can be used up to 250 Hz only (according to Fig. 51). And, if AC calibrations are required, the lock-in amplifier or an oscilloscope in XY mode is used as a null indicator.

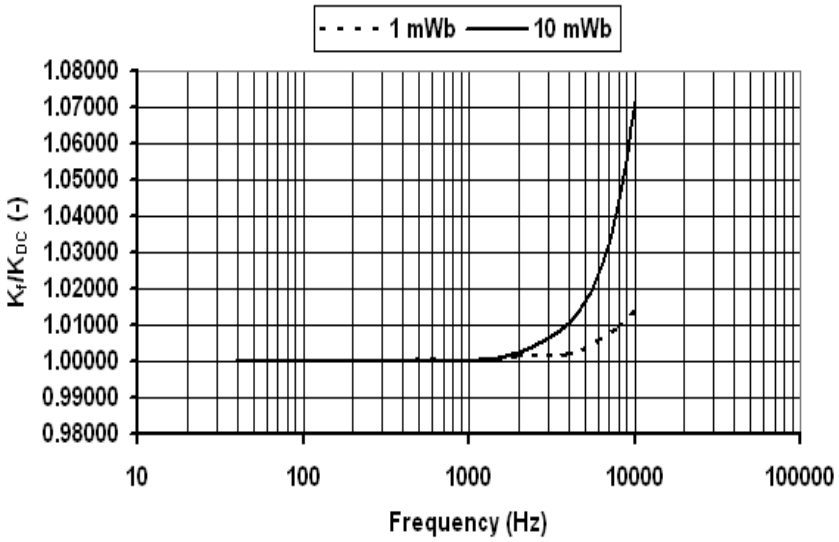

Fig. 49 Frequency dependence of Tinsley type 4229B variable mutual inductance.

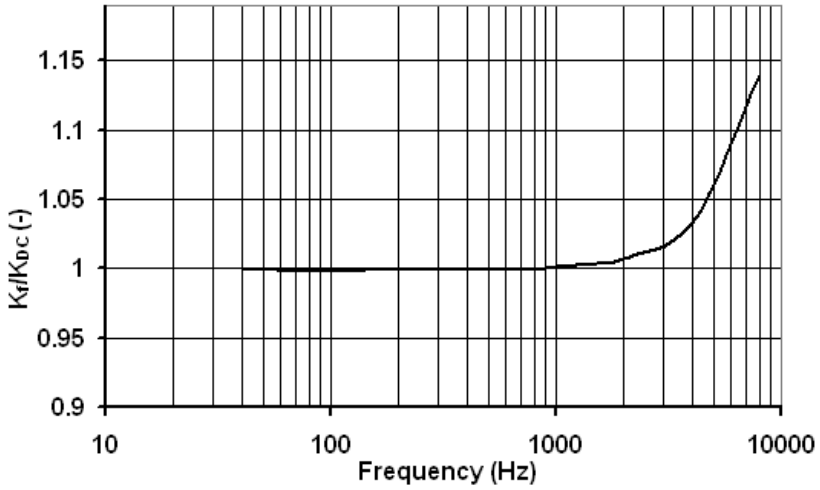

Fig. 50 Frequency dependence of the the magnetic flux standard with a nominal value of 10 mWb/A.

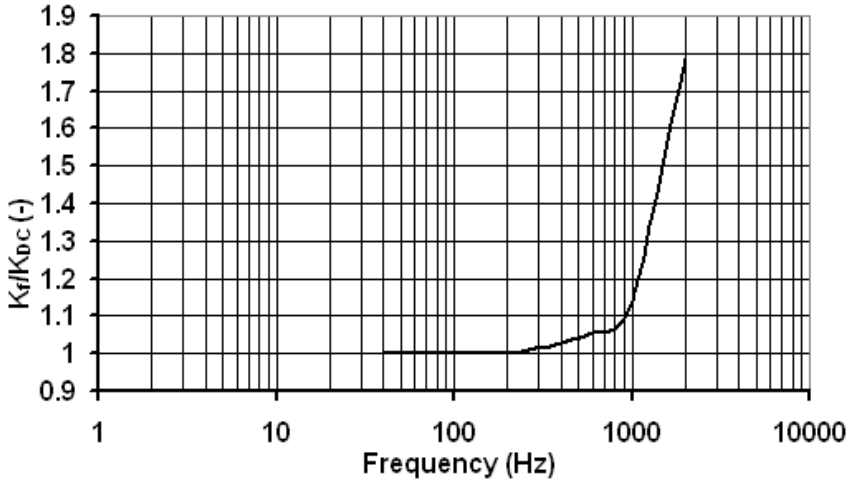

Fig. 51 Frequency dependence of the magnetic flux standard with a nominal value of 100 mWb/A.

Of course, the simplest method for AC calibration of a search coil is based on placing the search coil in the center of a coil standard, and the output voltage of the search coil is measured by a digital multimeter. The same method is used in AC magnetic field meter calibration (Fig. 47) in Chapter 4.4.1. Assuming a sinusoidal waveform, constant K_S of the calibrated search coil is then calculated as

$$K_S = \frac{U_{RMS}}{2\pi B_{RMS} f} \text{ resp. } K_S = \frac{U_{AVG}}{4B_{RMS} f \sqrt{2}} \text{ resp. } K_S = \frac{U_{AVG}}{4B_m f}, \tag{32}$$

where U_{RMS} is the RMS value, or U_{AVG} is the arithmetic mean value of the output voltage of the search coil, measured using a digital multimeter. B_{RMS}, or B_m, is the adjusted RMS value, or the maximum value of the magnetic flux density inside the MFD standard, and f is the frequency measured by an HP 53131A digital counter.

There is another way that can be used for determining the constant of the search coil. If there is no digital multimeter for measuring the arithmetic mean output voltage value, a digital oscilloscope with mathematical functions (integration of the input signal) can be used. The search coil output is connected to the oscilloscope, and if the voltage has a sinusoidal waveform, integration on this signal can be applied. Then the amplitude of the magnetic flux from one period of the integration waveform can be measured. The constant of the search coil can then be calculated from

$$K_S = \frac{\Phi_m R_N}{K_B U_N \sqrt{2}}, \tag{33}$$

where $\bar{\boldsymbol{u}}_m$ is the amplitude of the magnetic flux measured from one period, and K_B is the calibrated constant of the MFD. The use of an oscilloscope is not very accurate, so this method should be used only for indicative measurements.

If the impedance of the search coil is not negligible in relation to the input resistance of the measuring device (the oscilloscope or the multimeter), it is necessary to make a correction to the measured value of the output voltage. The actual voltage value induced in the search coil is greater than the measured voltage value. The impedance of the coil to the input resistance of the device consists of a voltage divider, so it is necessary to multiply the value of K_S by the correction factor k, which is to be determined as

$$k = \frac{R_{in} + Z_{SC}}{R_{in}}, \tag{34}$$

where R_{in} is the input resistance of the multimeter or oscilloscope, and Z_{SC} is the impedance of the search coil. As an alternative to measurements with an oscilloscope, we can also take advantage of the direct measurement method of the AC magnetic flux effective or the maximum value from the search coil. However, it is necessary to use a webermeter that is able to measure the AC magnetic flux. However, most commercially-available webermeters are not able to measure the sinusoidal waveform. The constant of the search coil can then be calculated according to (33). Another option is to calculate constant K_S from the frequency dependence of the coil constant, which can be determined approximately from equation (18). The uncertainty value depends on the search coil calibration method that is used, and also on the search coil parameters (constant value, resistance). The results of a comparison of the methods for AC calibration of a search coil with a nominal constant value of 90 m^2 can be found in [C1].

4.4.3 Calibration of loop antennas (monitoring loops)

Loop antennas (monitoring loops) are often used for recording (measuring) low frequency magnetic fields up 300 kHz (Fig. 52). The anntenna factor K_{AF} is determined by the calibration as the ratio between the measured magnetic field and the voltage induced in the loop. The loops can be calibrated in several ways. Firstly, a single transmit loop antenna is used to generate a known magnetic field. The receiving loop is placed at a known distance from the transmiting loop, and the output voltage is measured [86]. Secondly, the loop is placed in the center of the Helhmoltz coils, which can generate a well-known defined magnetic field *H*, and the induced voltage of the loop is measured [86], [87]. The voltage from the loop is usually measured with a 50Ý impedance load. The antenna factor can also be calculated from the loop impedances [87].

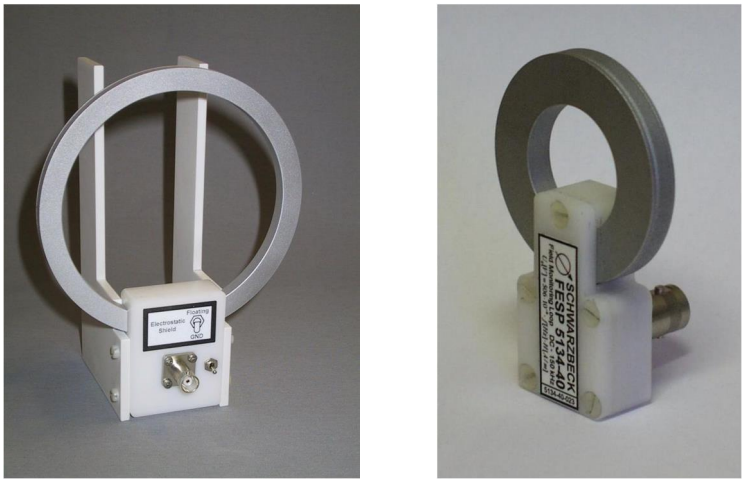

Fig. 52 An FESP 5133-7/41 monitoring loop (left) and an FESP 5134-40 monitoring loop (right). Pictures taken from the website of Schwarzbeck Mess - Elektronik OHG.

The schematic diagram of the method in which Helmholtz coils (or other coil standards) are used is similiar to the diagram in Fig. 47. A monitoring loop is placed in the coil standard instead of the magnetic field analyzer. The induced voltage *U* from the loop is measured via the 50Ý impedance load by a 3458A multimeter. An example of FESP 5134-40 calibration is presented in Table 11. The antenna factor *AF* is calculated as

$$AF = 20\log\frac{H}{U}\ \text{dB(S/m)} \tag{35}$$

$$AF = 20\log\mu_0 10^6\frac{H}{U} = 20\log\frac{H}{U} + 1.9841\ \text{dB(pT/}\varepsilon\text{V)} \tag{36}$$

Table 11 An example of FESP 5134-40 calibration.

Frequency (kHz)	**The value of the magnetic field strength set in the CMI standard (A/m)**	**Voltage across 50 q (dBε V)**	**AF dB(S/m)**	**AF dB(pT/ε V)**
0.005	100.3	47.47	112.56	114.55
0.010	100.3	53.40	106.62	108.61
0.020	100.2	59.42	100.60	102.58
0.030	100.2	62.93	97.09	99.07
0.050	100.0	67.37	92.63	94.61
0.070	100.2	70.28	89.74	91.72
0.10	100.1	73.37	86.64	88.62
0.20	100.6	79.39	80.66	82.64
0.30	100.2	82.83	77.19	79.18
0.50	100.1	87.09	72.93	74.91
0.70	100.1	89.78	70.23	72.21
1.00	100.4	92.51	67.52	69.51
3.00	100.2	100.05	59.97	61.95
5.00	100.3	103.76	56.27	58.25
7.00	100.2	106.35	53.67	55.65
10.00	100.1	109.19	50.82	52.81
30.00	100.0	117.75	42.25	44.23
50.00	100.0	121.23	38.77	40.75
70.00	100.1	123.22	36.79	38.77
100.00	100.0	124.88	35.12	37.11

4.5 Summary

The design of the single-layer Helmholtz-type solenoid for generating AC MFD in the frequency range up to 100 kHz has been proposed, and a full characterization has been presented here. The analytical design and the FEM design have been compared with a real solenoid. The results from the DC analysis show good agreement between the theoretical and measured values in the center of the solenoid. The results from the AC analysis show that the relative difference of the MFD frequency dependence in the center of the solenoid between theoretical and measured values is in the range of (0.25 %ï 0.7 %) for the frequency range of (3ï 100) kHz. The relative difference of the MFD frequency dependence in the center of the solenoid is about 2% at 100 kHz. Good agreement between the theoretical and measured homogeneity values in the *z*- and ***ȷ***-axis was also proven.

A programmable capacitor array that enables a high-frequency MFD value to be generated in a single-layer Helmholtz-type solenoid up to 150 kHz with inexpensive low voltage AC power sources has been realized and has been successfully tested. A transimpedance amplifier that expands the upper range of useful frequencies for multi-layer search coils has also been realized and successfully tested.

The methods for calibrating AC coil standards have also been described, analyzed and compared. The possibilities of using coil standards in metrology has been described in detail.

5 A system for AC calibration of Hall probes up to 1 T

Teslameters with Hall probes are widely used for measuring the magnetic flux density in industry, in the health sector, and in testing. In other well-known approaches, the DC ranges of these teslameters are calibrated using an MFD coil standard, or by comparison with an NMR magnetometer. However, it is a more complex matter to calibrate the AC ranges, which are mostly the same as the DC ranges (usually up to 2 T). A few tens of mT at a frequency of 50 Hz can usually be generated by an AC MFD coil standard. However, the AC MFD value decreases in proportion to the frequency. For generating AC MFD values greater than about 30 mT, it is necessary to use a system with a laboratory AC electromagnet.

5.1 Design of an AC electromagnet

5.1.1 Analytical electromagnet design

An analytical analysis of the electromagnet can be made from Ampereôs law or from Hopkinsonôs law [88]-[90]. The MFD value B_g in the the cross-sectional area of the air gap A_g, the cross-sectional area of the yoke A_c, the mean path length l_c, and the air gap length l_g are defined. The number of turns $N = N_1+N_2$ for the stated current value I and the MFD value in the core B_c are needed (Fig. 53).

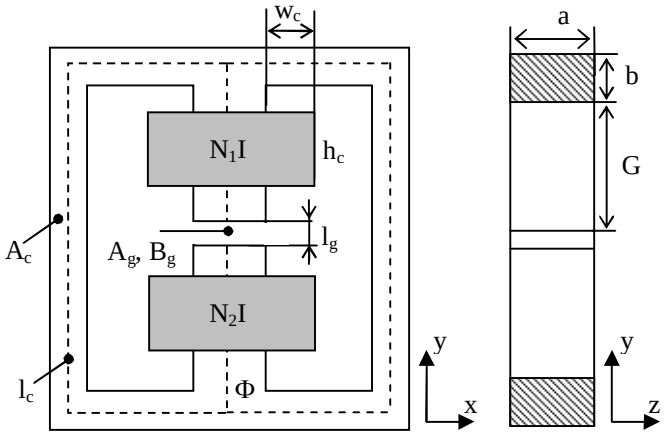

Fig. 53 Parameters of the core for analytical analysis (N_1=N_2 are connected in series).

When fringing fields and leakage flux are neglected, it holds (from Ampereôs law) that

$$H_g = \frac{\Phi}{\mu_0 A_g} \Rightarrow \Phi = H_g \mu_0 A_g \tag{37}$$

$$B_g = B_c = \frac{\Phi}{A_g} \tag{38}$$

$$NI = H_c l_c + H_g l_g \tag{39}$$

where H_g is the value of the magnetic field strength in the air gap, and the H_c value for the calculated B_c value is obtained from the B(H) characteristics of the material that is used. According to Hopkinsonôs law, it holds that

$$R_g = \frac{l_g}{\mu_0 A_g} \tag{40}$$

$$R_c = \frac{l_c}{\mu_0 \mu_a A_c} \tag{41}$$

$$R_T = R_c + R_g \tag{42}$$

$$\Phi = B_g A_g \tag{43}$$

$$F = \Phi R_T = NI \tag{44}$$

where R_c is core reluctance, R_g is air gap reluctance, R_T is total reluctance, μ_a is the amplitude permeability of the material, and F is magnetomotive force. The calculated number of turns N = 1681 turns (Ampereôs law) and N = 1679 turns (Hopkinsonôs law) for current value I = 5 A is valid for the stated parameters: $A_g = 2 \cdot A_c$ = 36 cm^2 (core dimensions a = 60, b = 30 mm), l_g = 10 mm, B_g = 1 T, l_c = 0.55 m and ε_a = 1000 (3% silicon steel, for B_m=1 T). The inductance value L can be calculated from [88], [91]

$$L = \frac{N^2}{R_T} = \frac{\mu_{re} \mu_0 A_c N^2}{l_c}, \mu_{re} = \frac{\mu_a}{1 + \frac{\mu_a l_g}{l_c}} \tag{45}$$

where μ_{re} is the effective permeability.

Placing the coil winding as close to the air gap as possible should keep the leakage flux to a minimum [92]. However, the effect of the fringing fields cannot be neglected, which means that the B_c value should be higher than the B_g value. The core induction value B_{cr} needed for generating B_g = 1T is calculated from

$$B_{cr} = B_c FF \tag{46}$$

where FF is the fringing factor. Empirical equations for determining the FF value can be found in McLyman [88]

$$FF = 1 + \frac{l_g}{\sqrt{A_c}} \ln \frac{2G_l}{l_g} \tag{47}$$

where G_l is the middle column length (see Fig. 53). Other formulas for determining the FF value can be found in Kazimierczuk [90], and the dependence of the fringing factor FF on the core cross-sectional area A_c is presented in Fig. 54. According to (47), the value of FF for A_c = 36 cm^2 and for G_l = 50 mm the value is about 1.4, which means that the value of B_{cr} = 1.4 T. The value of FF decreases with increasing A_c. Because the fringing effect increases the inductance value, the new inductance value L_r is calculated as

$$L_r = L \cdot FF \tag{48}$$

The number of windings N should be recalculated due to the fringing factor FF, or the current value I must be increased.

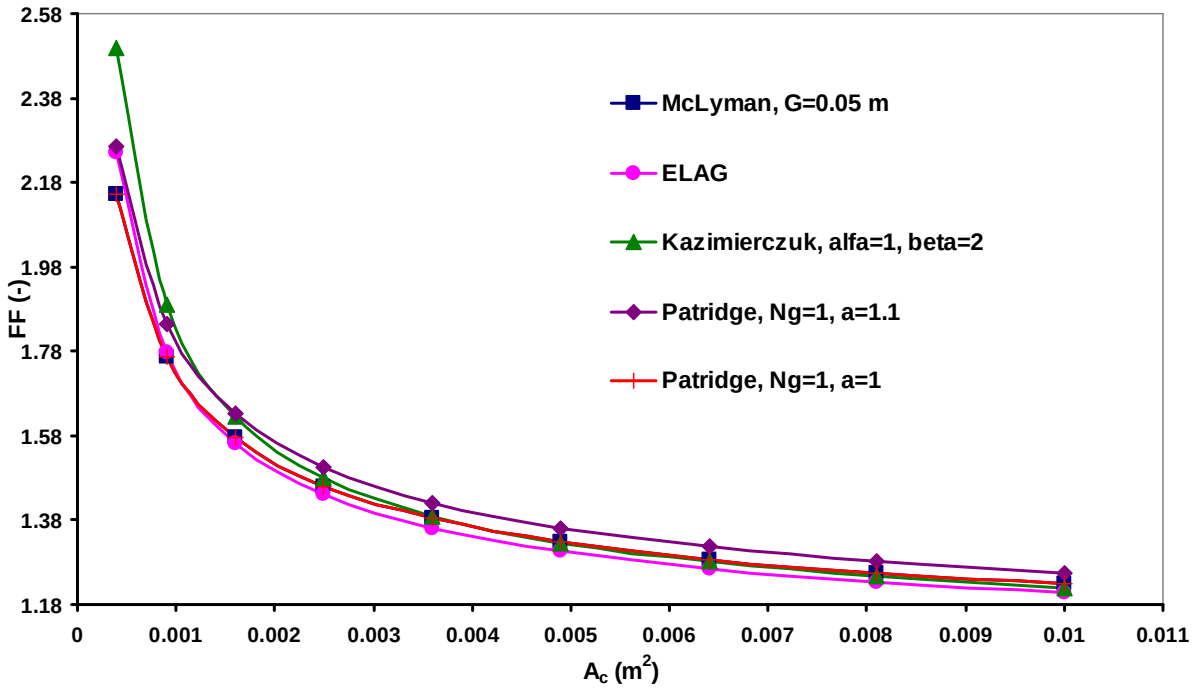

Fig. 54 Dependence of the fringing factor *FF* on the core cross-sectional area A_c (ELAG = effective length of the air gap).

5.1.2 FEM method results

The number of turns N and the core induction B_{cr} were obtained from analytical analysis. The last step was to compare several cores of different shapes (Fig. 55) by the FEM method (FLUX 3D software was used). The FEM method was used to choose a suitable core type from the point of view of the maximum MFD value in the air gap and homogeneity in the air gap. All models have the same parameters, as follows: A_g = 36 cm^2, l_g = 0.01 m, l_c = 0.55 m, material Steel 1010. The value of G_1 = 70 mm and window width of 65 mm was valid for the H shape (H1, H2) and for both UNCIORE cores. The windings of the models have N = 1600 turns (2x800 turns connected in series), a wire diameter of 1.6 mm, winding width w_c = 40 mm, winding height h_c = 51.2 mm, winding position - 1 mm from the air gap and 0.5 mm from the core. Only the winding of the toroid model is wound in 4 layers homogeneously along the core. Simulations were run for a frequency of 50 Hz and a current of 5 A. Table 12 shows the results for the AC MFD value (B_g) in the center of the air gap. It is obvious that the toroid is not appropriate, because its MFD value is almost 45% less than the values for the other models. This big difference is probably caused by the higher *FF* value. Because the G_1 value in (47) is equal to l_c = 0.55 m (for the toroid model), the *FF* value is about 2.6. The differences between the other model values are less than 10%. The homogeneity results on all three axes are shown in Fig. 56, 57 and 58, and in detail in Table 13. Some of the asymmetry in the homogeneity results for the *y*-axis is probably caused by an insufficient mesh in the air gap area. The homogeneity values are very similar, and are acceptable, with the exception of the homogeneity of the toroid model.

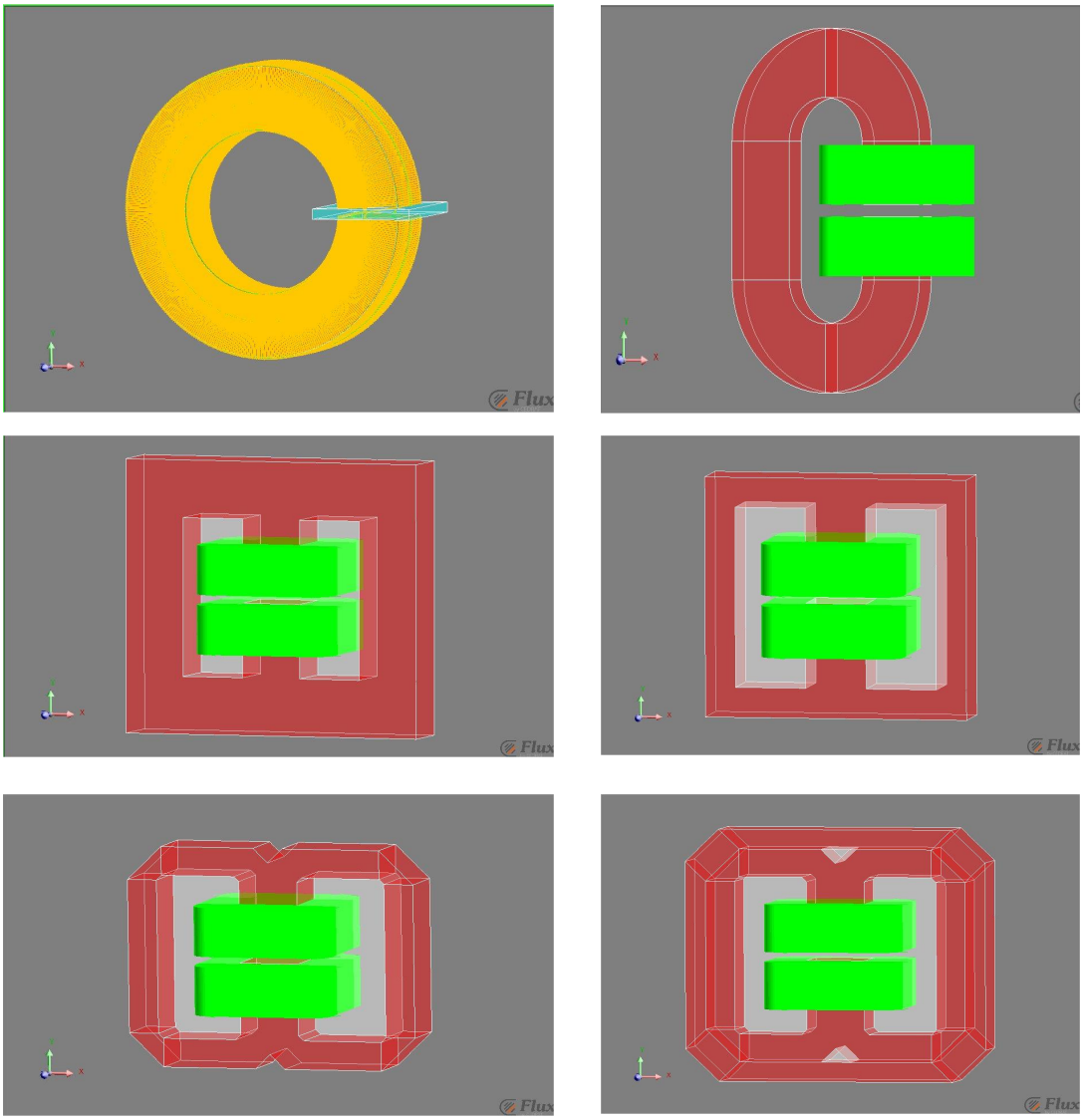

Fig. 55 Models of the compared core types in FLUX 3D software: (from the left) toroid, C shape, H shape (H1; with same A_c value in all legs), H shape (H2; center leg with A_c, side legs with $A_c/2$), UNICORE, 3-phase UNICORE (UNICORE 3f).

Table 12 A comparison of the AC MFD values B_g of the tested core types in the center of the air gap.

Shape	**B_g (T)**
toroid	0.754
C	0.992
H1	1.090
H2	1.023
UNICORE	0.993
UNICORE 3f	1.084

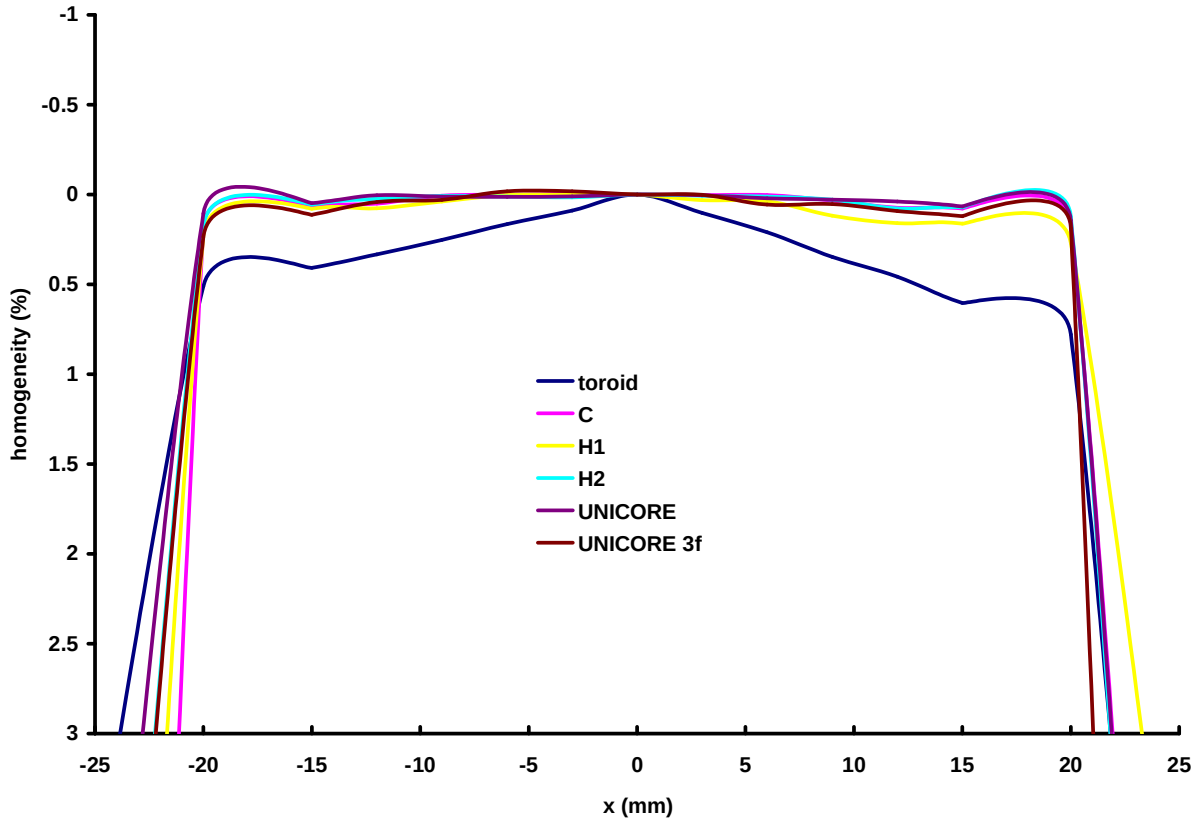

Fig. 56 Homogeneity in the air gap of the compared core types on the *x*-axis.

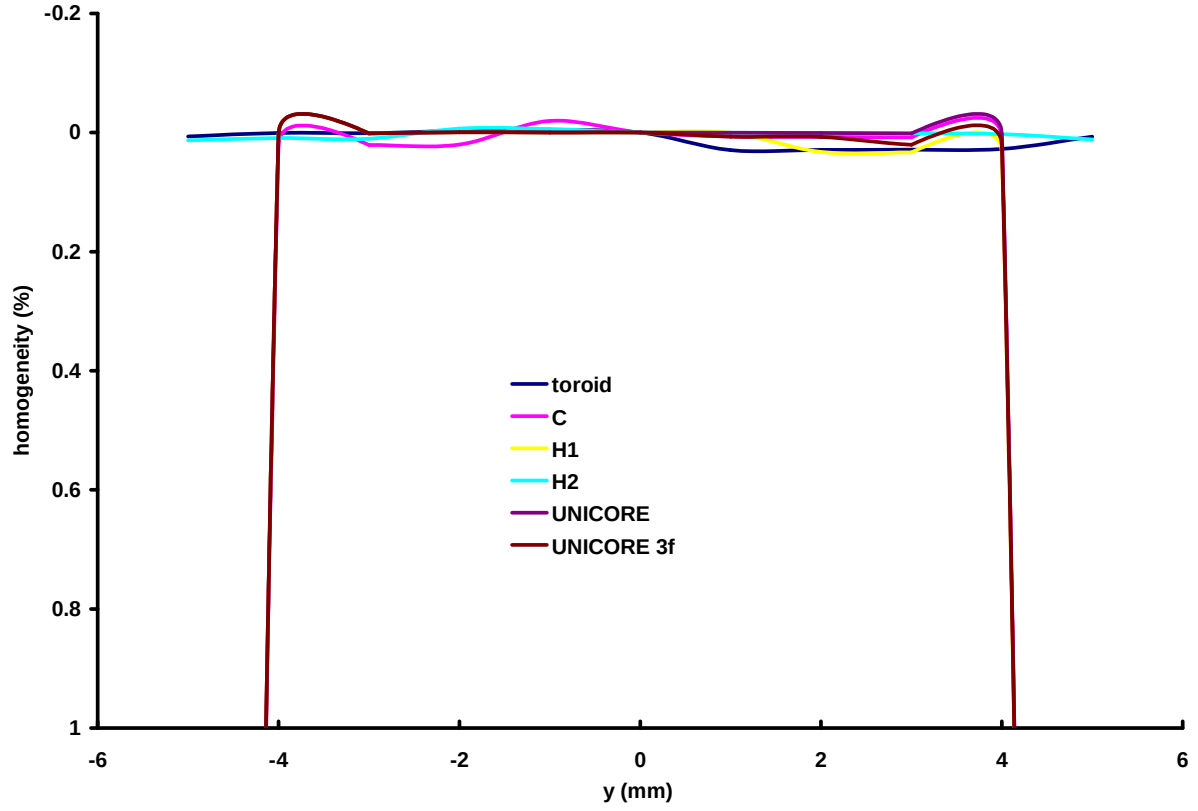

Fig. 57 Homogeneity in the air gap of the compared core types on the *y*-axis.

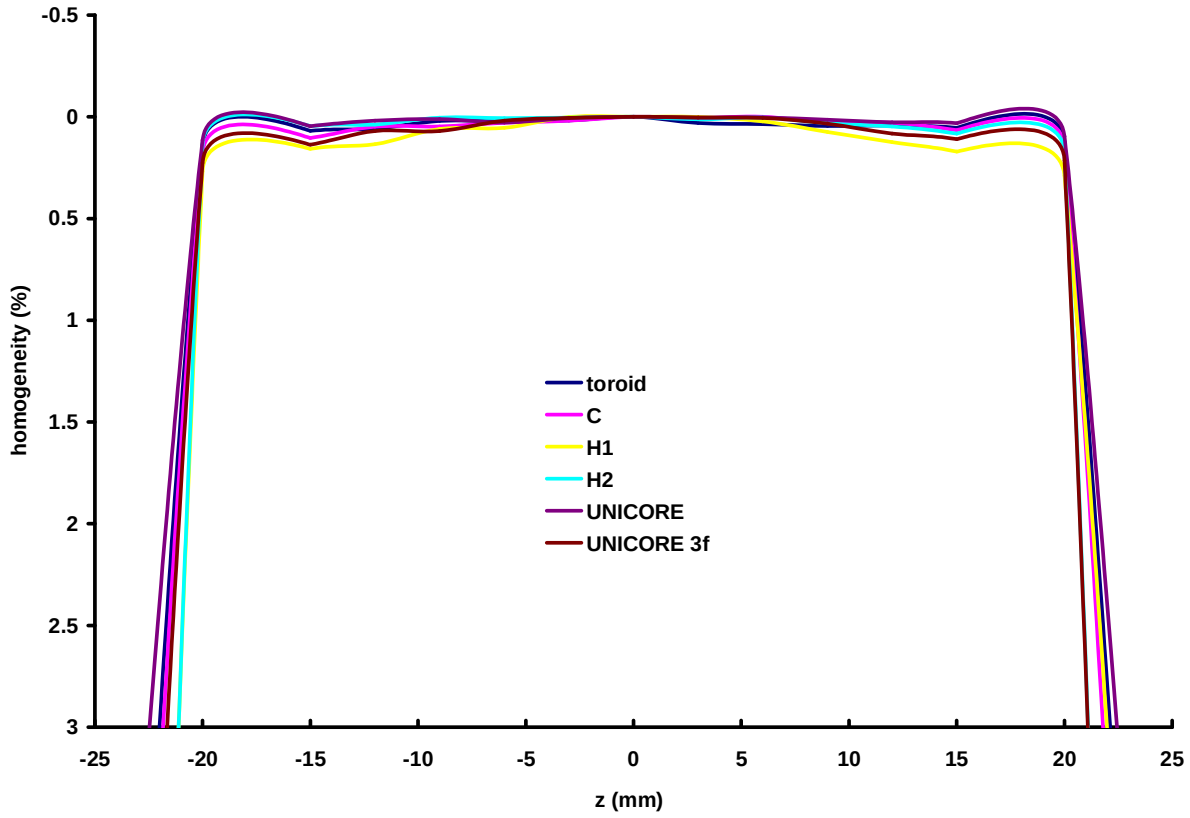

Fig. 58 Homogeneity in the air gap of the compared core types on the *z*-axis.

Table 13 Detailed homogeneity values inside the air gap of the tested core types.

Homogeneity on the x-axis (%)						
x (mm)	**toroid**	**C**	**H1**	**H2**	**UNICORE**	**UNICORE 3f**
15	0.60	0.08	0.16	0.07	0.07	0.12
-15	0.41	0.07	0.08	0.06	0.05	0.11
Homogeneity on the y-axis (%)						
y (mm)	**toroid**	**C**	**H1**	**H2**	**UNICORE**	**UNICORE 3f**
3	0.03	0.008	0.03	0.0006	0.002	0.02
-3	0.001	0.02	0.001	0.01	0.001	0.001
Homogeneity on the z-axis (%)						
z (mm)	**toroid**	**C**	**H1**	**H2**	**UNICORE**	**UNICORE 3f**
15	0.05	0.07	0.17	0.08	0.03	0.11
-15	0.07	0.10	0.16	0.05	0.05	0.14

Due to the the maximum generated value in the air gap and the homogeneity inside the air gap, the UNICORE core was chosen for other simulations and also for realizing the AC electromagnet. It was found during the simulation that the value of MFD in the center of the air gap also depends on the ratio of the winding width w_c and the winding height h_c, and also depends on the position of the winding (Fig. 60). The dependence of the MFD value for various w_c/h_c ratios simulated with the UNICORE core is shown in Fig. 59. There is a difference of less than 0.2% between ratio value 2 and ratio value 1, and there is a difference of about 2.2% between ratio value 1 and ratio value 0.5.

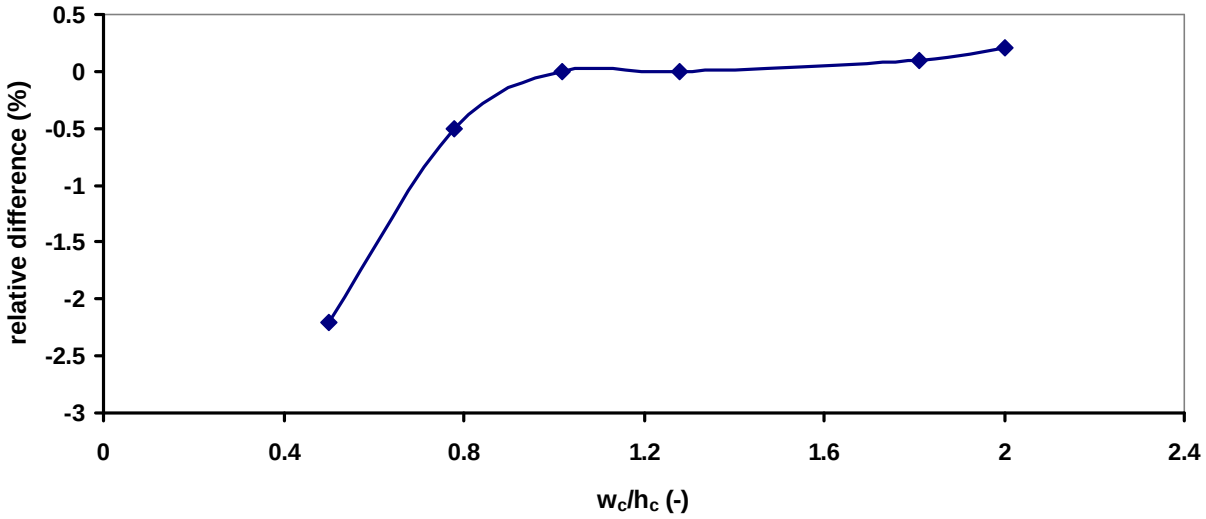

Fig. 59 Dependence of the B_g value on the ratio of the width to the height of the winding. The relative difference is related to the ratio $w_c/h_c = 1$.

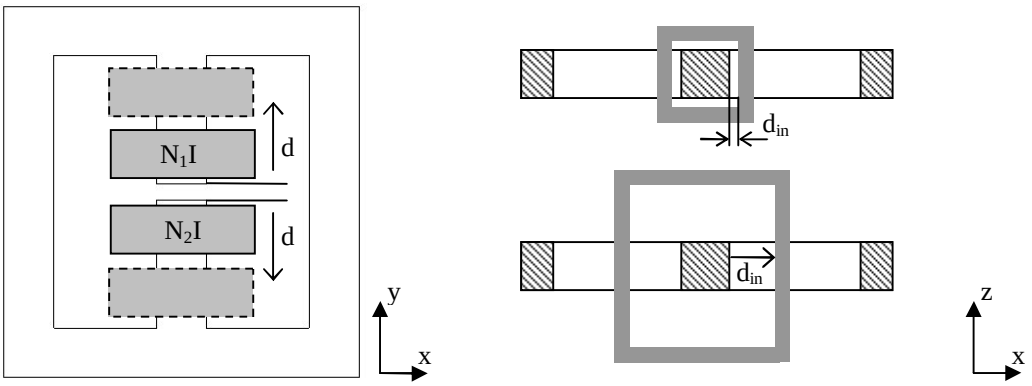

Fig. 60 Position of the winding for a simulation of the dependence of the B_g value on the winding distance d from the air gap (left), the distance d_{in} from the core (right).

As is shown in Fig. 61, the B_g value is very dependent on the distance d of the winding from the air gap (there is a difference of about 28% at 20 mm), so the winding should be placed very close to the air gap. By contrast, the dependence of B_g on the distance of the winding from the core (where the inner diameter of the winding d_{in} was increasing) is much smaller ï there is a difference of 0.4% for a distance of 10 mm and a difference of 1.6% for a distance of 20 mm.

Considering the results of the simulations above and the possibilities of producing such a electromagnet, the final design of the UNICORE core was simulated with the following parameters: $A_g = 2 \cdot A_c = 36$ cm^2, $l_g = 0.01$ m, $l_c = 0.55$ m, $G_l = 45$ mm, material Steel 1010. The windings of the model have $N = 1600$ turns (2x800 turns connected in series), wire diameter 1.6 mm, winding width $w_c = 61$ mm and winding height $h_c = 34$ mm (the w_c/h_c ratio about 1.8), winding position ï $d = 1$ mm from the air gap and $d_{in} = 2$ mm from the core. Simulations were run for a frequency of 50 Hz and 5 A current (Fig. 62), and $B_g = 1.245$ T was generated in the air gap.

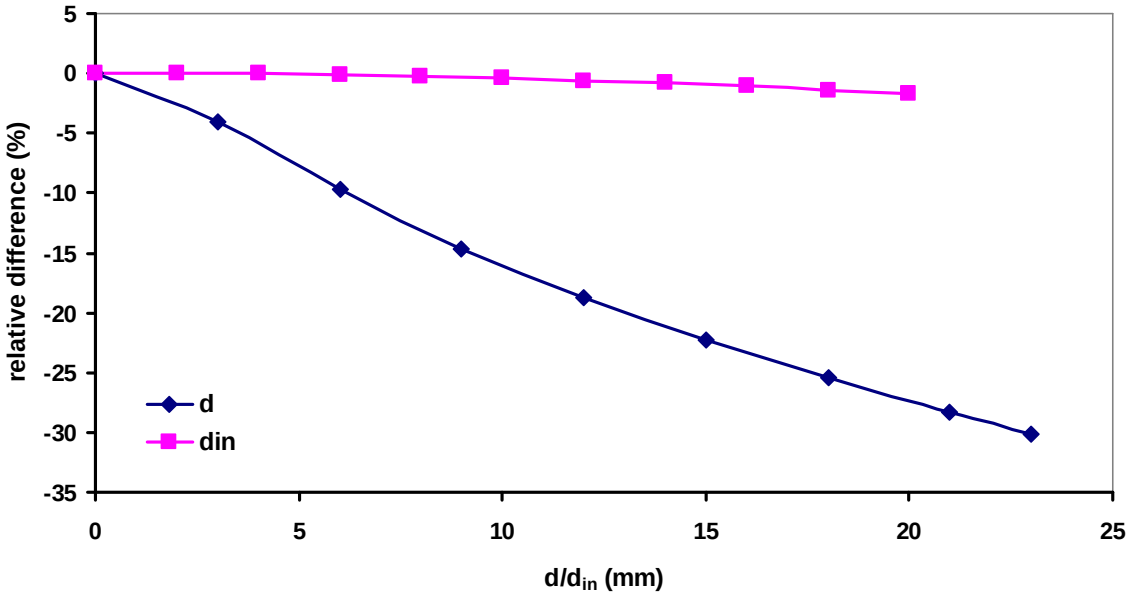

Fig. 61 Dependence of the B_g value on the winding distance d_{in} from the core and the distance d from the air gap for the UNICORE core.

a)

b)

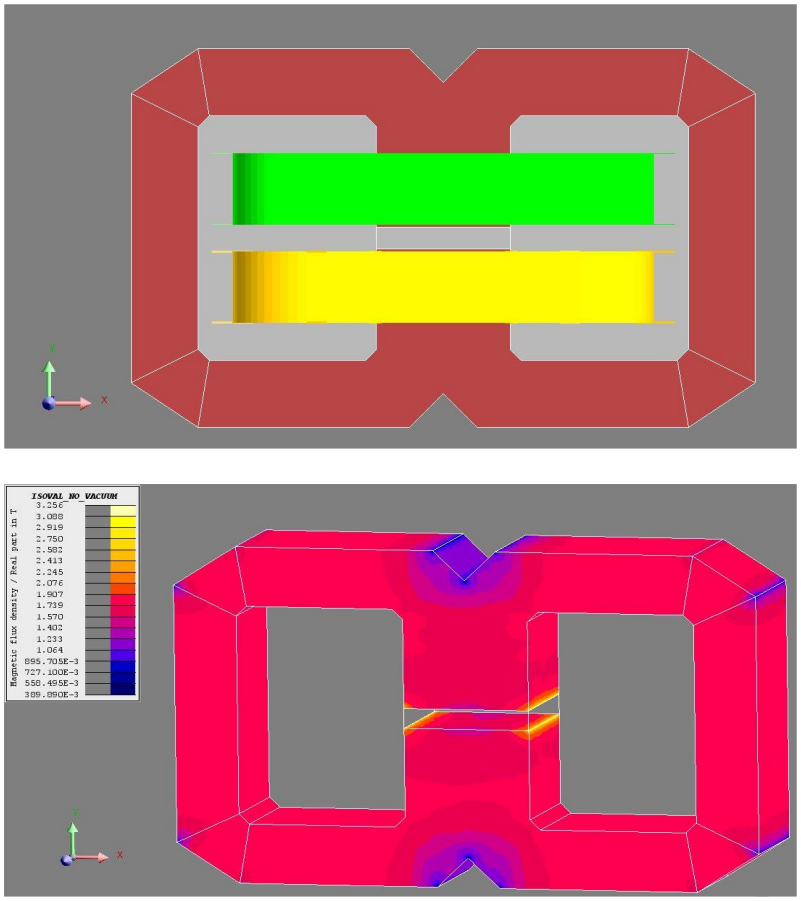

Fig. 62 Final model of the AC electromagnet with UNICORE shape a), and simulation results ï magnetic flux density distribution at 50 Hz b).

5.2 PCB search coils

The set MFD value in the air gap of the AC electromagnet, the design of which was described above, must be precisely measured to ensure traceability of the calibrated magnetometer. This traceability will be ensured by a search coil with a voltmeter. When a search coil is used, the area turns (the search coil constant) is very important for calculating the MFD value. Its inductance value or resonance frequency value, which is determined by its impedance, is important for determining the frequency dependence of the search coil. The estimated electromagnet air gap length is 10 mm and the homogeneity of the magnetic flux density within an area of (60x60) mm. The search coil that is used must therefore be thin, with the highest area turns value within an area of about (10x10) mm and with a low inductance value. Hand-wound search coils are the most widely-used type of flat search coils. Their area turns value can vary from 1 cm^2 to 100 cm^2 with an outer diameter up to 10 mm. However, the thickness of these search coils varies from 1 mm to 2 mm, and they are only circular in shape. Integrated planar coils have many applications in sensors and in MEMS devices [93]-[95], and also in RF and microwave applications [96], [97], in biomedical applications [98]-[100], and in power applications [101]-[103]. If photolithography is used for fabricating planar search coils, a turn/space less than 20 ε m in width (down to a few ε m) can be achieved using this technology. A higher area turns value with a smaller diameter than the PCB search

coil, and with much smaller thickness than on a hand-wound search coil, can be achieved with this technology. However, the thickness of the copper will be reduced, and this rapidly increases the resistance of the coil. And as the turns will be closer to each other, the inductance value will also be higher. Another disadvantage of this method is its high price, which implies that usually only a single-layer or double-layer planar coil can be fabricated. In recent years, additive manufacturing (3D printing technology) has also been used for fabricating planar coils [104]-[106]. The PCB method is limited by the technology that is used. The minimum dimension of the turn/space is 100 ε m, and the smallest diameter of the drilled hole is also 100 ε m. However, the method is cheap and simple, it has good repeatability, uniform cross sections, and a planar coil with more than 10 layers can be fabricated. New planar single-layer, double-layer and 10-layer search coils for B_m measurements have been designed and produced by the PCB method, and are characterized in this work.

When assuming low values of w and s (w = s = 100 ε m), the following approximate formulas for area turns calculations can be used. The two most widely-used types of PCB coils are shown in Fig. 63. The area turns value of a single-layer square coil according to Fig. 64a is calculated from

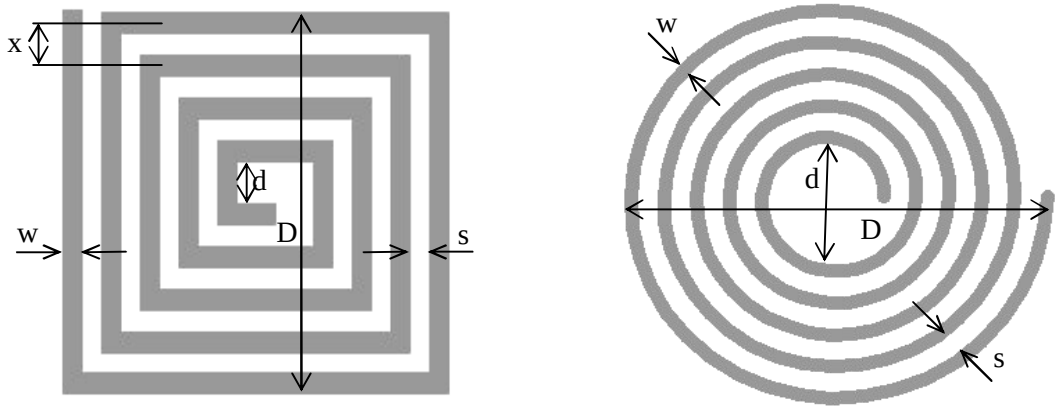

Fig. 63 Dimensions of the planar square and circular coils.

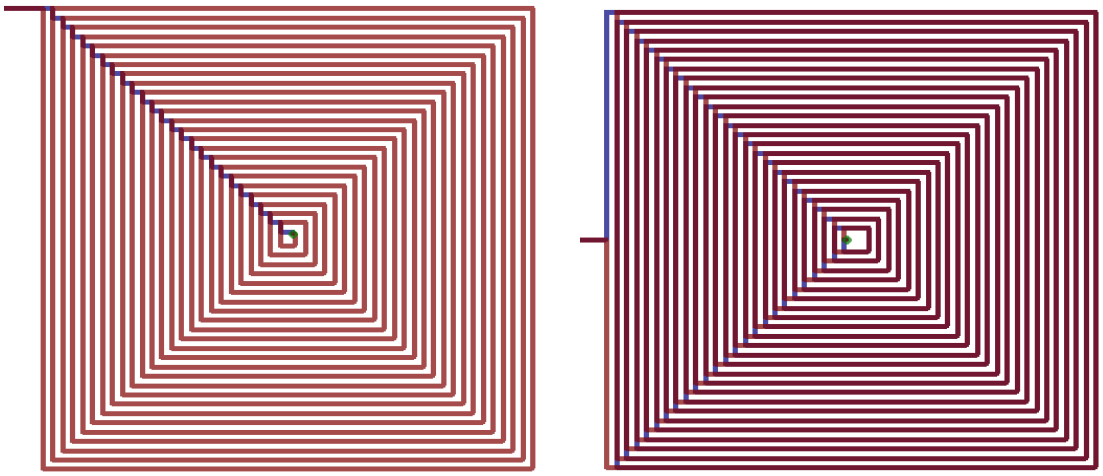

Fig. 64 Layout of a) a single-layer PCB search coil (left) with d=200 ε m, and b) a double-layer PCB search coil and a 10-layer PCB search coil (right) with d=400 ε m. The width of the turn/space is 100 ε m and the number of turns is 25. Red wire=top layer, blue wire=bottom layer.

$$S_{1L} = D^2 + \sum_{i=1}^{N} (D - xi)^2 , \tag{49}$$

where D is outer diameter, N is number of windings, and x is the difference between the center of the sides of the square (Fig. 63). The value of D can be calculated as [91]

$$D = \mathrm{d}_0 + 2\,\mathrm{Nw} + 2(\mathrm{N}\text{-}1)\mathrm{s}, \tag{50}$$

where d_0 is inner diameter, w is turn width and s is space width. For $w = s$ there applies $x = w + s$. Eq. (49) can be expressed as

$$S_{1L} = D^2 + ND^2 - 2xD\frac{N+1}{2}N + x^2\frac{1}{6}N(N+1)(2N+1). \tag{51}$$

Formula (49) can also be used for a circular single-layer PCB coil only multiplied by ´:

$$S = \pi\left[R^2 + \sum_{i=1}^{N}(R - xi)^2\right], \tag{52}$$

where $R = D/2$. It is obvious that the area turns value of a square PCB coil is higher than the area turns value of a circular PCB coil, so henceforth only square PCB coils will be considered here. It is rather more complicated to calculate the area turns value of the double-layer PCB coil according to Fig. 64b, because the calculation must be separated into the sum of the areas of the squares and the rectangles. For the bottom half of the area, S_1 applies

$$S_1 = D^2 + \sum_{i=1}^{N}(D - 2xi)^2 = D^2(N+1) - 2N(N+1)xD + \frac{2}{3}N(N+1)(2N+1)x^2 . \tag{53}$$

And for the top half of the area, S_2 applies

$$\begin{aligned} S_2 &= D(D-x) + \sum_{i=1}^{N}(D - 2xi)(D - 3ix) = \\ &^2(N+1) - \left[\frac{5}{2}N(N+1) + 1\right]xD + N(N+1)(2N+1)x^2 \end{aligned} \tag{54}$$

The total area turns value of the double-layer PCB rectangle coil is calculated as

$$S_{2L} = 2(S_1 + S_2) = 2D^2(N+1) - \left[\frac{9}{2}N(N+1) + 1\right]xD + \frac{5}{3}N(N+1)(2N+1)x^2 \tag{55}$$

The area turns value of the multi-layer PCB coil is then determined simply from the formula (55) by multiplying the number of layers/2. Formulas (49)-(55) can be used only for approximate calculations of the area turns value. Analytical formulas for resistance and inductance calculations of can be found in [J3].

Single-layer, double-layer and 10-layer PCB search coils were also designed and simulated in the CST Studio environment by FIT [107]. Search coil windings were designed with parameters and layout according to Fig. 64 on the assumed PCB FR-4 substrate with dimensions of (12x12) mm. A low-frequency (LF) domain solver with full wave analysis and adaptive mesh refinement to achieve higher accuracy was used for the simulations. A description of the simulation is presented in [J3].

A single-layer search coil (according to Fig. 64a), a double-layer search coil and a 10-layer (according to Fig. 64b) search coil were designed and produced on an FR-4 type PCB board 10 cm in length, 1.5 cm in width, and 0.5 mm thickness (the 10-layer coil is 1.2 mm in thickness), see Fig. 65. The dimensions of the search coils are: $w = s = 100$ εm, $N = 25$, $t = 18$ εm, d(1-layer) = 196 εm, d(2-layer) = 398 εm and d(10-layer) = 450 εm. Copper thickness

of t = 18 μm applies to the single-layer and double-layer search coils, and applies to the 10-layer coil only for the first layer and for the last layer. In the remaining 8 layers, the copper thickness is 65% of this value (11.7 εm). The diameter of the drilled holes is 100 εm, and the restring is 75%. The top and bottom wire from the coil to the connector are conducted one above the other to avoid an additional loop turn.

The calculated and measured parameters of the fabricated PCB search coils are presented in Table 14. It is clear from Table 14 that there is good agreement between the measured resistance value, the calculated resistance value and the simulated value from the CST Studio. Only the measured resistance value of the single-layer PCB search coil is much higher than the calculated value and the simulated value. This is probably caused by the PCB manufacturing process, due to the reproduction tolerances [108]. The effect of the via on the area turns value can be neglected, because the area of one via is only 0.04 mm^2. The thickness of the copper and the trace width have a very big influence on the resistance and inductance values. As concerns the inductance of the PCB search coils, there is very good agreement between the calculated values, the CST Studio values, and the values measured by an LCR bridge. A relative difference of less than 8% was determined for the single-layer PCB coil, a difference of less than 3.2% for the double-layer PCB coil, and a difference of less than 6.2% for the 10-layer PCB coil. The PCB search coil constant value was calibrated using the variable mutual inductance method [84], with a DC electromagnet used as the magnetic flux density standard. The search coil is placed in the center of a DC electromagnet to ensure that the greatest magnetic flux passes through. A magnetic flux density value of 1 T was used. The magnetic flux value was measured by an EF 5 fluxmeter (Magnet-Physik). Webermeter EF 5 was then calibrated by a coil standard of the magnetic flux. The current value through the magnetic flux standard was set to the same value as the measured magnetic flux value.

Table 14 Calculated and measured parameters of the fabricated PCB search coils.

Parameter	**Value**		
	SC1L (single-layer)	**SC2L (double-layer)**	**SC10L (10-layer)**
Calculated K_S value (cm^2)	8.57	16.03	81.4
K_S value from the CST Studio (cm^2)	8.58	16.41	81.0
Measured K_S value (cm^2)	8.52	16.31	81.6
Calculated resistance (q)	4.9	9.75	68.9
Resistance from the CST Studio (q)	4.7	9.8	63.4
Measured resistance (q)	6.2	9.6	62.7
Calculated inductance (Wheeler) (εH)	2.57	9.44	221
Calculated inductance (Rosa) (εH)	2.69	9.84	229
Inductance from the CST Studio (εH)	2.82	9.57	223
Measured inductance (εH)	2.79	9.75	210
Measured resonance frequency (MHz)	7.3	3.8	3.1
Coil diameter D (mm)	9.99	10.2	10.25
Coil length l (m)	0.51	1.02	5.1

A correct magnetic flux value was calculated from the current value and from the constant of the magnetic flux standard. The search coil DC constants were calibrated with expanded uncertainty of 0.08%. The differences from the calculated DC value according to (51) and according to (55), the simulated values from the CST Studio and the measured values are less than 0.7% (for the single-layer search coil), less than 2.4% (for the double-layer search coil) and less than 0.8% (for the 10-layer search coil). This also indicates very good agreement. A comparison of the calculated (according to (18)), simulated and measured frequency dependence of the PCB search coil constant is presented in [J3] as the comparison with hand-wounded search coils parameters.

In 2017, there was a bilateral comparison of measurements of magnetic quantities between CMI and VNIIM, Russia. One part of this comparison was the calibration of PCB search coils described above. A serious problem was revealed during this comparison. The first measurement was made with the connectors shown in Fig. 65. The results were not correct (the connector caused an additional loop) and the measurement at VNIIM was made without this connector [109]. The differences between the results were too great (from 0.7% up to 1.4%). On the recommendation of VNIIM, the original connector was dismounted and was replaced, as shown in Fig. 66. The results of the second measurement were then comparable (see Table 15).

Fig. 65 Fabricated PCB search coils: single-layer SC1L (top), double-layer SC2L (middle) and 10-layer SC10L (bottom).

Table 15 Reported results of the PCB search coils from the bilateral comparison.

	CMI		**VNIIM**	
Search coil	**K_S (cm^2)**	***U*(S) (%)**	**K_S (cm^2)**	***U*(S) (%)**
SC1L	8.599	0.08	8.589	0.1
SC2L	16.388	0.08	16.409	0.1
SC10L	83.02	0.08	83.08	0.09

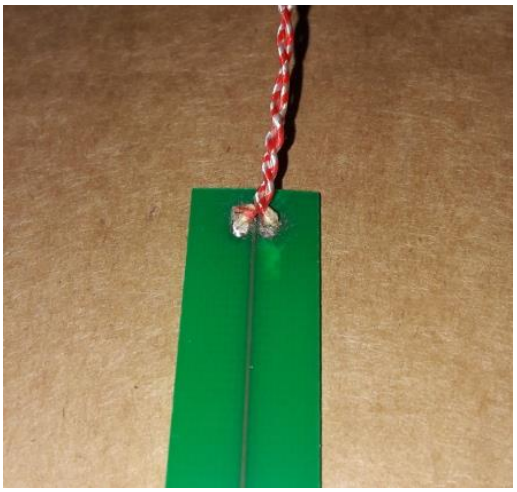

Fig. 66 The new connector of the PCB search coil.

The differences between the new measured DC value and the simulated values from the CST Studio are about 0.23% (for the single-layer search coil), about 0.13% (for the double-layer search coil) and about 2.4% (for the 10-layer search coil). The new differences between the calculated DC value according to (51) and according to (55) and the new measured values are about 0.35% (for the single-layer search coil), about 2.2% (for the double-layer search coil) and about 2% (for the 10-layer search coil).

5.3 Setup for Hall probes calibration up to 1 T

In general, it is necessary to use a material with a small loss value and with high permeability in AC applications (e.g. up to 1 kHz) to produce an AC electromagnet. A thin strip must be used to minimize the eddy current losses. Widely-available 3% silicon steel has a saturation value of about 2 T, strip thickness from 0.05 mm, a broad range of strip widths, and high total loss in higher frequencies. This means that it is useful for the low frequency range. A Co-Fe based material (VACOFLUX) has a high saturation value up to 2.3 T and total loss at B = 1 T at a frequency of 1 kHz about (55 to 70) W/kg [110]. The AC electromagnet with a UNICORE core and with the parameters described above was produced from grain-oriented silicon steel with a strip thickness of 0.15 mm and with w_c/h_c = 1.8 (Fig. 67). The electromagnet windings are rated at 5 kV. The calculated inductance value according to (44) was 1.4 H. The corrected inductance value according to (47) with FF = 1.4 was 1.96 H, and the measured inductance value was 1.8 H.

When an AC electromagnet is fed directly from the power amplifier, the AC MFD value in the air gap cannot be greater than [111]

$$B = \sqrt{\frac{\mu_0 P}{2\pi f V}}, \tag{56}$$

where P is the output power of the amplifier, f is the frequency of the generated AC MFD, and V is the volume of the air gap. It is not difficult to calculate that an amplifier with output power of at least 9 kW must be used to generate B = 1 T at a frequency of 50 Hz in an air gap volume of (60x60x10) mm^3.

Fig. 67 The AC electromagnet with a UNICORE core.

During the development of the system it was therefore decided to use the serial resonance effect, which can minimize the required voltage range of the amplifier. A block diagram of the system for generating AC magnetic flux density up to 1 T is shown in Fig. 68. The electromagnet winding is powered from the power amplifier. A high voltage capacitor C (which is composed of several capacitors of the same type), rated at 5 kV, is connected in series with the electromagnet winding to create an LC tank circuit. This enables us to use a common power amplifier. An OPA140AID operational amplifier produces a feedback to improve the stability of the MFD generated in the air gap of the electromagnet. One input of the OPA140AID is the output from the search coil S, which is located in the air gap of the electromagnet, and the second input is brought from the generator. The output voltage from the search coil is also sampled by the A/D converters of a 3458A multimeter. The 3458A is connected to the computer with measurement software created in LabWindows CVI via a GPIB bus. The RMS value, the peak value, the frequency and the form factor of the MFD value generated in the air gap are calculated from the sampled output voltage in this software. A single-layer PCB search coil 0.5 mm in thickness with a constant value of 8.6 cm^2, and a two-layer PCB search coil 0.5 mm in thickness with a constant value of 16.4 cm^2, were designed and fabricated for AC MFD measurements in the air gap of the electromagnet [J3].

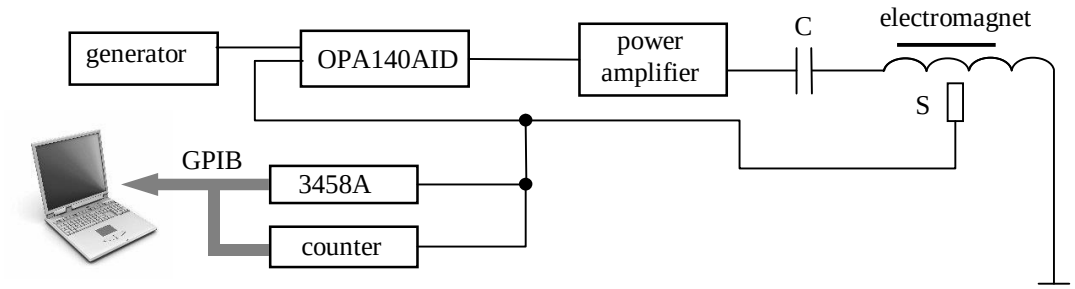

Fig. 68 Block diagram of the system for generating AC magnetic flux density up to 1 T.

5.4 Measurement results

A single-layer PCB search coil was used for the homogeneity measurements, and a comparison was made with the homogeneity simulated in Flux 3D (Fig. 69, Fig. 70 and Fig. 71). The measured homogeneity is better than 0.04% on the x-axis and on the z-axis at a distance of 10 mm from the center of the air gap, and it is better than 0.2% on the y-axis at a distance of 4 mm from the center of the air gap. The measured homogeneity is sufficient for widely-used Hall probes less than 2 mm in thickness and less than 6 mm in width. The measured AC MFD value is calculated from formula (19) or (20), where U_{RMS} is the RMS value of the output voltage (U_{AVG} is the arithmetic mean value of the output voltage) of the search coil sampled using an Agilent 3458A digital multimeter. The type B relative uncertainty of the measured AC MFD value can be calculated as

$$u_{\mathrm{Bc}} = \sqrt{u_{\mathrm{f}}^2 + u_{\mathrm{SC}}^2 + u_{\mathrm{U}}^2 + u_{\mathrm{d}}^2 + u_{\mathrm{h}}^2}\,, \tag{57}$$

where u_{f} is the relative standard uncertainty of the frequency measurement, u_{SC} is the uncertainty of the search coil constant, u_{U} is the uncertainty of the search coil output voltage (arithmetic mean or RMS) measurement, u_{d} is the uncertainty of the directional dependence measurement of the search coil, and u_{h} is the uncertainty of the influence of the homogeneity inside the electromagnet air gap. The input quantities of the type B uncertainty sources are assumed to be uncorrelated. The maximum uncertainty value of the frequency measurement usually varies within tens of ppm, so it can be neglected, because the other uncertainties are typically higher. The uncertainty of the PCB search coil was 0.04%. The value of u_{U} can lie in the order of thousandths of one percent. The value of u_{d} can lie in the order of hundredths to tenths of one percent, and the value of u_{h} can lie in the order of hundredths to tenths of one percent.

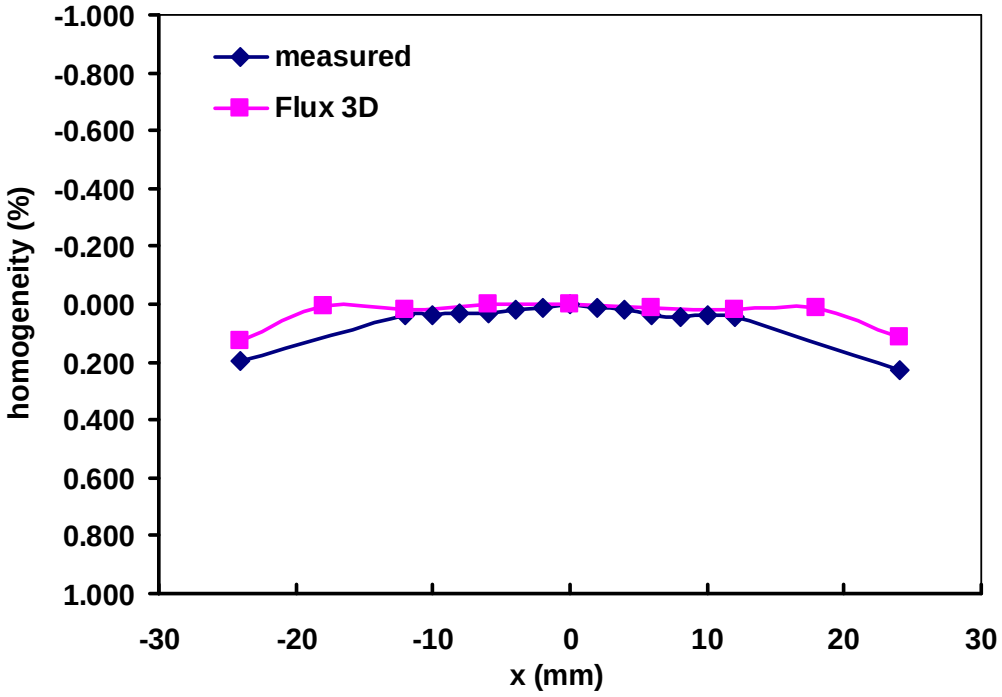

Fig. 69 Homogeneity in the air gap of the UNICORE core on the *x*-axis.

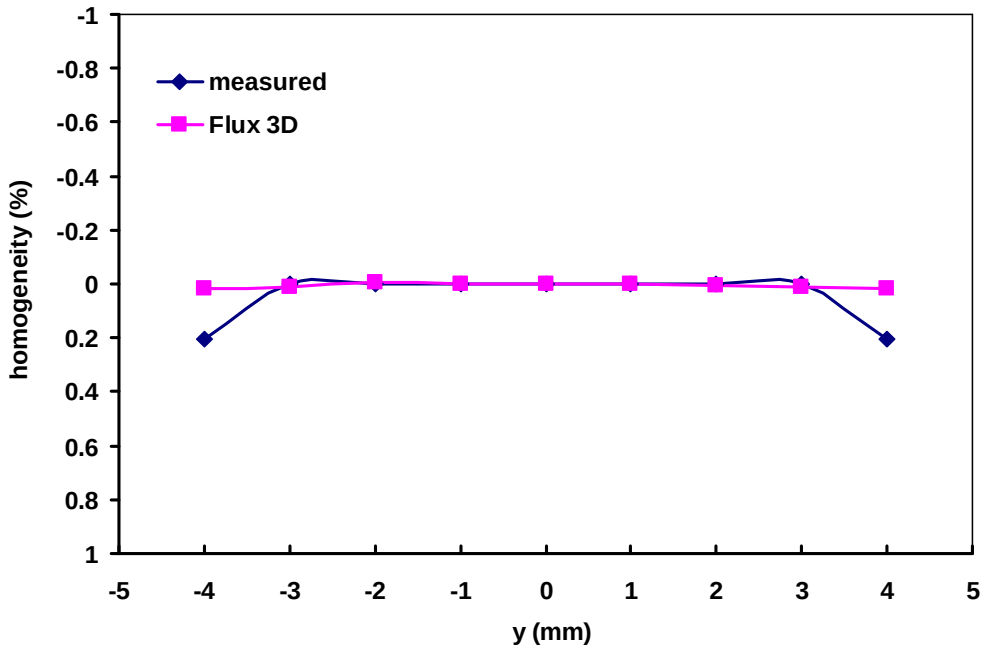

Fig. 70 Homogeneity in the air gap of the UNICORE core on the *y*-axis.

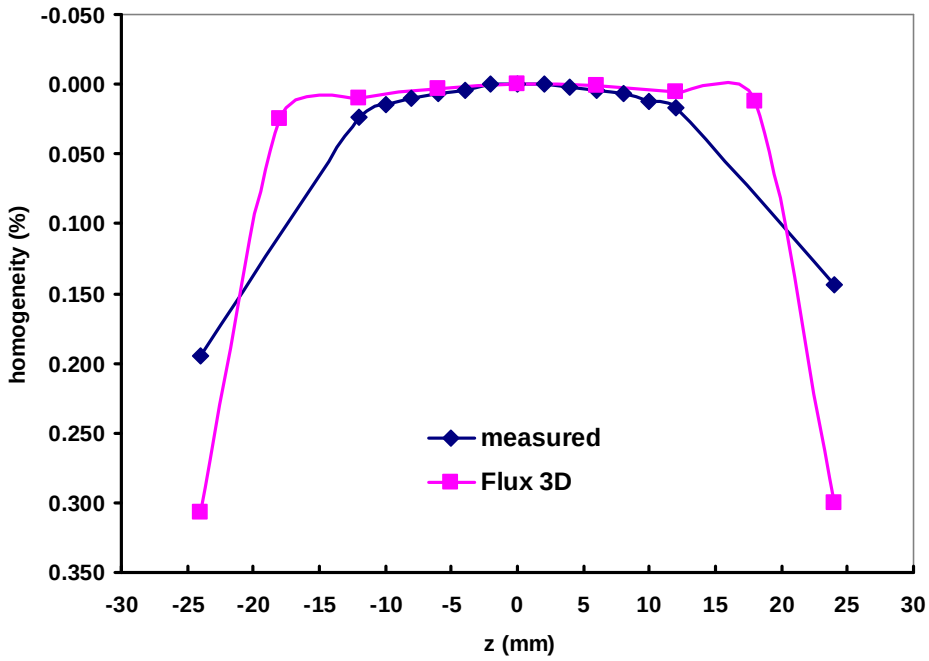

Fig. 71 Homogeneity in the air gap of the UNICORE core on the *z*-axis.

The system was tested at a frequency of 50 Hz, where an AC magnetic flux density value of 0.9 T (RMS) was reached, due to the limitations of the power amplifier that was used. The AC magnetic flux density value was measured using a double-layer PCB search coil with expanded uncertainty of 0.2%. Fig. 72 shows the measured stability of the AC MFD value generated in the air gap with and without the feedback. Stability of 1 mT was measured without the feedback, and stability of 0.08 mT was measured with the feedback. The form factor of the AC MFD was about 1.121 using the feedback. These are sufficient values.

However, the feedback was usable only up to about 0.35 T. Above this value, the feedback became unstable, probably due to the technical limitations of the power amplifier. Fig. 73 shows the main window of the software used for the AC MFD measurements.

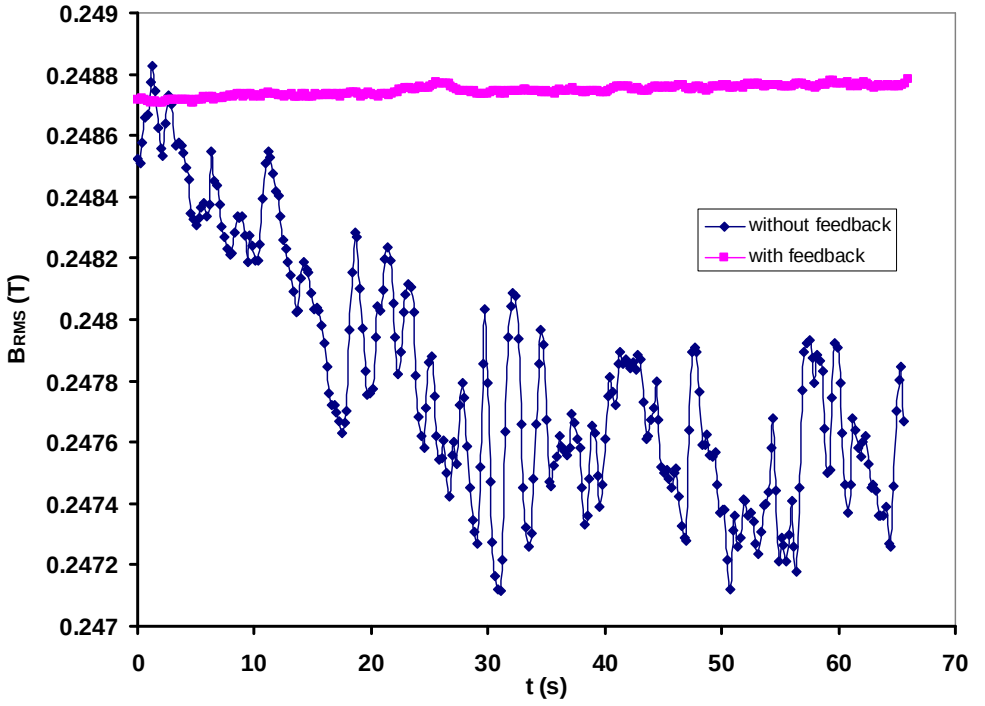

Fig. 72 Measured stability of the AC MFD generated in the air gap with and without the feedback.

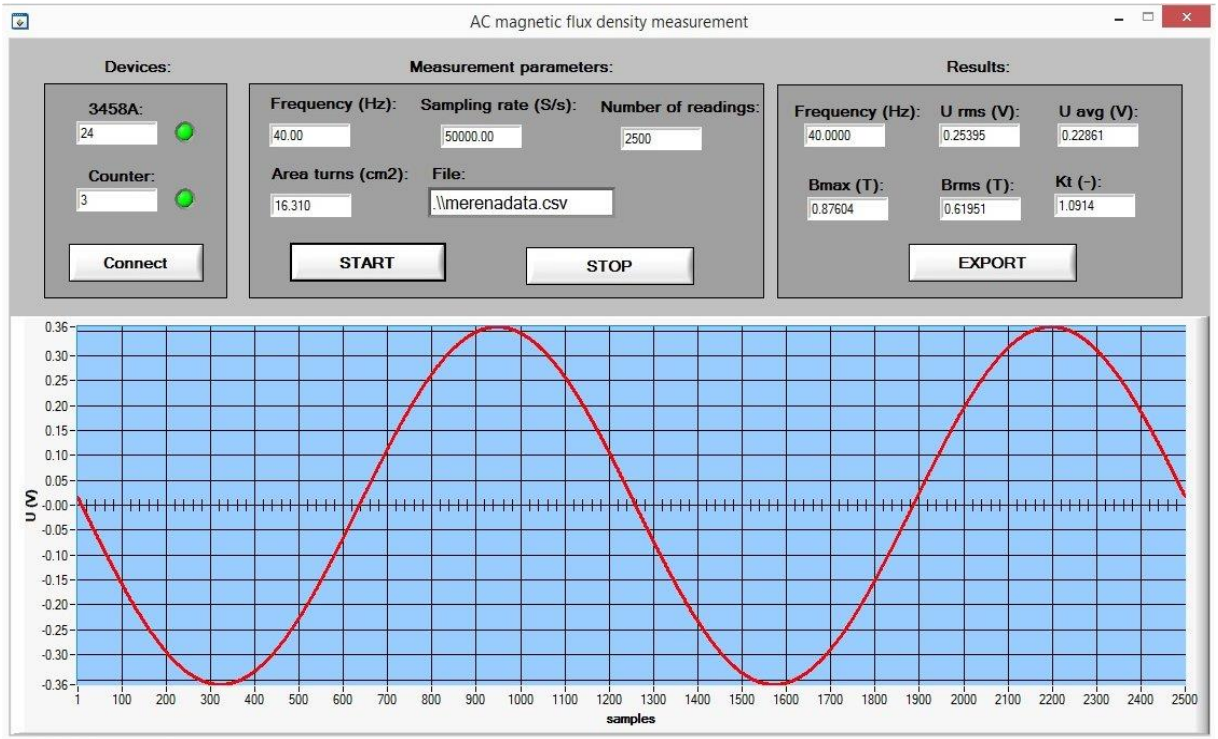

Fig. 73 Main window of the software created for AC MFD measurements.

5.5 Expanding the frequency range up to 1 kHz with an amorphous AC electromagnet

The AC electromagnet made from grain-oriented steel described above can be used only in the low frequency range (up to 70 Hz). At higher frequencies, above 70 Hz, an AC electromagnet with a core made from a material with a low loss value should be used. A nanocrystalline and amourphous material has a low loss value at higher frequencies, high permeability, strip thickness from a few tens of ε m, but a low saturation value, and the maximum strip width is only 50 mm. Commonly available nanocrystalline materials such as Vitroperm (Fe-Si-B-Nb-Cu) and Finemet (Fe-Si-B-Nb-Cu) have a saturation value from about 1.2 T to 1.3 T [112], [113]. Materials such as Nanoperm (Fe-M-Nb-B, M = Zr, Nb or Hf), Hitperm (Fe-Co-M-B-Cu, M = Zr, Nb or Hf) and their modifications have a saturation value higher than 1.6 T [114], [115] and total losses of a few tenths of W/kg at lower frequencies. NanoMet material (Fe-Si-B-P-Cu) has a saturation value of 1.8 T [116]-[118], but it is not yet available for commercial use. Co-based amorphous materials such as Vitrovac have a saturation value lower than 1 T [119]. The typical saturation value of an Fe-based amorphous material is about 1.5 T (the saturation value of MetGlass 2605HB1 is about 1.64 T [120]). The strip thickness of MetGlas 2605 is 25 ε m, while the strip thickness of the grain-oriented steel used in the UNICORE core is 0.15 mm.

A core made from Metglas 2605SA1 material with a cross-sectional area of 36 cm^2 and with an air gap length of 10 mm was manufactured (Fig. 74a). The electromagnet windings are the same as in the case of the UNICORE yoke - 2x800 turns connected in series and wound with a copper wire 1.6 mm in diameter. The electromagnet windings are also rated at 5 kV. The core was eventually pulled down by a steel structure (Fig. 74b). The winding resistance values and the inductance values are similar to those for the winding of the UNICORE electromagnet (R = 6.3 q ; L = 1.88 H). The system described above was used to measure the AC magnetic flux density in the center of the air gap in the amorphous electromagnet. A serial resonance effect was also used ï a capacitors with a nominal value of 2.7 ε F, 84 nF and 15 nF and with a nominalvoltage value of 6 kV were connected in series with the electromagnet winding. The measured RMS values of the AC magnetic flux density were 280 mT (80 Hz), 160 mT (405 Hz) and 90 mT (930 Hz). Again, a single-layer PCB search coil was used for the homogeneity measurements, and a comparison was made with the homogeneity simulated in Flux 3D (Fig. 75, Fig. 76 and Fig. 77). The measured homogeneity

Fig. 74 a) Core made from Metglas 2605SA1, b) the AC electromagnet made from Metglas 2605SA1 material.

was better than 0.1% on the x-axis and on the z-axis at a distance of 20 mm from the center of the air gap and it was better than 0.01% on the y-axis at a distance of 3 mm from the center of the air gap.

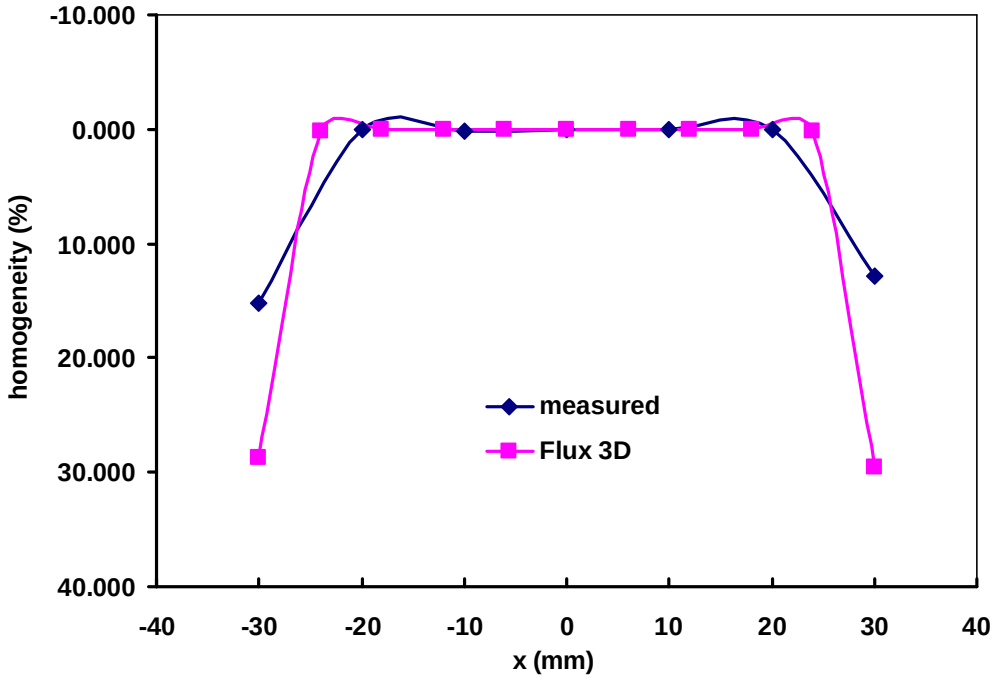

Fig. 75 Homogeneity in the air gap of the amorphous core on the *x*-axis.

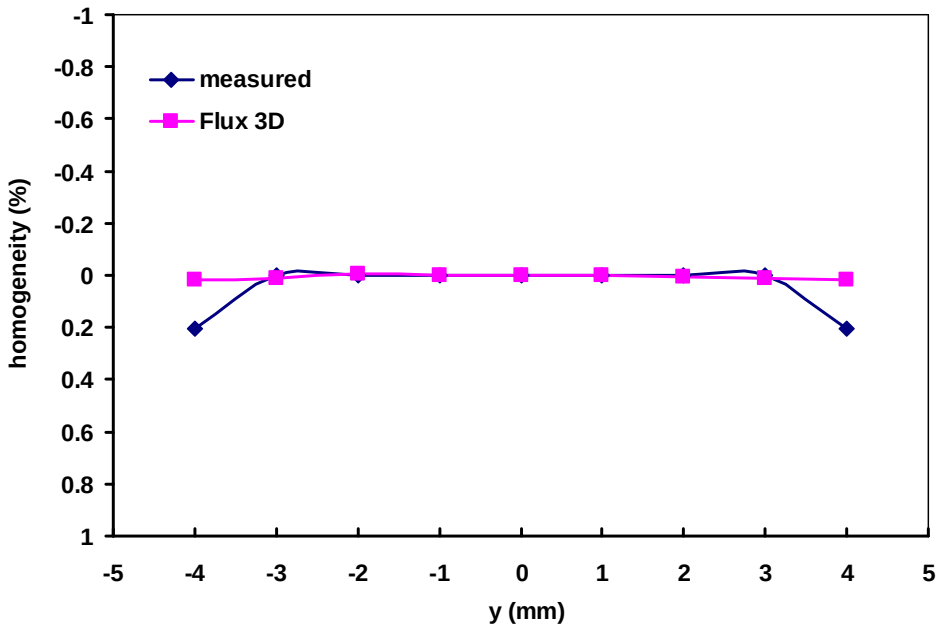

Fig. 76 Homogeneity in the air gap of the amorphous core on the *y*-axis.

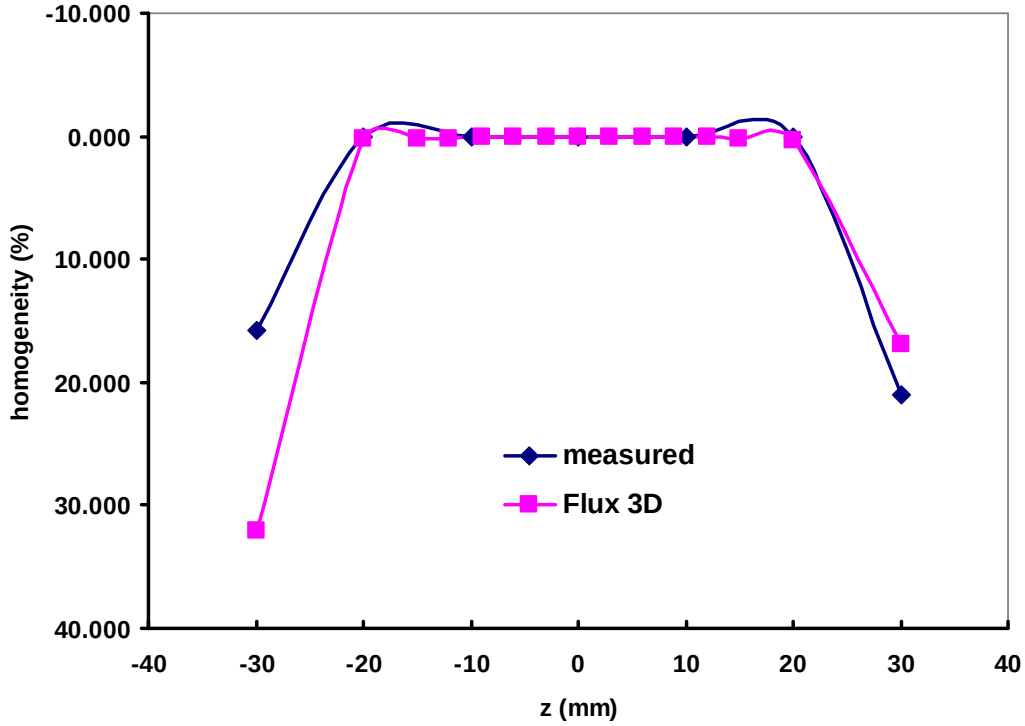

Fig. 77 Homogeneity in the air gap of the amorphous core on the *z*-axis.

5.6 Summary

A system for generating AC magnetic flux density up to 1 T for lower frequencies has been designed and realized. An AC electromagnet with a UNICORE shape made from grain-oriented steel was designed by an analytical approach and by the FEM method and was manufactured. Capacitors for employing serial resonance were created.

The design of a single-layer, a double-layer and a 10-layer PCB search coil for AC magnetic flux density measurements has been proposed, and a full characterization has been presented. The results show very good agreement between the theoretical (calculated), simulated (FIT) and measured values of resistance, inductance and the search coil constant.

Homogeneity of realized AC electromagnet was measured using the single-layer PCB search coils and double-layer PCB search coil was used for measurement of AC magnetic flux density in the air gap. A software for measurement of AC magnetic flux density using a multimeter 3458A as a digital sampler was created in LabWindows CVI. The system was tested at a frequency of 50 Hz, where AC magnetic flux density value of 0.9 T was reached. The stability of the generated MFD was improved using a feedback.

The AC electromagnet made from amorphous material MetGlas 2605SA1 and with the same cross-sectional area, the same winding parameters and the same air gap as in the case of UNICORE yoke was also realized to extend the frequency range of generated MFD values up to 1 kHz.

6 Conclusions

There were some coil standards at CMI that are used for calibrating Hall probes at 50 Hz or for calibrating AC magnetic field analyzers up to 20 kHz, but there was no AC electromagnet for use in Hall probe calibration at CMI before this dissertation work was begun. The main goal of the work presented in this dissertation was to develop new AC magnetic flux density standards for use in expanding the options available for calibrating Hall probes up to 1 T in the low frequency range (up to 100 Hz) and for calibrating magnetometers up to 100 µT in the frequency range up to 100 kHz.

The setup for generating an AC magnetic flux density value up to 100 kHz was presented in detail in Chapter 4. The design of the single-layer Helmholtz-type solenoid for generating AC MFD in the frequency range up to 100 kHz has been proposed, and a full characterization has been presented here. The analytical design and the FEM design have been compared with a real solenoid. The results from the DC analysis show that the relative difference of the MFD theoretical values in the center of the solenoid is from 0.04% to 0.19%, depending on the method that is used. The results from the AC analysis show that the relative difference of the MFD frequency dependence in the center of the solenoid is in the range of (0.25 %ï 0.7 %) for the frequency range of (3ï 100) kHz - about 2% at 100 kHz ï in comparison with the values measured by a special search coil. Good agreement between the theoretical (calculated) and measured homogeneity values in the *z*- and ***J***-axis was also proven.

A programmable capacitor array that enables a high-frequency MFD value to be generated in a single-layer Helmholtz-type solenoid up to 150 kHz with inexpensive low voltage AC power sources has been realized and has been successfully tested. Specifically, an AC amplitude MFD value up to 150 εT up to 140 kHz and an AC amplitude MFD value up to 220 εT up to 120 kHz can be generated with expanded uncertainty of (0.2 to 1.0)% for k=2. An AC amplitude MFD value of 110 εT at maximum can be generated at a frequency of 150 kHz for a short time. A transimpedance amplifier that expands the upper range of useful frequencies for multi-layer search coils has also been realized and successfully tested. With this amplifier, a part of the frequency range of single-layer and multi-layer search coils conveniently overlaps and allows a large frequency range to be covered with ease, without blind spots. In particular, the measurement differences with EP 01/00 and with K_{II} with the transimpedance amplifier were lower than 0.28% in the overlapping range of 2 kHz to 30 kHz. The methods for calibrating AC coil standards have also been described, analyzed and compared.

In metrology, coil standards are used for calibrating AC magnetic field meters, loop antennas and search coils. The method for calibrating AC magnetic field meters by a special search coil and calibrating loop antennas has been described in detail. Five different search coil calibration methods have also been analyzed, described and compared.

A system for generating AC magnetic flux density up to 1 T for lower frequencies was presented in detail in Chapter 5. An AC electromagnet with a UNICORE shape made from grain-oriented steel and with winding of 1600 turns was designed by an analytical approach and by the FEM method and was manufactured. Capacitors for employing serial resonance were created and were dimensioned for 5 kV.

The design of a single-layer, a double-layer and a 10-layer PCB search coil for AC magnetic flux density measurements has been proposed, and a full characterization has been presented. The design of the PCB search coils was adapted for use in an AC electromagnet air gap of 10 mm. The analytical design and the FIT design were compared with the fabricated PCB search coils. A single-layer PCB search coil with a constant value of 8.52 cm^2 and 0.5 mm in thickness, a double-layer PCB search coil with a constant value of 16.31 cm^2 and

0.5 mm in thickness, and a 10-layer PCB search coil with a constant value of 81.6 cm^2 and 1.2 mm in thickness, were fabricated. PCB search coils can have a better value for certain parameters (thickness, inductance vs. area turns, diameter) than the parameters of hand-wound search coils. The results show very good agreement between the theoretical (calculated), simulated (FIT) and measured values of resistance, inductance and the search coil constant. It has also be proven that the search coil constants of all three PCB coil types are frequency-independent up to 20 kHz. The fabricated search coils can therefore easily be used for AC magnetic flux density measurements in the given frequency range up to 10 kHz.

Homogeneity of realized AC electromagnet was measured using the single-layer PCB search coils and double-layer PCB search coil was used for measurement of AC magnetic flux density in the air gap. A software for measurement of AC magnetic flux density using a multimeter 3458A as a digital sampler was created in LabWindows CVI. The system was tested at a frequency of 50 Hz, where AC magnetic flux density value of 0.9 T was reached. According to the results of the homogeneity measurements, this is sufficient for common Hall probes less than 2 mm in thickness and less than 6 mm in width. Hall probes can be calibrated up to 1 T in the frequency range from 30 Hz up to 70 Hz by the system described here. The stability of the generated MFD is about 0.08 mT using a feedback. The expanded uncertainty of the generated MFD value is 0.2 %.

The AC electromagnet made from amorphous material MetGlas 2605SA1 and with the same cross-sectional area, the same winding parameters and the same air gap as in the case of UNICORE yoke was also realized to extend the frequency range of generated MFD values. RMS values of AC magnetic flux density up to 280 mT (80 Hz), up to 160 mT (405 Hz) and up to 90 mT (930 Hz) can be generated by mean of this electromagnet.

6.1 Achieved objectives

All partial tasks defined in Chapter 3 have been fulfilled, i.e.:

- A new single-layer Helmholtz- type solenoid for generating AC magnetic flux density up to 100 kHz is presented in Chapter 4.1. The design, realization and characterization of this solenoid are discussed.
- The setup with the Helmholtz-type solenoid was improved by a programmable capacitor array to be able to generate AC magnetic flux density up to 100 µT in the frequency range up to 100 kHz. The MFD value can be generated up to 150 kHz beyond the objectives of this dissertation. The results are presented in Chapter 4.2.
- Methods that can be used for calibrating a coil standard up to 100 kHz have been presented. The frequency dependence of a single-layer Helmholtz-type solenoid was calibrated up to 100 kHz by a method using two search coils with nominally the same values (method 1), with expanded uncertainty from 0.2% up to 0.35% and by a method using a precise AC current shunt (method 2), with expanded uncertainty from 0.12% up to 0.25%. The frequency dependence of the constant of the search coils was verified and calibrated in special Helmholtz coils. The results are presented in Chapter 4.3.
- The design of a new AC electromagnet for generating AC magnetic flux density up to 1 T at low freqeuncies is presented in Chapter 5.1. Hall probes can be calibrated up to 1 T in the frequency range from 30 Hz up to 70 Hz by the system described in Chapter 5.3. The results are presented in Chapter 5.4.

- The design of a single-layer, double-layer and 10-layer PCB search coil for AC magnetic flux density measurements in the air gap of the AC electromagnet has been proposed, and a full characterization has been presented in Chapter 5.2.

The possibilities of using AC coil standards in metrology, including calibration results, are presented in Chapter 4.4. An AC electromagnet made from amorphous MetGlas 2605SA1 material was also fabricated to extend the frequency range of the generated MFD values up to 1 kHz. Measured RMS values of AC magnetic flux density are presented in Chapter 5.5.

6.2 Future research

There are several further improvements that can be investigate and realized. Specifically:

- Extend the frequency range of AC coil standard calibration from 100 kHz up to 200 kHz using a single-turn shielded search coil with lock-in amplifier.
- Fabricate a power transformer to improve the power supply of an AC electromagnet.
- Improve the feedback for stabilizing the AC MFD up to 1 T, perhaps with the use of digital control [121].
- Extend the frequency range of the AC MFD by an amorphous electromagnet up to 10 kHz.
- Fabricate a high voltage programmable capacitor array for use with an AC electromagnet.

7 References

[1] E. Tiesinga, P. J. Mohr, D. B. Newell and B. N. Taylor: ĂCODATA recommended values of the fundamental physical constants: 2018ñ, 2019. [Online]. Available: https://physics.nist.gov/cuu/pdf/wallet_2018.pdf

[2] W. F. Gauster: ĂSome basic concepts for magnet coil designñ, *Transactions of the American Institute of Electrical Engineers, Part I: Communication and Electronics*, vol. 79, no. 6, pp. 822-828, Jan. 1961.

[3] S. R. Trout: ĂUse of Helmholtz coils for magnetic measurementsñ, in *IEEE Transactions on Magnetics*, vol. 24, no. 4, pp. 2108-2111, July 1988.

[4] S. Tumanski: ĂHandbook of Magnetic Measurementsò, CRC Press, 2011.

[5] F. J. Nieves, A. Bayón and F. Gascón: ĂOptimization of the magnetic field homogeneity of circular and conical coil pairsñ, *Review of Scientific Instruments* 90, 045120 (2019).

[6] W. M. Frix, G. G. Karady and B. A. Venetz: ĂComparison of calibration systems for magnetic field measurement equipmentñ, in *IEEE Transactions on Power Delivery*, vol. 9, no. 1, pp. 100-108, Jan. 1994.

[7] A. F. R. Alvarez, E. Franco-Mejía and C. R. Pinedo-Jaramillo: ĂStudy and Analysis of Magnetic Field Homogeneity of Square and Circular Helmholtz Coil Pairs: A Taylor Series Approximationñ, *2012 VI Andean Region International Conference*, Cuenca, 2012, pp. 77-80.

[8] V. E. Baranova and P. F. Baranov: ĂThe Helmholtz coils simulating and improved in COMSOL,ñ *2014 Dynamics of Systems, Mechanisms and Machines (Dynamics)*, Omsk, 2014, pp. 1-4.

[9] A. F. Restrepo, E. Franco, H. Cadavid and C. R. Pinedo: ĂA comparative study of the magnetic field homogeneity for circular, square and equilateral triangular helmholtz coilsñ, *2017 International Conference on Electrical, Electronics, Communication, Computer, and Optimization Techniques (ICEECCOT)*, Mysuru, 2017, pp. 13-20.

[10] James Clerk Maxwell: ĂA Treatise on Electricity and Magnetismñ, Clarendon Press, Oxford, p. 319, 1873.

[11] Q. Cao, X. Han, B. Zhang and L. Li: ĂAnalysis and Optimal Design of Magnetic Navigation System Using Helmholtz and Maxwell Coilsñ, in *IEEE Transactions on Applied Superconductivity*, vol. 22, no. 3, pp. 4401504-4401504, June 2012, Art no. 4401504.

[12] B. Mihailescu, I. Plotog and M. N. Velcea: ĂComparative assessment of maxwell and Helmholtz coils magnetic field for biotechnological applicationsñ, *2015 IEEE 21st International Symposium for Design and Technology in Electronic Packaging (SIITME)*, Brasov, 2015, pp. 157-160.

[13] W. Braunbek: ĂDie Erzeugung weitgehend homogener Magnetfelder durch Kreisstraemeñ, *Zeitschrift fuer Physik*, Vol. 88, pp. 399-402, 1934.

[14] A. Zikmund: ĂMagnetic calibration by using non-linear optimization methodñ, Disertaļní práce, Ļ,VUT, 2014.

[15] Wang, P., Liu, H., Cheng, X. et al.: ĂDesign of Braunbek Coil for Nuclear Magnetic Resonance Gyro Magnetic Field Excitationñ, J. Shanghai Jiaotong Univ. (Sci.) (2018), vol. 23, no. 6, pp. 740-745.

[16] R. Merritt, C. Purcell, G. Stroik: ĂUniform magnetic field produced by three, four, and five square coilsñ, *Review of Scientific Instruments* **54**, 879 (1983).

[17] S. M. Rubens: ĂCube-Surface Coil for Producing a Uniform Magnetic Fieldñ, *Review of Scientific Instruments* 16, 243 (1945).

[18] G. E. Lee-Whiting: ĂUniform magnetic fieldsñ, Atomic Energy of Canada Limited, 1957.

[19] J. C. Alldred, I. Scollar: ĂSquare cross section coils for the production of uniform magnetic fieldsñ, *Journal of Scientific Instruments*, Volume 44, Number 9, 1967.

[20] J. L. Kirschvink: ĂUniform magnetic fields and double - wrapped coil systems: Improved techniques for the design of bioelectromagnetic experimentsñ, *Bioelectromagnetics*, 13: 401-411 (1992).

[21] P. Baranov, V. Baranova, S. Uchaikin and Y. Pisarenko: ĂCreating a uniform magnetic field using axial coils system for calibration of magnetometers,ñ *2016 Dynamics of Systems, Mechanisms and Machines (Dynamics)*, Omsk, 2016, pp. 1-5.

[22] A. Modi *et al*.: ĂHexagonal coil systems for uniform magnetic field generation,ñ *2016 IEEE Asia-Pacific Conference on Applied Electromagnetics (APACE)*, Langkawi, 2016, pp. 47-51.

[23] MIT Lecture Notes, Chapter 9, pp. 20-23. [Online]. Available: http://web.mit.edu/viz/EM/visualizations/coursenotes/modules/guide09.pdf

[24] J. V. Afanasjev et al: ĂSredstva izmerenij parametrov magnitnogo poljañ, Leningrad, Energia 1979 (in Russian).

[25] M. W. Garrett: ĂAxially Symmetric Systems for Generating and Measuring Magnetic Fieldsñ, *Journal of Applied Physics* 22, 1951.

[26] M. W. Garrett: ĂThick Cylindrical Coil Systems for Strong Magnetic Fields with Field or Gradient Homogeneities of the 6th to 20th Orderñ, *Journal of Applied Physics* 38, 1967.

[27] J. R. Barker: ĂNew Coil Systems for the Production of Uniform Magnetic Fieldsñ, *Journal of Scientific Instruments*, Vol. 26, No. 8, 1949.

[28] Annieamma George, Balasubramaniam (B.A.R.C.), V.Y. Dhapre, Arun Patil, R.V. Iyengar and P.D. Saraf: ĂVector PPM setup using four coil Barker system and 0.1 nT PPMñ, *Journal of Instrumentation Society of India*, v.37/4, p.277-281, 2007.

[29] J. Kupec: ĂEtalony a vybrané metody mČření magnetické indukceñ, Kandidátská dizertační práce, Praha, 1984.

[30] D. B. Montgomery: ĂSolenoid Magnet Designñ, Wiley, New York (1969).

[31] B. Girard and M. Sauzade: ĂCalcul des solenoides compenses du 6^{éme} ordre a volume de bobinage minimumñ, *Nuclear Instruments and Methods* 25 (1964) 269-284.

[32] F. Bitter: ĂWater cooled magnetsñ, *Review of Scientific Instruments* **33**, 342 (1962).

[33] D. B. Montgomery: ĂThe generation of high magnetic fieldsñ, *Reports on Progress in Physics*, Vol. 26, No. 1, 1963.

[34] A. V. Gavrilin, M. D. Bird, V. E. Keilin, and A. V. Dudarev: ĂNew concepts in transverse ýeld magnet design,ñ *IEEE Trans. Appl. Supercond.*, vol. 13, no. 2, pp. 1213ï 1216, Jun. 2003.

[35] Wang, X., Chen, Y., Huang, C., Wang, X., Zhao, L., Zhang, X. and Tang, J.: ĂContribution of a 300 kHz Alternating Magnetic Field on Magnetic Hyperthermia Treatment of HepG2 Cellsñ, *Bioelectromagnetics*, 34(2), pp. 95-103, (2013).

[36] Bekovic, M. and Hamler, A.: ĂDetermination of the Heating Effect of Magnetic Fluid in Alternating Magnetic Fieldñ, *IEEE Trans. on Magnetics*, 46(2), (2010).

[37] Mahdi Mohseni, Amirhossein Rajaei: ĂDesign of Alternating Magnetic Field Generator for Magnetic Fluid Hyperthermia Research Applicationñ, *Scientia Iranica*, Vol. 25, No. 6, 2018, pp. 3507-3516.

[38] D. E. Bordelon *et al.*: ĂModified Solenoid Coil That Efficiently Produces High Amplitude AC Magnetic Fields With Enhanced Uniformity for Biomedical Applications,ñ in *IEEE Transactions on Magnetics*, vol. 48, no. 1, pp. 47-52, Jan. 2012.

[39] Konefağ-Janocha M, BanaŜ-ZŃbczyk A, Bester M, et al.: ĂThe Effect of Stationary and Variable Electromagnetic Fields on the Germination and Early Growth of Radish (Raphanus sativus) ñ, *Polish Journal of Environmental Studies*, vol. 28, no. 2, 2019, pp. 709-715.

[40] M. Enokizono, T. Todaka, S. Hasebe and K. Bessho: ĂLaminated eddy-current type solenoid coil for alternating high magnetic field,ñ in *IEEE Transactions on Magnetics*, vol. 26, no. 5, pp. 2759-2761, Sept. 1990.

[41] M. Chiampi, G. Crotti, and D. Giordano: ĂSet up and characterization of a system for the generation of reference magnetic fields from 1 to 100 kHz,ñ *IEEE Trans. Instrum. Meas.*, vol. 56, no. 2, pp. 300ï 304, Apr. 2007.

[42] D. A. Rollett and A. E. Drake: ĂTraceable magnetic field strength measurements to 120 kHz,ñ *IEE Proc. Sci., Meas. Technol.*, vol. 143, no. 4, pp. 255ï 258, Jul. 1996.

[43] S. A. Hanna, Y. Motai, W. J. Varhue and S. Titcomb: ĂVery-Low-Frequency Electromagnetic Field Detector With Data Acquisition,ñ in *IEEE Transactions on Instrumentation and Measurement*, vol. 58, no. 1, pp. 129-140, Jan. 2009.

[44] C. Fabricio de Melo, R. L. Araújo, L. M. Ardjomand, N. S. R. Quoirin, M. Ikeda, and A. A. Costa: ĂCalibration of magnetic field meters at 60 Hz using a Helmholtz coil: Constructive aspects and calculation of associated uncertainties,ñ in Proc. 18th IMEKO World Congr., Rio de Janeiro, Brazil, Sep. 2006, pp. 1942ï 1945.

[45] M. Ishii, R. Ketzler, M. Albrecht, S. Kurokawa, and Y. Shimada: ĂImprovement of formula and uncertainty of the reference magnetic field for ac magnetometer calibrationñ, *IEEE Trans. Instrum. Meas.*, vol. 62, no. 6, pp. 1443ï 1449, Jun. 2013.

[46] A. M. de França, D. G. Costa, L. N. Pereira, M. A. Soares, P. C. de O. Vitorio, P. R. M. Nascimento: ĂLow frequency magnetic flux density meter calibrationñ, Proc. of 20th IMEKO World Congress 2012, pp. 796-798.

[47] ICNIRP: ĂGuidelines for limiting exposure to time-varying electric and magnetic fields (1 Hz to 100 kHz),ñ *Health Phys.*, vol. 99, no. 6, pp. 818ï 836, 2010.

[48] ñIEEE Standard for Calibration of Electromagnetic Field Sensors and Probes (Excluding Antennas) from 9 kHz to 40 GHzò, IEEE Standard, 1309-2013, 2013.

[49] A. Marrella et al.: ĂA combined low-frequency electromagnetic and fluidic stimulation for a controlled drug release from superparamagnetic calcium phosphate nanoparticles: potential application for cardiovascular diseasesñ, *Journal of the Royal Society*, Interface **15**, 2018.

[50] Silkstone G, Wilson MT: ĂA Further Investigation of the Effects of Extremely Low Frequency Magnetic Fields on Alkaline Phosphatase and Acetylcholinesteraseñ, PLoS ONE 11(3), 2016.

[51] D. Cvetkovic, E. Jovanov and I. Cosic: ĂAlterations in Human EEG Activity Caused by Extremely Low Frequency Electromagnetic Fields,ñ *2006 International Conference of the IEEE Engineering in Medicine and Biology Society*, New York, NY, 2006, pp. 3206-3209.

[52] Rácuciu, M.: ĂInfluence of extremely low frequency magnetic field on assimilatory pigments and nucleic acids in *Zea mays* and *Cucurbita pepo* seedlingsñ, *Rom. Biotech. Lett.*, 2012, vol. 17, pp. 7662ï 7672.

[53] M. Ljesevic, B. Loncarevic, I. N. Bubanja, V. Beskoski, G. Gojgic-Cvijovic, Z. Velikic, D. Stanisavljev: ĂInfluence of the low frequency 10-1000 Hz magnetic field on Saccharomyces cerevisiae respiration aktivityñ, 55th Meeting of the Serbian Chemical Society, Novi Sad, Serbia, June 8-9, 2018. Proceedings, p. 31-35.

[54] Yost MG, Liburdy RP.: ĂTime-varying and static magnetic fields act in combination to alter calcium signal transduction in the lymphocyteñ, FEBS Lett 1992; 296:117ï 22.

[55] E. L. Bronaugh: ĂHelmholtz coils for EMI immunity testing: stretching the uniform field area,ñ *Seventh International Conference on Electromagnetic Compatibility, 1990*, York, UK, 1990, pp. 169-172.

[56] E. R. Javor and T. Anderson: ĂDesign of a Helmholtz coil for low frequency magnetic field susceptibility testing,ñ *1998 IEEE EMC Symposium. International Symposium on Electromagnetic Compatibility. Symposium Record (Cat. No.98CH36253)*, Denver, CO, USA, 1998, pp. 912-917 vol.2.

[57] Seidman, Seth J et al.: ĂFeasibility results of an electromagnetic compatibility test protocol to evaluate medical devices to radio frequency identification exposureñ, *Biomedical engineering online* vol. 13 110. 3 Aug. 2014.

[58] Herceg, D., A. Juhas, and M. Milutinov: ĂA design of a four square coil system for a biomagnetic experiment,ñ *Facta Universitatis Series: Electronics and Energetics*, Vol. 22, No. 3, 285ï 292, 2009.

[59] Yamazaki, K. , Fujinami, H. , Shigemitsu, T. and Nishimura, I.: ĂLow stray ELF magnetic field exposure system for in vitro studyñ, *Bioelectromagnetics*, 21: 75-83, 1990.

[60] Shigemitsu, T., Negishi, T., Yamazaki, K. , Kawahara, Y., Haga, A. , Kobayashi, K. and Muramatsu, K.: ĂA newly designed and constructed 20 kHz magnetic field exposure facility for in vivo studyñ, *Bioelectromagnetics*, 30: 36-44, 2009.

[61] Wada K., Kogure S., Suzuki Y.: ĂOptimal design of a magnetic-field generator at 20 kHz for biological researchñ, Proceedings of the 32nd Annual Meeting of the Bioelectromagnetics Society, Seoul, Korea, 14ï 18 June 2010, pp. 455ï 456.

[62] K. Caputa and M. A. Stuchly: ĂComputer controlled system for producing uniform magnetic fields and its application in biomedical research,ñ in *IEEE Transactions on Instrumentation and Measurement*, vol. 45, no. 3, pp. 701-709, June 1996.

[63] Smith, R. F., Clarke, R. L. and Justesen, D. R.: ĂBehavioral sensitivity of rats to extremely - low - frequency magnetic fieldsñ, *Bioelectromagnetics*, 15: 411-426, 1994.

[64] Kumar, V. S., Kumar, D. A., Kalaivani, K., Gangadharan, A. C., Raju, K. N., Thejomoorthy, P. , Manohar, B. M. and Puvanakrishnan, R.: ĂOptimization of pulsed electromagnetic field therapy for management of arthritis in ratsñ, *Bioelectromagnetics*, 26: 431-439, 2005.

[65] J. Kupec, M. Ulvr: ĂZpráva ļ. 8017-ZV-C0001-17 o státním etalonu magnetické indukceñ, Ļeský metrologický institut, 2017.

[66] M. Ulvr: ĂCalibration of magnetic field meters up to 50 kHz at CMI, ñ Proc. of 19th Symposium IMEKO TC 4 Symposium and 17th IWADC Workshop Advances in Instrumentation and Sensors Interoperability, Barcelona, Spain, July 18-19, 2013.

[67] GMW: ĂModel: 5403AC 63MM LAMINATED ELECTROMAGNET - Userôs manualñ, Canada, 2005.

[68] GMW: Ă3470HFAC Dipole Electromagnet, High Frequency ACñ, Canada, 2014.

[69] Ece Bayēr, Eyüp Bilgi, Aylin ķendemir-Ürkmez and E. Esin Hamek-Kocabaĸ: ĂThe effects of different intensities, frequencies and exposure times of extremely low-frequency electromagnetic fields on the growth of *Staphylococcus aureus* and *Escherichia coli* O157:H7ñ, *Electromagnetic Biology and Medicine*, 34:1, pp. 14-18, 2015.

[70] Christiansen, M. G., Howe, C. M., Bono, D. C., Perreault, D. J. & Anikeeva, P.: ĂPractical methods for generating alternating magnetic fields for biomedical researchñ, *Rev. Sci. Instrum.* 88, 084301 (2017).

[71] De Souza, A., Garcí, D., Sueiro, L., Gilart, F., Porras, E. and Licea, L.: ĂPre - sowing magnetic treatments of tomato seeds increase the growth and yield of plantsñ, *Bioelectromagnetics*, 27: 247-257, 2006.

[72] G. Podaru, J. Moore, R. K. Dani, P. Prakash, and V. Chikan: ĂNested Helmholtz coil design for producing homogeneous transient rotating magnetic fieldsñ, *Rev. Sci. Instrum.* 86, 034701 (2015).

[73] Oleg Zaitov, Vladimir A. Kolchuzhin: ĂBitter coil design methodology for electromagnetic pulse metal processing techniquesñ, *Journal of Manufacturing Processes*, Volume 16, Issue 4, 2014, pp. 551-562.

[74] S. Ninomiya, K. Hatanaka, Y. Sakemi, T. Kawaguchi, and N. Takahashi: ĂThe study of high magnetic field and AC operation of high temperature superconducting magnet,ñ in Proc. Asian Particle Accelerator Conference 2004, Gyeongju, 2004, pp. 507ï 509.

[75] 0. Miura, I. Inoue, T. Suzuki, K. Matsumoto, Y. Tanaka, K. Funaki, M. Iwakuma, K. Yamafuji, and T. Matsushita: ĂThe development of a 2.5 T/100 kV a AC superconducting magnet using a high-Jc NbTi superconducting wire having Nb artificial pinsñ, *Superconducting Sci. Technol.*, vol. 6, pp. 748-754, (1993).

[76] V. E. Czernyshev: ĂRasczot czastotnoj pogreshnosti mier magnitnoj indukciiñ, in *Trudy Metrologiceskich Institutov SSSR*, vol. 140, Moscow, Russia: Izd. standartov, 1972.

[77] Ionel DumbravŁ, Georgiana Roĸu, Ion PŁtru, Aurelia Scornea, Octavian Baltag, Andrei Marinescu: ĂCalibration of Magnetic Field Sensors up to 10 kHz Based on 50 Hz Helmholtz Coilsñ, Proc. of 22nd IMEKO TC4 International Symposium, Romania, 2017.

[78] P. Kaġpar, P. Ripka: ĂInduction Coils: Voltage versus Current Outputñ, XVI IMEKO World Congress, Vienna, 2000.

[79] K. Weyand, R. Ketzler: ĂImproved AC-Field Calibration-Setupñ, in Proc. of CPEM 2004, London, 2004, pp 396-397.

[80] Po Gyu Park, Y. G. Kim, V. N. Kalabin, V. Ya. Shifrin: ĂAC magnetic flux density standards in the low frequency rangeñ, in Proc. of CPEM 2008, USA, 2008.

[81] V. N. Kalabin, P. G. Park, and V. Ya. Shifrin: ĂPrecision low-frequency AC magnetic field transducerñ, CPEM 2006 Conf. Digest, Torino, Italy, pp. 140-141, July 9-14, 2006.

[82] K. Weyand et all: ĂFinal Report of CCEM Key Comparison CCEM. M.-K1: Magnetic Flux Density by means of Transfer Standard Coilñ, *Metrologia*, Volume 42, Technical Supplement, 2005.

[83] R. Haugh: ĂAlternating current bridge methodsñ, Sir I. Pitman & Sons, 5th Edition, London, 1957.

[84] V. Nováková Zachovalová: ĂOn the Current Shunts Modelingñ, *IEEE Transaction on Instrumentation and Measurement*, vol. 63, no. 6, 2014, pp. 1620-1627.

[85] M. Ulvr: ĂA system for calibration of search coils with area turns up to 100 m^2ñ, Proc. of CPEM 2012, Washington, 2012.

[86] D. Overturf, N. Lumsden, J. Dea, D. Rodriguez and J. D. Rockway: ĂAir core loop antenna calibration methods,ñ *2017 IEEE International Symposium on Antennas and Propagation & USNC/URSI National Radio Science Meeting*, San Diego, CA, 2017, pp. 377-378.

[87] A. Aykan: ĂCalibration of circular loop antennas,ñ in *IEEE Transactions on Instrumentation and Measurement*, vol. 47, no. 2, pp. 446-452, April 1998.

[88] C. W. T. McLyman: ĂTransformer and Inductor Design Handbookñ, Fourth Edition,CRC Press, 2011.

[89] W. G. Hurley, W. H. Wölfle: ĂTransformers and Inductors for Power Electronics ï Theory, Design and Applicationsñ, Wiley, 2013.

[90] A. E. Fitzgerald, C. Kingsley Jr., S. Umans: ĂElectric Machineryñ, 6th Edition, McGraw-Hill, 2003.

[91] M. K. Kazimierczuk: ĂHigh Frequency Magnetic Componentsò, 2nd Edition, Wiley, 2014.

[92] MIT, Dept. of Electrical Engineering: ĂMagnetic Circuits and Transformersñ, MIT Press, 1965.

[93] R. E. Pawinanto, J. Yunas, M. M. Said, M. Mohd. Noor and B. Y. Majlis: ĂDesign and Fabrication of PCB Based Planar Micro-coil For Magnetic MEMS Actuatorñ, P*roceedings of IEEE International Conference on Semiconductor Electronics*, Kuala Lumpur, Malaysia, 27.-29. August 2014, (IEEE, 2014), pp 487-490.

[94] S. Duric, L. Nad, B. Biberdġic, M. Damnjanovic, and Lj. Ćivanov: ĂPlanar Inductive Sensor for Small Displacementñ, *Proceedings of 26th International Conference on Microelectronics*, Niġ, Serbia, 11.-14. May 2008, (Electron Devices Society of IEEE, 2008), pp. 345-348.

[95] T. M. Liakopoulos, C. H. Ahn: ĂA micro-fluxgate magnetic sensor using micromachined planar solenoid coilsñ, Sensors and Actuators **77**, 66ï 72 (1999).

[96] B.Y. Liu, H.W Zhang, X.L Tang, H. Su: ĂRF Integrated Planar Inductor Fabricated on Ferrite Substratesñ, *Proceedings of 2006 International Conference on Communications, Circuits and Systems*, Guilin, China, 25.-28. June 2006, (IEEE, 2006), pp. 2623 ï 2624.

[97] J. N. Burghartz, B. Rejaei: ĂOn the Design of RF Spiral Inductors on Siliconñ, *IEEE Trans. Electron Devices* **50**, 718-729 (2003).

[98] A. B. Islam, S. K. Islam, F. S. Tulip: ĂDesign and Optimization of Printed Circuit Board Inductors for Wireless Power Transfer Systemñ, *Circuits and Systems* **4**, 237-244 (2013).

[99] J. Uei-Ming and M. Ghovanloo: ĂDesign and Optimization of Printed Spiral Coils for Efficient Transcutaneous Inductive Power Transmissionñ, *IEEE Trans. Biomed. Circuits Syst.***1**, 193-202 (2007).

[100] Y. Mi, X. Tang, S. Rui, Y. Chu, C. Bian, C. Yao and C. Li: ĂDevelopment of High dB/dt Pulsed Magnetic Field Generator Based on Printed Circuit Board Archimedes Spiral Coil for Biomedical Applicationsñ, *IEEE Trans. Plasma Sci.* **44**, 1879-1887 (2016).

[101] E. J. Brandon, E. E.Wesseling, V. Chang, and W. B.Kuhn: ĂPrinted microinductors on flexible substrate for power applicationsñ, *IEEE Trans. Compon. Packag. Technol.* **26**, 517ï 523 (2003).

[102] E.Waffenschmidt, B. Ackermann, and M.Wille: ĂIntegrated ultra thin flexible inductors for low power converters,ñ in *Proceedings of IEEE 36th Power Electronics Specialists Conference*, Recife, Brazil, 12.-16. June 2005, (IEEE, 2005), pp. 1528ï 1534.

[103] M. Ludwig, M. Duffy, T. OôDonnell, P. McCloskey, and S. C. Ó. Mathùna: ĂPCB integrated inductors for low power DC/DC converterñ, *IEEE Trans. Power Electron.* **18**, 937ï 945 (2003).

[104] Y. Yan, Ch. Ding, K. D. T. Ngo, Y. Mei, and G.-Q. Lu: ĂAdditive Manufacturing of Planar Inductor for Power Electronics Applicationsñ, in *Proceedings of 2016 International Symposium on 3D Power Electronics Integration and Manufacturing*, Raleigh, USA, 13.-15. June 2016, (IEEE, 2016).

[105] N. Lazarus, C. Meyer, S. Bedair, H. Nochetto, and I. Kierzewski: ĂMultilayer liquid metal stretchable inductors,ñ *Smart Mater Struct.* **23**, pp. 1ï 10 (2014).

[106] S.-Y. Wu, C. Yang, W. Hsu and L. Lin: Ă3D-printed microelectronics for integrated circuitry and passive wireless sensorsñ, *Microsystems & Nanoengineering* **1** (2015).

[107] M. Clemens and T. Weiland: ĂDiscrete Electromagnetism with the Finite Integration Techniqueñ, *Progress In Electromagnetics Research* **32**, 65ï 87 (2001).

[108] S. Stalf: ĂPrinted inductors in RF consumer applicationsñ, *IEEE Trans. Consum. Electron.* **47**, 426-435 (2001).

[109] M. Ulvr, J. Kupec: ĂBilateral comparison of measurement of magnetic quantities CMI-VNIIM - Final reportñ, February 2018.

[110] Soft Magnetic Cobalt-Iron-Alloys, VACUUMSCHMELZE GMBH & CO. KG, 2001.

[111] M. I.Vasserman: ĂUstrojstvo dlja poverki teslametrov peremenych polej v diametru 0.01 ï 1 Tñ, *Trudy Metrologiceskich Institutov SSSR*, No. 233 (293), Energia, Leningrad, 1979.

[112] Nanocrystalline VITROPERM, VACUUMSCHMELZE GMBH & CO. KG, 2010.

[113] Nanocrystalline soft magnetic material FINEMET, brochure No. HL-FM10-C, Hitachi Metals Ltd. 2005.

[114] M. E. McHenry, M. A. Willard, D. E. Laughlin: ĂAmorphous and nanocrystalline materials for applications as soft magnetsñ, *Progress in Materials Science* 44 (1999), pp 291-433.

[115] G. Herzer: Nanocrystalline Soft Magnetic Alloys, Handbook of Magnetic Materials, Vol. 10, Ch. 3, Ed. K.H.J. Buschow, 1997, Elsevier.

[116] A. Urata, H. Matsumoto, S. Yoshida, A. Makino: ĂFeï Siï Bï Pï Cu Nanocrystalline Alloy Ribbons With High Saturation Magnetic Flux Density Prepared Using Industrial Materialsñ, *IEEE Transactions on Magnetics*, vol. 47, no. 10, 2011.

[117] A. Makino, H. Men, T. Kubota, K. Yubuta. A. Inoue: ĂFeSiBPCu Nanocrystalline Soft Magnetic Alloys with High Bs of 1.9 Tesla Produced by Crystallizing Hetero-Amorphous Phaseñ, *Materials Transactions*, Vol. 50, No. 1 (2009) pp. 204-209.

[118] K. Takenaka, A. D. Setyawan, Y. Zhang, P. Sharma, N. Nishiyama, A. Makino: ĂProduction of Nanocrystalline (Fe, Co)-Si-B-P-Cu Alloy with Excellent Soft Magnetic Properties for Commercial Applicationsñ, *Materials Transactions*, Vol. 56, No. 3, 2015.

[119] Soft Magnetic Materials and Semi-finished Products, VACUUMSCHMELZE GMBH & CO. KG, 2002.

[120] Chang-Hung Hsu, Yeong-Hwa Chang: ĂImpacts of Fe-Based Amorphous HB1 Core Transformers on Energy Efficiency and Environment Protectionñ, Proceedings of the 8th WSEAS International Conference on Instrumentation, USA, 2009.

[121] Aleş Havránek: ĂAlgoritmy Śízení magnetovacího procesu kompenzaţ ních ferometrŢñ, Disertaţ ní práce, Ţ VUT, 2017.

8 Publications of the autor

8.1 Thesis related

8.1.1 Publications in journals with impact factor

[J1] M. Ulvr: ĂSetup for generating an AC magnetic field from 3 kHz up to 100 kHzñ, *IEEE Transaction on Magnetics*, vol. 51, No. 1, 2015.

[J2] M. Ulvr, J. Polonský: ĂGenerating an AC amplitude magnetic flux density value up to 150 εT at a frequency up to 100 kHzñ, *Journal of ELECTRICAL ENGINEERING*, vol. 68, No. 3, 2017. *co-authorship 60 %*

[J3] M. Ulvr: ĂDesign of PCB search coils for AC magnetic flux density measurementñ, *AIP Advances*, vol. 8, no. 4, pp. 047505-1 - 047505-9, 2018.

8.1.2 Conference proceedings ï others

[C1] M. Ulvr, P. Kaġpar: ĂA COMPARISON OF DC AND AC METHODS FOR CALIBRATION OF SEARCH COILS WITH A HIGH AREA TURNS VALUEñ, Proc. of IMEKO World Congress of Metrology 2015, Praha, Ţ.R. *co-authorship 60 %*

[C2] M. Ulvr: ĂAC calibration methods of magnetic flux density coil standard up to 100 kHzñ, *2018 Conference on Precision Electromagnetic Measurements (CPEM 2018)*, Paris, 2018.

8.2 Other author publications

8.2.1 Publications in journals with impact factor

[O1] A. Zikmund, M. Janoġek, M. Ulvr, J. Kupec: ĂPrecise calibration method for triaxial magnetometers not requiring Earth's field compensationñ, *IEEE Transaction on Intrumentation and Measurement*, vol. 64, No. 5, 2015. *co-authorship 25 %*

[O2] M. Ulvr, A. Zikmund, J. Kupec, M. Janoġek, M. Vlk, T. Bayer: ĂDetermination of the Overhauser magnetometer uncertaintyñ, *Journal of ELECTRICAL ENGINEERING*, vol. 66, no. 7/s, 2015. *co-authorship 16,67 %*

[O3] M. Ulvr, J. Kupec: ĂImprovements to the NMR method with flowing water at CMIñ, *IEEE Transaction on Instrumentation and Measurement*, vol. 67, No. 1, 2018, pp. 204-208. *co-authorship 50 %*

[O4] M. Ulvr, J. Kupec: ĂVerification of low-ε indicator standard insertsñ, *Journal of ELECTRICAL ENGINEERING*, vol. 69, No. 6, 2018. *co-authorship 50 %*

8.3 Response to authorôs publications

[J1] M. Ulvr: ĂSetup for generating an AC magnetic field from 3 kHz up to 100 kHzñ, *IEEE Transaction on Magnetics*, vol. 51, No. 1, 2015.

- R. Beiranvand: ĂEffects of the Winding Cross-Section Shape on the Magnetic Field Uniformity of the High Field Circular Helmholtz Coil Systems,ñ in *IEEE Transactions on Industrial Electronics*, vol. 64, no. 9, pp. 7120-7131, Sept. 2017.
- J. Menclová: ĂNávrh a realizace cívek a napájecího obvodu pro hypertermii využívající magnetické pole a feromagnetické nanoļásticeñ, BakaláŚská práce, ĻVUT, 2017.
- M. Ishii: ĂAC Magnetometer Calibrations from 50 Hz up to 100 kHz at NMIJ, ñ *2018 Conference on Precision Electromagnetic Measurements (CPEM 2018)*, Paris, 2018, pp. 1-2.

[J3] M. Ulvr: ĂDesign of PCB search coils for AC magnetic flux density measurementñ, *AIP Advances*, vol. 8, no. 4, pp. 047505-1 - 047505-9, 2018.

- D. Murzin, D. J. Mapps, K. Levada, V. Belyaev, A. Omelyanchik, L. Panina and V. Rodionova: ĂUltrasensitive Magnetic Field Sensors for Biomedical Applicationsñ, *Sensors*, Vol. 20, Iss. 6, p. 1569 (2020).
- J. Kulíżek: ĂOvlŠení možnosti zvýšení efektivity repetitivní transkraniální magnetické stimulace pro léļbu pacientŢ s orofaciální bolestíñ, Diplomová práce, ĻVUT, 2020.

[O1] A. Zikmund, M. Janošek, M. Ulvr, J. Kupec: ĂPrecise calibration method for triaxial magnetometers not requiring Earth's field compensationñ, *IEEE Transaction on Intrumentation and Measurement*, vol. 64, No. 5, 2015.

- R. C. da Silva, I. S. K. Ishioka, C. Cappelletti, S. Battistini and R. A. Borgis: ĂHelmholtz cage design and validation for nanosatellites HWIL testing,ñ in *IEEE Transactions on Aerospace and Electronic Systems*, vol. 55, no. 6, pp. 3050-3061, Dec. 2019.
- M. Tahir, A. Moazzam and K. Ali: ĂA Stochastic Optimization Approach to Magnetometer Calibration With Gradient Estimates Using Simultaneous Perturbations,ñ in *IEEE Transactions on Instrumentation and Measurement*, vol. 68, no. 10, pp. 4152-4161, Oct. 2019.
- Y. Mu, C. Wang, X. Zhang and W. Xie: ĂA Novel Calibration Method for Magnetometer Array in Nonuniform Background Field,ñ in *IEEE Transactions on Instrumentation and Measurement*, vol. 68, no. 10, pp. 3677-3685, Oct. 2019.
- M. V. Gheorghe, M. C. Bodea and L. Dobrescu: ĂCalibration of Skew Redundant Sensor Configurations in the Presence of Field Alignment Errors,ñ in *IEEE Transactions on Instrumentation and Measurement*, vol. 69, no. 4, pp. 1794-1804, April 2020.
- Huan Liu, Haobin Dong: ĂResearch on an improved Overhauser magnetometerñ, *Journal of Instrumentation*, TH 006, 2019.
- F. J. Nieves, A. Bayón and F. Gascón: ĂOptimization of the magnetic field homogeneity of circular and conical coil pairs,ñ in *Review of Scientific Instruments*, vol. 90, no. 4, pp. 045120-1 - 045120-10, 2019.
- M. Janosek, M. Dressler, V. Petrucha and A. Chirtsov: ĂMagnetic Calibration System With Interference Compensation,ñ in *IEEE Transactions on Magnetics*, vol. 55, no. 1, pp. 1-4, Jan. 2019.

- Long, D., Zhang, X., Wei, X., Luo, Z., Cao, J.: ĂA Fast Calibration and Compensation Method for Magnetometers in Strap-Down Spinning Projectilesñ, *Sensors* **2018**, *18*, 4157.
- H. Liu, H. Donga, Z. Liu, J. Gea, W. Luo, C. Zhang, Z. Yuan, J. Zhu and H. Zhang: ĂA comprehensive study on the weak magnetic sensor character of different geometries for proton precession magnetometerñ, *Journal of Instrumentation*, vol. 13, September 2018, T09003.
- M. V. Gheorghe and M. C. Bodea: ĂAdvanced rate and position table leveling algorithm,ñ *2018 IEEE International Instrumentation and Measurement Technology Conference (I2MTC)*, Houston, TX, 2018, pp. 1-6.
- Shi, G., Li, X., Bai, Y., Zheng, C., Shu, X..: ĂResearch on a vehicle status based measurement equation for yaw estimationñ, *Chinese Journal of Scientific Instrument* 39(10), pp. 176-183, 2018.
- J. V. L. de Loiola *et al*.: Ă3 Axis simulator of the Earth magnetic field,ñ *2018 IEEE Aerospace Conference*, Big Sky, MT, 2018, pp. 1-8.
- Yan, X., Chen, G., Tian, X.: ĂTwo-step fast reconfigurable unscented kalman filter algorithm for measurement of missile rolling angleñ, *Chinese Journal of Scientific Instrument* 39(6), pp. 140-147, 2018.
- M. V. Gheorghe and M. C. Bodea: ĂCalibration Optimization Study for Tilt-Compensated Compasses,ñ in *IEEE Transactions on Instrumentation and Measurement*, vol. 67, no. 6, pp. 1486-1494, June 2018.
- D. S. Batista, F. Granziera, M. C. Tosin and L. F. de Melo: ĂThree-Axial Helmholtz Coil Design and Validation for Aerospace Applications,ñ in *IEEE Transactions on Aerospace and Electronic Systems*, vol. 54, no. 1, pp. 392-403, Feb. 2018.
- Li, Q., Li, Z., Zhang, Y., Yin, G.: ĂArtificial Vector Calibration Method for Differencing Magnetic Gradient Tensor Systemsñ, *Sensors* **2018**, *18*, 361.
- Liu, H., Dong, H., Liu, Z. et al.: ĂApplication of Hilbert-Huang Decomposition to Reduce Noise and Characterize for NMR FID Signal of Proton Precession Magnetometerñ, *Instrum Exp Tech* (2018) 61: 55.
- Gheorghe, M.V., Bodea, M.C.: ĂPractical optimization of reference-free calibration methods for directional drilling sensor modulesñ, UPB Scientific Bulletin, Series C: Electrical Engineering and Computer Science 80(2), pp. 109-120, 2018.
- R. Beiranvand: ĂEffects of the Winding Cross-Section Shape on the Magnetic Field Uniformity of the High Field Circular Helmholtz Coil Systems,ñ in *IEEE Transactions on Industrial Electronics*, vol. 64, no. 9, pp. 7120-7131, Sept. 2017.
- H. Liu, H. Dong, Z. Liu, J. Ge, B. Bai and C. Zhang: ĂNoise characterization for the FID signal from proton precession magnetometerñ, *Journal of Instrumentation*, Volume 12, July 2017.
- C. Wang, X. Qu, X. Zhang, W. Zhu and G. Fang ĂA Fast Calibration Method for Magnetometer Array and the Application of Ferromagnetic Target Localization,ñ in *IEEE Transactions on Instrumentation and Measurement*, vol. 66, no. 7, pp. 1743-1750, July 2017.
- Yang, D., You, Z., Li, B., Duan, W., Yuan, B.: ĂComplete Tri-Axis Magnetometer Calibration with a Gyro Auxiliaryñ, *Sensors* **2017**, 17, 1223.
- Shi, G., Li, X., Liu, Y., Kang, R., Shu, X.: ĂEquivalent two-step algorithm for the calibration of three-axis magnetic sensor in heading measurement systemñ, *Chinese Journal of Scientific Instrument*, Volume 38, Issue 2, 1 February 2017, Pages 402-407.

- H. Liu, H. Dong, J. Ge, P. Guo, B. Bai, and C. Zhang: ĂAn Improved Tuning Control Algorithm Based on SVD for FID Signal,ñ *J. Adv. Comput. Intell. Intell. Inform.*, Vol. 21, No.1, pp. 133-138, 2017.
- K. Han, H. Han, Z. Wang and F. Xu: ĂExtended Kalman Filter-Based Gyroscope-Aided Magnetometer Calibration for Consumer Electronic Devices,ñ in *IEEE Sensors Journal*, vol. 17, no. 1, pp. 63-71, 1 Jan.1, 2017.
- Huan Liu, Haobin Dong, Jian Ge, Bingjie Bai, Zhiwen Yuan and Zhizhuo Zhao: ĂResearch on a secondary tuning algorithm based on SVD & STFT for FID signalñ, *Measurement Science and Technology*, Volume 27, Number 10, 2016.
- Y. Zhang, Z. Su, M. Chi, Y. Huang and D. Wang: ĂMagnitude and Orientation Error Correction of a Superimposed Spatial Universal Rotating Magnetic Vector,ñ in *IEEE Transactions on Magnetics*, vol. 52, no. 5, pp. 1-9, May 2016.
- P. Szulim, S. Gontarz, J. MŃczak: ĂCalibration of magnetic field sensor used for diagnosis of steel constructionñ, *Journal of ELECTRICAL ENGINEERING*, Vol. 66, No. 7/s, 2015, pp. 203-207.

[O2] M. Ulvr, A. Zikmund, J. Kupec, M. Janoġek, M. Vlk, T. Bayer: ĂDetermination of the Overhauser magnetometer uncertaintyñ, *Journal of ELECTRICAL ENGINEERING*, vol. 66, no. 7/s, 2015.

- Chao Tan, Jiacheng Wang, Zongliao Li: ĂA frequency measurement method based on optimal multi-average for increasing proton magnetometer measurement precisionñ, *Measurement*, Volume 135, 2019, pp. 418-423.

[O3] M. Ulvr, J. Kupec: ĂImprovements to the NMR method with flowing water at CMIñ, *IEEE Transaction on Instrumentation and Measurement*, vol. 67, No. 1, 2018, pp. 204-208.

- Marco Grisi, Gaurasundar Marc Conley, Pascal Sommer, Jacques Tinembart, and Giovanni Boero: ĂA single-chip integrated transceiver for high field NMR magnetometryñ, *Review of Scientific Instruments*, vol. 90, no. 1, 2019.
- M. Janosek, M. Dressler, V. Petrucha and A. Chirtsov: ĂMagnetic Calibration System With Interference Compensation,ñ in *IEEE Transactions on Magnetics*, vol. 55, no. 1, pp. 1-4, Jan. 2019.
- Y. Huang *et al.*: ĂA Pure Shift-Based NMR Method for Transverse Relaxation Measurements on Complex Samples,ñ in *IEEE Transactions on Instrumentation and Measurement*, vol. 69, no. 1, pp. 201-211, Jan. 2020.
- G. G. Rodriguez, G. Forte, E. Anoardo: ĂUsing Proton Nuclear Magnetic Resonance (NMR) as a calibrating reference for magnetic field measurement instruments: Sensitive volume and magnetic field homogeneityñ, *Measurement*, vol. 151, 2020.